STARS

Electronic Theses and Dissertations, 2004-2019

2010

Heat Transfer In Multi-layer Energetic Nanofilm On Composites Substrate

Navid Amini Manesh
University of Central Florida

HEAT TRANSFER IN MULTI-LAYER ENERGETIC
NANOFILM ON COMPOSITES SUBSTRATE

by

NAVID AMINI MANESH
B.S. Bahá'í Institute of Higher Education, 1996
B.S. University of Central Florida, 2005
M.S. University of Central Florida, 2007

A dissertation submitted in partial fulfillment of the requirements
for the degree of Doctor of Philosophy
in the Department of Mechanical, Materials and Aerospace Engineering
in the College of Engineering and Computer Science
at the University of Central Florida
Orlando, Florida

Fall Term
2010

Major Professor: Ranganathan Kumar

ABSTRACT

The main purpose of this work is to find a physical and numerical description related to the reaction of the multilayer nano energetic material (nEM) in dense film. Energy density of nEM is much higher than the conventional energetic material; therefore, nEM finds more applications in propulsions, thermal batteries, material synthesis, nano igniters, waste disposals, and power generations. The reaction model of a multilayer nEM in a dense film of aluminum and copper oxide deposits on a composite substrate of silica/silicon is studied and solved in different stages. The two main interests in this study are propagation speed and maximum temperature of the reaction. In order to relate speed of reaction and maximum flame temperature a number of other variables such as heat loss, the product porosity, and the reaction length should be estimated. The main aim of this study is to introduce a numerical model which estimates and relates these values in multilayer nEM in a dense film. The following is a summary of the execution steps to achieve this goal.

In Part I of this thesis, flame front speed and the reaction heat loss were the main targets. The time-of-flight technique has been developed to measure the speed of flame front with an accuracy of 0.1 m/s. This measurement technique was used to measure the speed of propagation on multilayer nEM over different substrate material up to 65 m/s. A controllable environment (composite silicon\silica) was created for a multilayer standard thin film of aluminum and copper oxide to control the reaction heat loss through the substrate. A number of experimental results show that as the thickness of silica decreases, the reaction is completely quenched. Reaction is not in self-sustaining mode if the silica thickness is less than 200 nm. It is also observed that by

increasing silica's thickness in substrate, the quenching effect is progressively diminished. The speed of reaction seems to be constant at slightly more than 40 m/s for a silica layer with thickness greater than 500 nm. This would be the maximum heat penetration depth within the silica substrate, so the flame length was calculated based on the measured speed.

In Part II, a numerical analysis of the thermal transport of the reacting film deposited on the substrate was combined with a hybrid approach in which a traditional two-dimensional black box theory was used, in conjunction with the sandwich model, to estimate the maximum flame temperature. The appropriate heat flux of the heat sources is responsible for the heat loss to the surroundings. A procedure to estimate this heat flux using stoichiometric calculations is based on the previous author's work. This work highlights two important findings. One, there is very little difference in the temperature profiles between a single substrate of silica and a composite substrate of silicon\silica. Secondly, by increasing the substrate thickness, the quenching effect is progressively diminished at given speed. These results also show that the average speed and quenching of flames depend on the thickness of the silica substrate and can be controlled by a careful choice of the substrate.

In Part III, a numerical model was developed based on the moving heat source for multilayer thin film of aluminum and copper oxide over composite substrate of silicon\silica. The maximum combustion flame temperature corresponding to the speed of flame front is the main target of this model. Composite substrate was used as a mechanism to control the heat loss during the reaction. Thickness of the substrate, the length of flame front, and the density of the product were utilized for the standard multilayer thin film with 43 m/s flame front speed. The calculated heat penetration depth in this case was compared to the experimental result for the same flame front

speed. Numerical model was also used to estimate three major variables for a range of 30-60 m/s. In fact, the maximum combustion flame temperature that corresponds to flame speed along with the length of the flame, density of the product behind the flame, and maximum penetration depth in steady reaction, were calculated.

These studies will aid in the design of nEM multilayer thin film. As further numerical and experimental results are obtained for different nEM thicknesses, a unified model involving various parameters can be developed.

TABLE OF CONTENTS

LIST OF FIGURES

LIST OF TABLES

LIST OF NOMENCLATURE

CHAPTER 1
INTRODUCTION

Motivation

Nano energetic material (nEM) in multilayer thin film offers higher energy density, reaction rate, stability, and precision [1-11]. This study has broad practical applications ranging from propulsions, thermal batteries, material synthesis, nano igniters [12-17], waste disposals, and power generations [18-23]. The study of energetic material in nano scale geometry is growing rapidly due to the significant improvement in ignition process, energy release, and mechanical properties.

Bulk reaction of energetic material (ball milling) had significant drawbacks in performance relative to nEM in thin film. Traditional energetic materials are produced by mixing oxidizer and fuel which creates monomolecular, such as nitrocellulose, nitroglycerine, and trinitrotoluene. The mixing of oxidizer and fuel powder produce composite energetic materials. Although the composites release a higher energy compare to traditional energetic material, the energy release rates are slower due to higher mass transport of the reactants. Traditional energetic materials are relatively easy to prepare, and their performances can be predicted and the stoichiometry of the chemical reactants can be adjusted. [24-27]. Nanotechnology plays a major role to improve the reaction of nEM in thin film. Reducing the size of reactive material in nano scale increases the surface area between the reactants and the random hot spot within the reaction zone. This advantage reduces the diffusion distance of the reaction [28-31] and results in less heat and mass transport within the reaction zone. Increasing heat and mass transport leads to enhance heat conduction rate. New nEM in thin film is also a strong competitor to organic energetic material.

1

For comparison, traditional energetic compounds based on organic materials have almost similar energy per unit weight, but nEM in multilayer thin film offers much higher energy density and burn rate capacity. This field of study is relatively young, yet it is showing a great promise and potential as an alternative substance for explosive and propellant systems. Energy density and burn rate are the two main mechanical criteria for evaluation and comparisons of energetic materials.

Nano multilayer thin film includes a number of configurations such as nano particles in powder, gel, air- gel, or sputtering multilayer foil of oxidizer and fuel [32-41]. In general, two classes of new nEM are studied; Metastable intermolculer compositions (MIC) and energetic material in multilayer dense film or foil. MIC is a class of energetic materials that is composed by compressing individual fuel and oxidizer particles down to nano-scale dimensions. These same composites can be prepared using micron-size particles and this process is classified as pyrotechnics. Despite the high rate of reaction in this class of energetic material, inconsistent results generate many gray areas for study in this field. The second type of nEM in multilayer dense film or foil is the main target for this study. They have a slower speed of flame front and relatively precise and consistent reactions.

Nano energetic material in multilayer dense film has shown that a positive correlation exists between the burn rate, and the geometry, the deposition process and type of oxidizer [1]. Upper limits for the burn rate of nEM materials have not been yet determined. Although many earlier studies have shown the burn rate of nEM in dense thin film to be much lower than traditional materials a number of reports show a great improvement in this area [42-44]. Utilizing different processing technique and improving the geometry have increased the burn rate significantly [46-

2

49]. The challenge has been to theoretically explain the actual physical results of these experiments and improvements. Theoretical analysis and modeling of the physical results show a good reason for utilization of nEM as an alternative energetic material for the explosive and propellant systems [44]. These improvements have given hope and motivation to continue the intensity of the exploration in order to create a unified, consistent and predictable process.

A number of materials were used to produce nEM in multilayer thin film [18]. Study shows that aluminum and copper oxide are consistent in stochiometric ratio in macro and nanoscale reaction. Aluminum and copper oxide in nanoscale have similar stochiometric ratio in nanoscale as well as macroscale reaction which makes it easier to study the reaction in nanoscale with known composition for a complete reaction. In this study aluminum and copper oxide were used as main components for numerical model and experimental exercises.

Main Objective

The main objective of this study is to describe the physical process of self-propagating reactions in multilayer thin films by specifying the process as a combustion phenomenon. A physical understanding of this process is the key point in defining some of the unknown variables that influence the reaction. The speed of flame front and the maximum flame temperature are two key factors in the reaction. Establishing the proper way to measure the speed of flame front was the first target of this study. Heat loss and the geometry (layered structure) of the thin film directly impact the temperature and speed of the flame. Controlling the heat loss was the second target of this study. Measuring the speed of flame front and controlling the heat loss helps to calculate the maximum flame temperature for different flame front speeds. A physical mechanism to accommodate for heat loss, speed of flame front, and maximum flame

3

temperature was the third target for this study. Additional variables such as length of flame, porosity of the products are required in solving a numerical model. Estimate of required characteristics of the flame front relative to the speed of flame front was the last target for this study. The following section is a summary of the overall progress to achieve these objectives.

Problem Statement

The reaction model of a multilayer nEM in a dense film of aluminum and copper oxide deposited over acomposite substrate of silicon\silica is proposed and solved in different stages. Three major steps are needed to fully engage all the involved variables in one numerical model.

1. In first section of this study, speed of flame front, one of distinctive characters of thin film reaction, is clearly specified and proper measurement techniques (time-of-flight technique) were proposed in order to measure the speed of flame front. Long strips of multilayer of aluminum and copper oxide in thicknesses of 26 nm and 54 nm, respectively, have been prepared by magnetron sputter deposition (Fig. 1.1). Forty units of these strips forming a total thickness of 3.2 μm were used as the standard multilayer thin film. Simple and composite substrates were used to control the reaction heat loss through the substrate. A number of experiments show that heat loss can control the speed of flame front and even quench the flame.
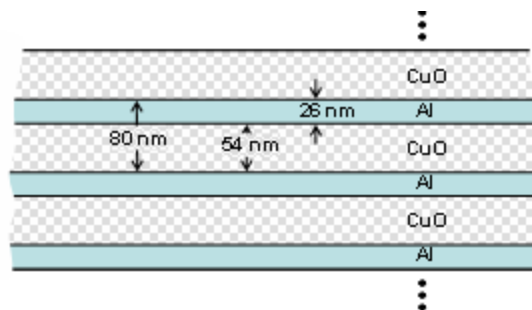
Fig. 1-1 CuO/Al MIC Layers

4

2. A numerical approach was used to explain some of the experimental results in the first section based on moving heat flux over composite substrate. This model estimates the theoretical maximum temperature of the reaction for the measured speeds in section 1. Maximum combustion temperature was calculated with limited heat loss of the thin film; hence maximum combustion temperature should be modified if reactions have significant heat loss through the environment. Due to the additional heat loss through the substrate, using the sandwich model alone to estimate the flame temperature reaction of aluminum and copper oxide over the substrate is not sufficient. Using the black box theory, a moving heat source model would be an appropriate alternative to represent the heat transfer simulation. The black box model alone would not successfully represent the actual diffusion process within the reaction zone. Hence, it is vital to integrate the two theories supplemented by experimental results to successfully relate the speed of flame front and the heat loss to the maximum flame temperature.

3. A two-dimensional numerical model for full reaction of multilayer thin film over composite substrate is proposed. The calculated maximum flame temperature was used to estimate the following characteristics of the flame for different speeds of flame front

   a. **Length of flame** represents the certain amount of multilayer thin film which is participating in the reaction at any instant.

   b. **Reaction Heat loss** is controlled by the thickness of the silica within the composite substrate. As the thickness of the silica increases, more heat flow is

blocked by the silica which causes the maximum flame temperature to rise. Excessive heat loss throughout the substrate can be adjusted by changing the thickness of the silica.

c. **Density of the product** behind the flame is reduced during the reaction. The porosity of the product can be adjusted by the properties of the materials, and it impacts the heat loss and the flame temperature.

Thickness of the substrate, length of flame front, and density of product were utilized for the standard multilayer thin film with 43 m/s flame front speed. The calculated heat penetration depth in this case was compared to the experimental result for the same flame front speed. A numerical model also was used to estimate three major variables for speed of flame front in a range of 30-60 m/s. In fact, the maximum combustion flame temperature that corresponds to speed along with the length of the flame, density of the product behind the flame, and maximum penetration depth in steady reaction were calculated when the total thickness of the thin film is 3200nm.

Literature Review

Combination reactions between chalcogen elements and metals are the most widely studied mechanically induced self-sustaining reactions. Takacs [49] summarized the result of a series of five papers by Chakurov and his colleagues in 1980s, which represents the first results on self-sustaining reactions. Following these early studies, the field of mechanochemistry has had a rich history, which has led to the use of ball mills for processing a wide range of materials, ranging

6

from minerals to advanced materials. Bakhshai et al. [50] used the ball milling method to demonstrate a self-propagated reaction of a mixture of Cu_2O, CuO, and Al powders. Combustible multilayer materials are introduced by depositing alternating layers of materials, which react exothermically during thermally induced intermixing. Several research teams have studied analytical and theoretical processes of various layers and have introduced the general thermodynamic and kinetics of a broad range of the thin film reactions.

The characterization of a self-propagating CuOx-Al in multilayer foil geometry was investigated. Armstrong's group [51-53] developed a model to find the heat rate of any possible multilayer reaction. This was later used by the Weihs' group. A one-dimensional model can be used to calculate the heat transfer of the reaction based on the rate of reaction.

The experimental results showed that the highly exothermic nature of the reaction is only a prerequisite for initiating combustion. Whether combustion takes place or not depends on the dynamic state of the reaction system. The influence of the crystalline structures of the reactants on the ignition of the combustion reactions instigated by high-energy ball milling is not always predictable. The calculation of the results of some reactions may be different due to internal and external variables yet unknown. The factors influencing the outcome of the reaction and the variables are being studied. In this section, aluminum and copper oxide in a multilayer thin film and bulk reactions are discussed in detail as the selected, physical and numerical model; and also, a number of other related investigations are highlighted and discussed briefly.

Ball Milling

Mechano-chemical process (MCP) uses mechanical energy to activate chemical reactions and structural changes. Mechanically activated processes date back to the early history of

7

humankind. The field of mechano-chemistry has had a rich history, particularly in Europe, which has led to the use of ball milling for processing a wide range of materials, ranging from minerals to advanced materials.

Self–propagating reaction was induced by ball milling in the mixture of Cu_2O and Al powder. Bakhshai et al. [50] presented the result of a self–propagating reaction between Cu_2O and Al. Zeck et al. [54] continued the same type of reaction process with other materials. They investigated the self-propagating reaction between CuO and Al and compared the two results. Bakhshai et al. [56] used the ball milling method to demonstrate a self-propagated reaction of a mixture of a Cu_2O and Al powders. Ball milling has been used to induce chemical reaction and alloying in variety of powder mixtures.

Zeck et al. [54] used the ball milling method to demonstrate a self-propagated reaction of the mixture of CuO and Al powders. Aself-propagating reaction of CuO and Al had been compared with Cu_2O and Al. All major components of their experiments were nearly similar.

Thin Film Reaction

The extreme minimization integrated circuits and digital devices have lead to an increase in the concern about the performance, reliability and precision of these devices such a small scale. Thin film material has increasingly played a main role in many of the new consumer electronic devices such as storage media, read and write heads, and flat panel displays. Such a remarkable array of applications has created a sense of excitement among the thin film scientists and engineers. Specifically, nano energetic materials (nEM) are potentially better alternatives than organic materials for explosive and propellant systems. Michaelsent et al. [56] investigated the thermodynamics and kinetics of thin film reactions by using differential scanning calorimetry of

8

several materials. The result of this research was published in 1997. Following that investigation Weihs' group [57] presented modeling and characterization of the propagation velocity of exothermic reaction in multilayer foils. They studied the CuO_x and Al reaction to identify the path and reaction kinetics. Experimental evidence showed that in the first reaction, CuO_x is reduced to the mixture of CuO and Cu_2O which coalesces with an interfacial layer of Al_2O_3. They discovered two different paths of reactions in their studies and the results are as follows.

1) The exothermic reduction-oxidation reaction of CuO_x and Al to form Cu and Al_2O_3 were studied in multilayer foil. Using DTA, XRD, Auger depth profiling, and TEM, the reaction path and kinetics of the two-step reaction were analyzed [34]. Weihs' group were able to identify likely rate determining processes for each of the two reaction steps Based on their experimental results. In the first exothermic reaction, the lateral growth of Al_2O_3 nuclei appears to control the rate of heat generation and, therefore, the reaction rate. This reaction slows as nuclei impinge and end when a continuous layer has formed. The activation energy for this step of the reaction was calculated to be 2.9 eV. Although CuO and Cu_2O are also reduced in this exothermic reaction, resulting in the formation of a copper layer, the heat generated is attributed to the formation of Al_2O_3 [34].

2) In the second stage of the CuO_x /Al reaction, diffusion of oxygen through the Al_2O_3 most likely controls the reaction rate in the first half of the exothermic reaction, and the heat generated is attributed to thickening of Al_2O_3 layers [57]. The rate of the reaction in the second half of the reaction, though, may also be limited by thickening of Cu product or non-uniform reduction in oxygen source, CuO_x.

9

Blobaum et al. [34] studied self-propagating formation reaction in multilayer foils and, they investigated one of the applications in joining and ignition. This work involves the multilayer foil reaction, which contains a reduction-oxidation thermite reaction between CuO_x and Al. Fischer and Grubelich [29] tabulated the experimental reference temperatures of the reaction of aluminum and copper oxide. He proposed the energy release of the reaction of aluminum and copper oxide to be 974.1 cal/g.

Combustion synthesis of energetic thin film in nano scale

Energetic reactions describe different regimes based on reaction rates which included detonations or combustion, and they could be in diffusions or premix mode. Reactants can react in different phases such as solid-solid, solid-liquid, liquid-gas, etc. Combustion can be instantaneous or self-sustain mode, and adiabatic, maximum, and combustion flame temperature can impact the reaction. Characteristics of the flame can be estimated based on the external impact of the flame using black box theory, or they can be solved by the fundamental equations of equilibrium for mass, species, and energy [58-60].

Feng et al. presented a model for exothermic reactions which demonstrated the application of simultaneous combustion synthesis for the dense ceramic and ceramic-metal interpenetrating phase composites. A number of important processes and parameters such as reaction stoichiometry, diluents, green density, pressure, and temperature are discussed [61]. Moore et al. also published a series of papers and experimental results for combustion (self-propagating high temperature) synthesis (SHS) [62-63]. They used the application of thermochemical functions to theoretically predict the maximum adiabatic temperature combined with knowledge of the

ignition temperature. The actual combustion temperature has been used to determine the heat loss from the SHS reaction and the amount of heat needed to ignite the reaction and maintain it in the self-sustained propagating mode.

Ignition

Energetic reactions include a number of phases based on the type of reaction, but they always start with an ignition phase which is transient and unstable. Reduction of ignition time delay is one of the major benefits of the nEM in thin film [64-65]. Zanotti et al. divided the reaction of the energetic material into two separate phases: initiation and self-propagation[67]. Self-propagation is the major focus of this study. The relative amount of energy of the ignition compared to the overall reaction is negligible and all numerical and experimental studies have been focused on the self- propagation period. Feng [61] compared the various mathematical models that have been developed to simulate and predict the ignition temperature in the dense ceramic and ceramic-metal films.

Tunable environment

A controlled environment helps to compare and contrast a number of reactions and investigate the impact of any variables related to the process. Alexander et al. used different types of thin film geometry to create a controllable environment to measure the characteristics of the flame in microscale [67]. Controlling some of the characteristics of the flame such as heat loss is necessary to maintain the speed and length of the flame. Rossi et al. used different types of thin film geometry to create a controllable environment [68]. This environment is used in many micro and nano thin film materials in mechanical and electric devices. Shantanu used deposited material in patterns and over a controlled environment to estimate the burn rate of

11

energetic material [69]. The time-varying-resistance method was introduced to investigate the ignition of nano particles.

<u>Submicron heat transport model</u>

Using macroscale heat transfer theory in a nanostructure can create a significant error in the calculation of the heat transfer rate or temperature distribution. Nano structures must include a specific regime in which separate nanoscale from macroscale heat transfer theory and the risk mitigation can be estimated using the macroscale heat transfer as an alternative. Ziman (1960), Devienne (1965), and Tien et al. (1969) presented fundamentals and application for conduction in microscale. These applications were presented for microscale thermal conduction with the use of developed regime maps that show the boundary between the macroscale and microscale heat transfer. The maps relate the geometric dimension separating the two regimes for conduction heat transfer. Yeh (1988), Cravalho et al. (1967), and Armaly and Tien (1970) similarly contributed in microscale radiation [70-84]. Flik et al. shared some of the experimental results for the heat transfer regimes of silicon, diamond, and some of the superconductors in thin film [85].

As more nanoscale devices enter the field of study, interfaces between materials become increasingly important on small length scales. Cahill et al. developed thermal transport in micro/nanoscale solid state devices and structures. Computations and the numerical solutions of the Boltzmann transport equation (BTE) were presented based on experimental and theoretical results [86-87]. Goodson et al. used the Boltzmann transport equation to show the influence of low-dimensional structures in thermal conductivity of the silicon over-layer [88]. This study

12

measures the thermal conductivity of silicon wafers between 0.4 and 1.6 μm at temperatures between 20 and 320 K.

Majumdar et al. used stochastic or Monte Carlo techniques for electron transport simulations as an alternative for BTE and established additional experimental methods for high spatial-resolution and high time-resolution thermometry. The application of this method and related methods for measurements of thermal transport was demonstrated in low-dimensional structures. Scanning thermal microscopy (SThM) achieves lateral resolutions of 50 nm and a measurement bandwidth of 100nm [89].

Chen et al. presented a number of experimental results in reduction of both the in-plane and cross-plane thermal conductivities of superlattices. They also investigates the applicability of the Fourier law in nanoscale heat transfer and the impact of that in nanotechnology [90-92]. Mahan et al. showed that heat flow is severely decreased in transient phenomena, due to nonlocal effects. In fact the temperature profile evolves in all cases significantly slower than the local theories predict [93-94].

Numerical models for a moving heat source

Carslaw and Juger [95] introduced the moving heat source model. Rosenthal [96] solved the model (Rosenthal's theory) using the semi-infinite body subjected to an instant point heat source, line heat source, or surface heat source. These solutions can be used to predict the temperature profiles at a distance far from the heat source, but they are unable to predict the temperature in the interface of the heat source. Eagar and Tsai [97] modified Rosenthal's theory to include a two-dimensional (2-D) surface. Gaussian heat source distributed the hat source with a constant distribution parameter and found an analytical solution for the temperature of a semi-infinite

13

body subjected to this moving heat source. Jeong and Cho [98] used the conformal mapping technique, and they successfully transformed the solution of the temperature field in the plate with finite thickness for a welded joint [99-101]. Using the Gaussian heat sources could predict the temperature at regions close to the heat source but the solution is still limited by the effect of penetration. Goldak, *et al.* (Ref. 4 of the number 8), introduced the three-dimensional (3-D) double ellipsoidal moving heat source using finite element modeling (FEM). The purposed model could resolve the shortcoming of the previous 2-D Gaussian model to predict the temperature at welded joints with deeper penetration. [100] Nguyen et al. solved the proposed double ellipsoidal model and found a proper match between the numerical and experimental results.

Summary of Literature Search

In this section, a review of previous studies in all related areas to this research was presented in the same order as the manuscript. The`` reaction of aluminum and copper oxide in bulk and thin film geometry has been studied and most of its critical points are highlighted. Ball milling, one of the traditional activation techniques, was discussed for the bulk reaction of aluminum and copper oxide. There is evidence from the literature that thin films are a better and more effective option to increase the rate of reaction.

Studies of combustion phenomena in thin film advance material were presented as an effort to find the common point between the previous experiments and the energetic reaction of aluminum and copper oxide in thin film. This review also summarized some of the experimental and numerical investigations regarding igniting and controlling the reaction of self-propagating high temperature synthesis in thin film configuration. A nanoscale heat transfer study was

14

presented in the forth portion of this review in order to demonstrate some required correction in properties and geometries of the model in order to treat the nanoscale solution in a macroscale regime. In the final portion, the historical background of moving heat source models was described as a simple theory to finalize the applicable models.

CHAPTER 2
SPEED OF FLAME FRONT AND IMPACT OF REACTION HEAT LOSS

Introduction

The thermo-physical analysis of the reaction of Nano energetic material nEM in multilayer dense film is one of the emerging fields in nanotechnology. Although traditional energetic compounds based on organic materials have similar energy per unit weight, nEM materials offer much higher energy density and capacity of the burn rate in comparison to the organic materials. This field of study shows great promise and potential for nEM in multilayer dense film as an alternative substance for explosive and propellant systems. Energy density and burn rate are the two of the many mechanical criteria for evaluation and comparisons of energetic materials.

Although many earlier studies have shown the burn rate of nEM in multilayer dense film to be much lower than organic materials, a number of recent studies utilizing different technical processes and geometry of materials have improved the burn rate significantly [34, 43-48]. These improvements provide motivation to study nEM and flame in the presence of substrates. The challenge has been to explain the actual physical results of the experiments and improvements. Therefore, nEM in multilayer dense film material is a good alternative energetic material for the explosive and propellant systems.

Upper limits for the burn rate of nEM in multilayer dense film materials have not been yet determined. There are a number of reports for the propagation speed of dense nEM in multilayer dense film materials and many of them show rates no higher than 20 m/s [42, 43]. In contrast, this study will show a burn rate (or flame speed) in excess of 60 m/s experimentally for multilayer thin film of aluminum and copper oxide. Higher burn rates may be achieved

16

depending on the substrates used. Physical mechanisms can explain the speed of propagation and rate of reaction and help define some of the limitations and boundaries of the combustion process. It can also show better ways to process the samples in thin film scale.

In the literature, the analysis of thermal transport in thin multilayer film can be broadly divided into experimental and computational studies. Initial numerical analysis was based on one-dimensional model (sandwich theory) [51]. Subsequent work by Weihs et al defined the reaction in multilayer thin film of energetic material based on the theory of atomic diffusion and thermal transport [43, 46, and 57]. They used the two-dimensional sandwich theory to predict the speed of reaction. In reality, the flame dynamics is a strong function of many extraneous variables like the geometry and properties of the substrate on which the nanolayers are deposited. This is because the substrate acts as heat sink and can control the extent of self-sustainability of the thin film reaction. It is clear from the literature that the current models are insufficient to predict the overall thermal transport of multilayered thin films deposited on different substrates while black box type models require chemical kinetics models to successfully represent the flame heat release rate [58, 59].

Experimental analysis of the flame is crucial for the validation of the computational models. It is expected that the speed of propagation of the reaction is a complex function of properties and thickness of the substrate even for a standard geometry and controlled environment. The data available in the literature use free standing layers. The literature does not provide any detailed insight in very thin nEM in multilayer dense film materials or relate the flame speed with the properties and geometry of the substrate. The flame speed can range from 1 m/sec to 100 m/s depending on substrate properties. Thus, the objective of this study is to measure the flame speed

17

for different substrate configurations and determine the limiting quenching conditions. These quenching conditions can also be incorporated in numerical models. The purpose of the experiments is also to obtain a greater physical understanding of the reaction process that may allow an increase in the flame speed of thin nEM. A detailed analysis of the chemical kinetics is beyond the scope of this study.
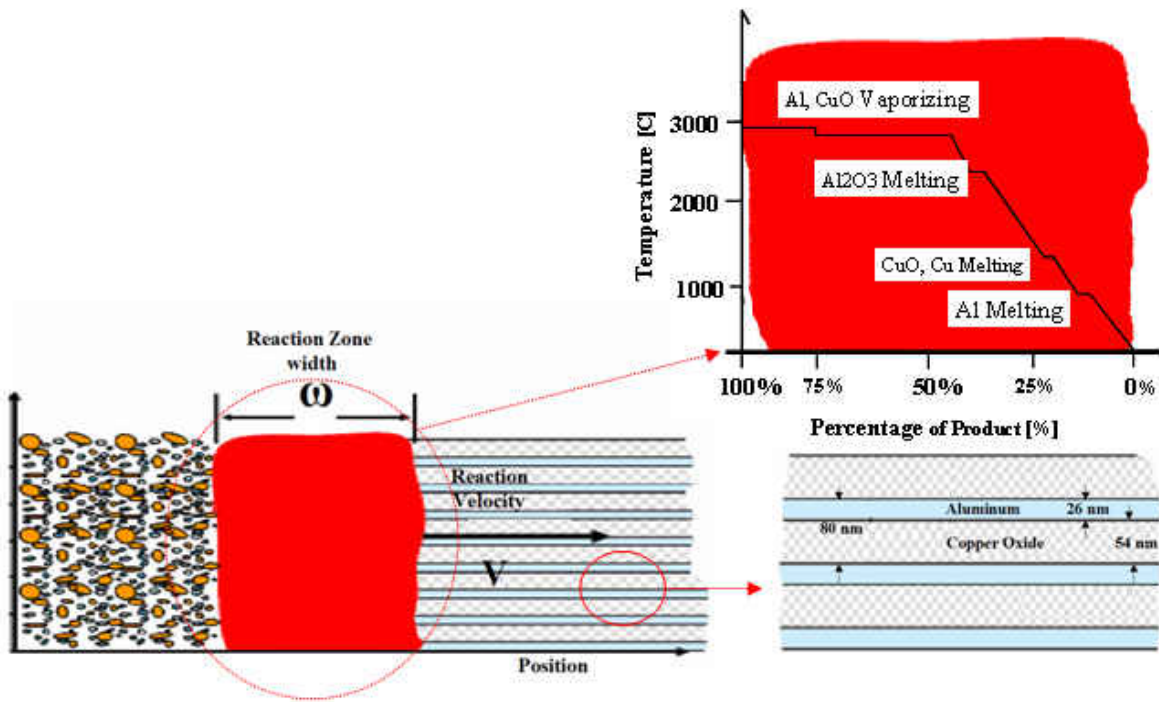
Fig. 2-1. Detailed schematic of the layered nEM in thin film reaction

Experimental procedure

To support the experimental effort, samples of Al/CuO have been prepared as multilayer thin films by vacuum deposition and deposited on the substrate. Layered Al/CuO in multilayer dense film having a total thickness of 3.2 µm was prepared by magnetron sputter deposition. An Al layer thickness of 26 nm and CuO layer thickness of 54 nm were used to provide a bi-layer of 80 nm for a standard sample configuration, as illustrated in Fig. 1.The thin film was subsequently deposited on substrates of various thickness and thermal conductivities as shown schematically in Fig. 2. Glass was one example of a single substrate investigated while silica on silicon and photoresist on silicon were the types of double substrates analyzed in this work.
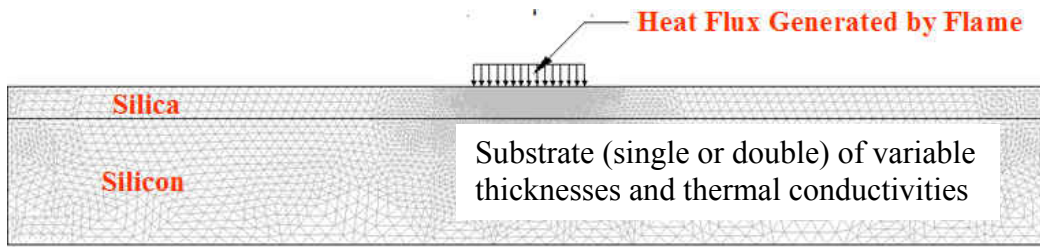
Fig. 2-2.Geometry and properties of the substrate on which the thin film is deposited

Measurement techniques for flame speed

High-speed photography is a popular but expensive technique for measurement of high flame speeds such as a million frames per second. The accuracy of this technique is decreased significantly in high-speed propagation reactions as in aluminum and copper oxide. For improved and accurate measurement of flame speed an electronic time-of-flight technique has been developed using patterned strips of layered nEM thin films on a substrate. Copper contacts were placed along the length of the strip in the passage of the flame front as shown in Fig. 3.

The flame is initiated via an electric spark at the end of the thin film strip and propagates down the length of the film. As the flame passes between each pair of copper contact strips (Fig. 3), the electrical conductivity between the pair is interrupted. This is because the reactants are electrically conducting due to the presence of the continuous Al layers, but the products (copper) are insulators as they do not form a continuous layer but solidify as isolated clusters on the substrate surface. The change in film electrical conductance can be sensed as a function of time to determine the velocity of flame propagation. This configuration produced a stepwise change in voltage, which is digitally acquired and analyzed to measure the propagation velocity. Each pair of copper probes is connected to resistances in a parallel circuit, as shown in Fig. 3. The voltage output undergoes a sharp drop in magnitude at the instant the flame passes across copper probes. This stepwise change in voltage decay is shown in Fig. 4. The data was captured using a data acquisition system with 1 MHz sampling rate.

The speed of flame along the propagation path can be considered as constant. In the time of flight technique, current through the secondary circuit is interrupted by the flame, causing voltage drop in several steps. If the speed of flame is constant, the time interval among successive voltage drops is expected to be the same due to the homogenous composition of the thin film and equidistant spacing of the copper contacts. All the experiments conducted support this hypothesis. Fig. 5 is a typical recorded data of voltage difference. Fig. 5 shows that as the flame passes through the thin film with four pairs of copper contacts the voltage dropped in four steps. Initial voltage interruption was recorded at sample 9885 and the last interruption at sample 10495. Comparison showed that each voltage interruption occurred after almost similar number of samples (between 150 to 159 samples). The actual time between each voltage drop is about

20

189 to 198 μs for 800 KHz sampling rate. This confirms the constant flame speed hypothesis. This experiment was repeated for four to six copper contacts to increase the time resolution and similar results were obtained. The time-of–flight technique provides an uncertainty of 50 μs for a speed of propagation of 50 m/s with an uncertainty of ± 1 m/s. The methodology for calculating the velocity is shown in Fig. 5. By comparing the voltage gradient at the lead and lag part of the drop (leading and trailing edge of the flame), the velocities were computed. This dual computation shows that there is adequate confidence in the velocity measurement.

Effect of Single and Double Substrate

Several types of substrates for nEM thin films were examined. In all cases, the total thickness of the thin film was held constant at 3.2 μm, composed of a thin film of 80 nm bi-layers. The physical domain shown in Fig. 2 is divided into three distinct segments namely 1) the moving heat source with a uniform heat generation rate, 2) the single or double substrate of varying thickness and thermal conductivities which serve as the heat sink. Combustion within the flame zone generates a fixed amount of heat which depends on the stoichiometry of the reaction. This generated heat is partially dissipated by the substrate depending on the thickness and thermal conductivity resulting in drastic reduction of flame speed and even quenching. The heat dissiptation rate can be controlled by utilizing different heat sinks for the flame. A material with high conductivity can possibly quench the reaction completely. By depositing a thin layer of material with low conductivity such as silica, part of the generated heat can be absorbed by the substrate. Thickness of deposition also affects the flame speed.

21

(a)

(b)

R	5000Ω
R1	4300Ω
R2	6100Ω
R3	5000Ω
R4	3000Ω
R5	2000Ω
R6	1000Ω

(c)
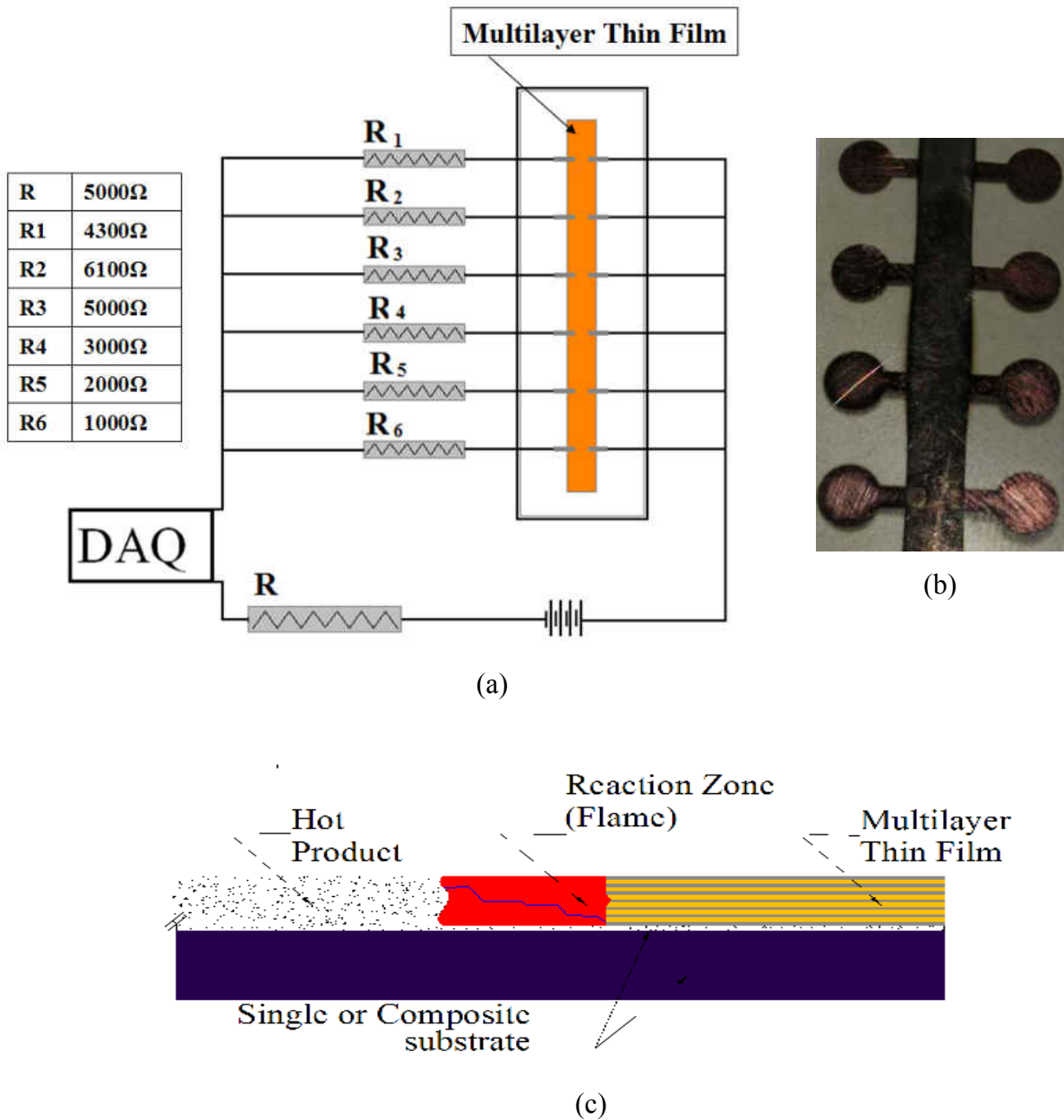
Fig. 2-3. Experimental configuration for Electronic Time of Flight technique for measurement of flame speed in MIC: a) Schematic; b) photograph of a section of the MIC material with the resistance arms c) Graphical description of thin film and substrate
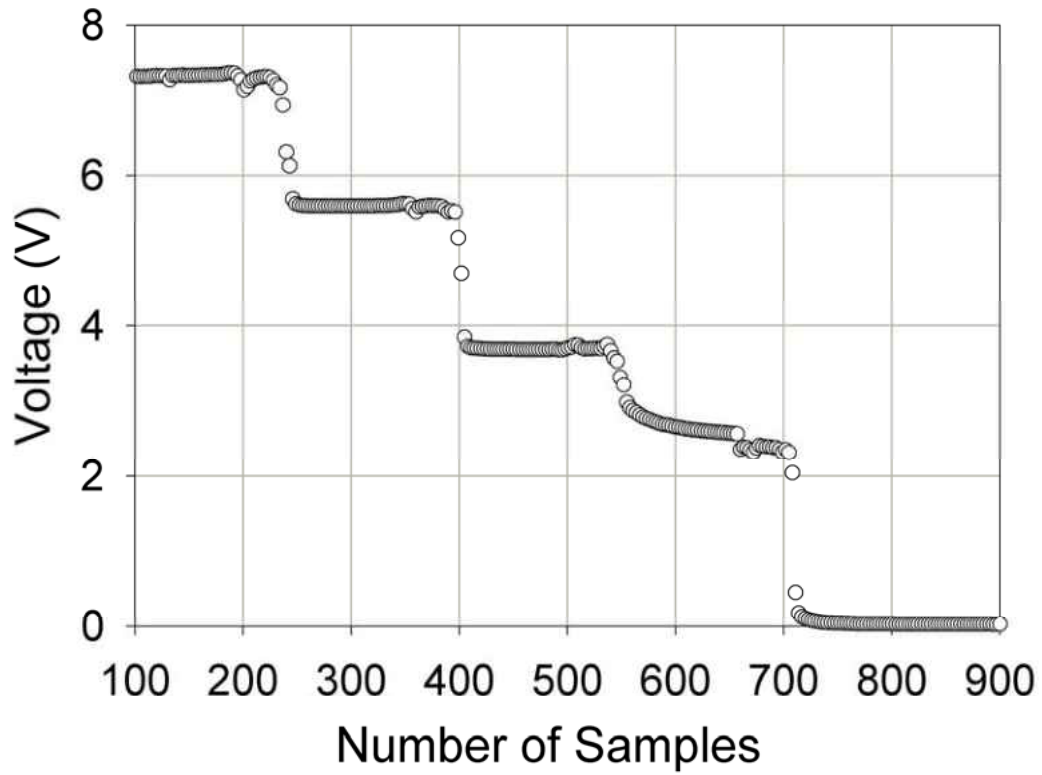
Fig. 2-4. Example of Electronic Time of Flight measurement of flame speed for layered Al/CuO MIC deposited on a substrate
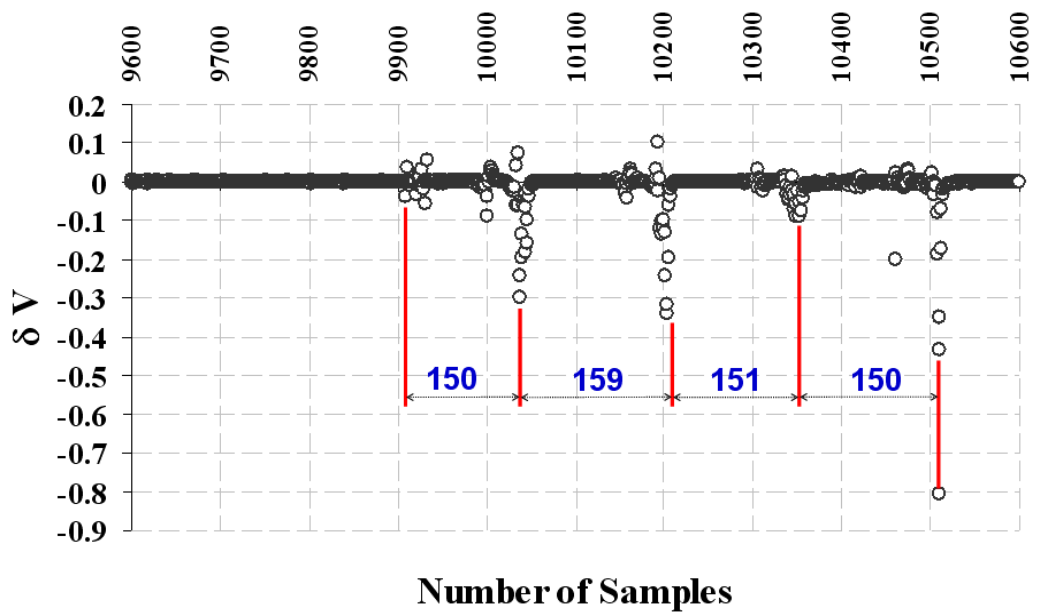
Fig. 2-5. Voltage difference using data in Fig. 4 for layered Al/CuO nano thin film deposited on a substrate

23
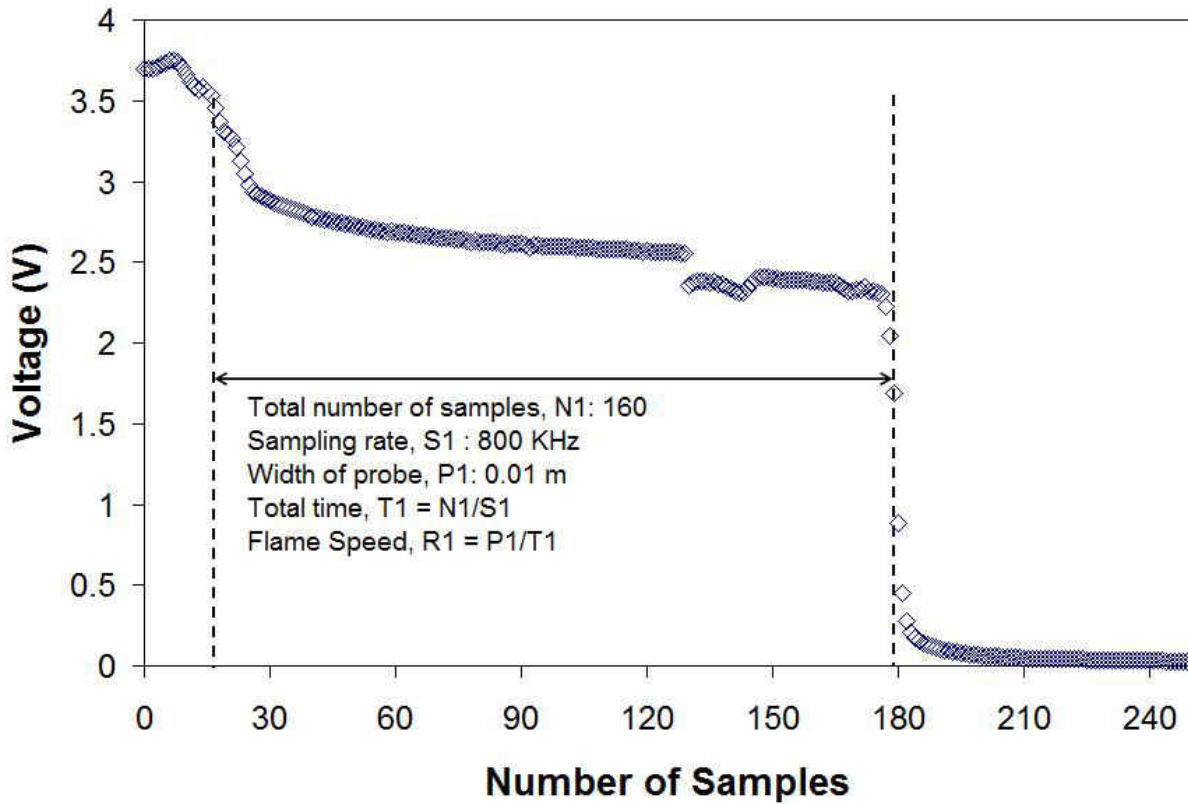
Fig. 2-6. Actual Voltage drop for reaction of Al/CuO nano thin film deposited on a substrate

Single substrate is made of only one individual material such as glass or deposited material on silicon. Deposited material is relatively thick so it can be considered as a single substrate. Single substrate samples were prepared on glass (Table 1) and photoresist on silicon. For the typical structure having an 80 nm bi-layers and total thickness of 3.2 μm, flame speeds in the range of 44-51 m/sec were observed (Fig. 6)for glass substrate having thickness of 1000 microns. Glass exhibits a high thermal conductivity of 1.1 W/m-K which is favorable for high heat dissipation responsible for reduction of flame speed. However 1000 micron thick substrate creates a thermal isolation layer resulting in negligible heat loss thereby sustaining the flame at reasonable speeds. For photoresist on silicon, flame speeds were measured for substrate thickness of 1.1 and 10 microns respectively. It is observed that for 1.1 micron substrate

24

thickness, the flame speed varies from 52-55 m/sec as shown in Fig. 6. For 10 micron substrate thickness the flame speed increases to 62 m/sec. When compared with glass, photoresist exhibits higher flame speed for a lower substrate thickness. This can be explained by the fact that photoresist has a thermal conductivity of 0.2 W/m-K which is five times lower than glass. As a result, photoresist cannot dissipate the heat generated by the flame effectively even for 1.1 micron substrate thickness. Increasing the thickness to 10 microns increases the thermal isolation effect, thereby increasing the flame speed to over 60 m/sec.

Table 2-1. Speed of Flame on Single and Composite Substrates

Substrate	Thermal conductivity (W/m.k)[104]	Thickness (μm)	Sample rate (kHz)	Speed of reaction (m/s)	Average Speed (m/s)
glass	1.1	1000	800, 1000	45.61, 44.78, 51, 44.76, 47.17	46.75
photo resist/Si	0.19-0.31	1.1	800	52.94, 54.97	53.96
photo resist/Si	0.19-0.31	10	800, 1000	61.05, 61.86,	61.45
SiO2/Si	1.03	0.03	1000	Quenched	Quenched
SiO2/Si	1.03	0.1	1000	Quenched	Quenched
SiO2/Si	1.03	0.2	1000	2	2
SiO2/Si	1.03	0.5	1000	41.66, 43.52, 42.97	42.72
SiO2/Si	1.03	2	1000	43.1,42.73, 41.78	42.54

Similar velocities to a single substrate were observed for thin films on Si substrates having a thick intervening layer of SiO$_2$ to provide thermal isolation. Silica has thermal conductivity of 1.06 W/m-K which is much lower than thermo conductivity of silicon (148 W/m-K). In thin films deposited directly on a Si substrate without a thermal isolation layer, no self-propagating reaction was observed, i.e., the reaction was effectively quenched. Fig. 6 shows the average speed and quenching of flames depending on the thickness of SiO$_2$ substrate. Thermal penetration depth, δ, of the moving reaction front into the thermally grown SiO$_2$ surface layer is measured by varying the thickness, D_{SiO2}, of the layer. Fig. 6 shows that the reaction is completely quenched for SiO$_2$ layer of less than or equal to 0.2 μm. The speed of the flame propagation seems to be more or less a constant at 40 m/s for SiO$_2$ layers of 1 μm and 2 μm. For the case of $D_{SiO2} >$ δ, the thermal penetration depth, the reaction velocity is expected to be similar to that of the bulk glass substrate as both have thermal conductivities values of around 1 W/m-K. For $D_{SiO2} <$ δ, a reduced flame speed is expected due to the increased loss of the heat of the reaction into the higher thermal conductivity silicon. The sudden decrease in velocity for $D_{SiO2} <$ 500 nm indicates this to be an upper bound for the thermal penetration depth, δ. If this distance and the thermal diffusivity of SiO$_2$ are used, δ, in the simple approximation, $\delta = \sqrt{4\alpha t}$, an estimate of the time, t, may be obtained that the composite substrate is exposed to the moving reaction front as $t = 69$ ns.
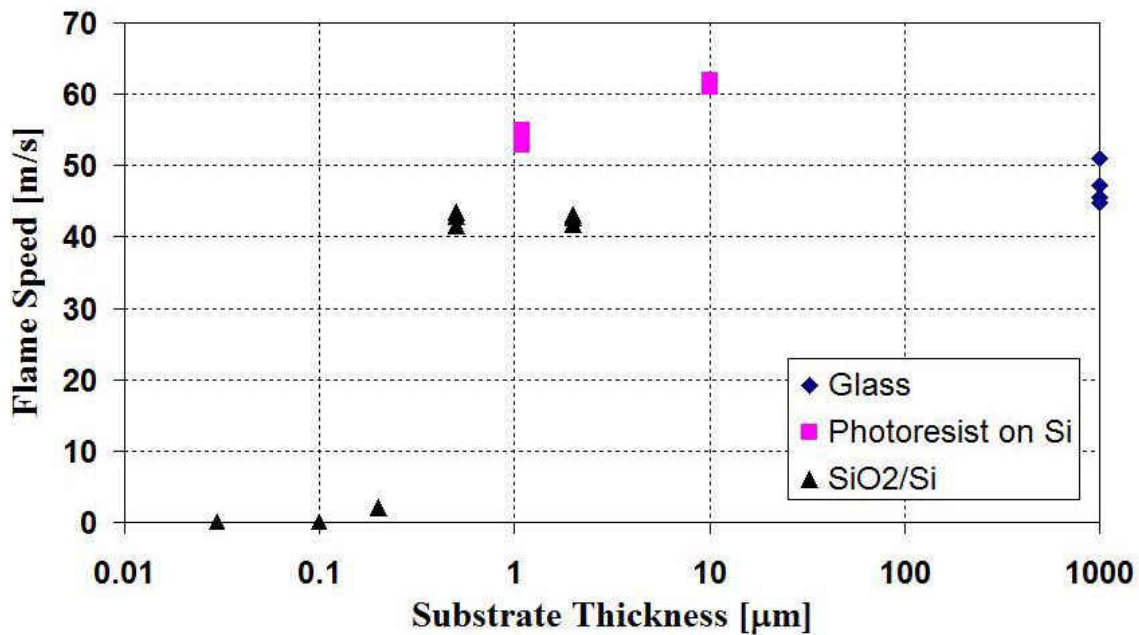
Fig. 2-7. nEM flame speed as function of thermal isolation thickness of substrate

Summary

This work deals with the reaction of nano energetic material in multilayer dense film. Energy density of nEM is much higher than that of conventional films. The problem of thermal transport of a multilayer thin film of Aluminum and Copper oxide has been analyzed for varying substrate material and thicknesses. The flame speed was experimentally determined using a time of–flight technique. Results show that the reaction is completely quenched and is not self-sustaining for the silica layer of less than 200 nm. It is also observed that with increase in substrate thickness the quenching effect is progressively diminished. The speed of reaction seems to be constant at slightly over 40 m/s for silica layers over 1 μm. For substrate thickness greater than 500 nm, flame speeds as low as 2-5 m/sec could be achieved. Heat dissipates less in photoresist than silica, so the flame speed in MIC with a photoresist substrate is much higher than silica, and can reach up to 60 m/s.

27

CHAPTER 3
MODELING OF A REACTING NANOFILM ON A COMPOSITE SUBSTRATE

Introduction

The energy density of a multilayer nanocomposite material is much higher than that of conventional organic energetic material. Nanoscaling can improve the reactivity but not necessarily the heat release rate. Usually, the energy density and the flame speed are the key variables that characterize the energetic material. Aluminum and copper oxide are used as nano-bi-layers that have increased the flame speed up to 60 m/s in several studies including a recent experimental study by the authors [34, 43-48, 103]. The foil geometry and deposition process affect the flame speed.

Although it is possible to estimate the adiabatic temperature and speed of flame [104], upper limits for the flame speed of multilayer dense nanofilms have not been yet determined experimentally. Earlier papers [42-43] showed that the flame speed of these films was no greater than 20 m/s [42-43]. In our recent study [103], the flame speed was experimentally determined using a time of–flight technique for various single and composite substrate configurations. The flame speed was found to be dependent on the substrate properties. These results show that the reaction can be completely quenched and is not self-sustaining for a silica layer of less than 200 nm. It is also observed that with increase in substrate thickness the quenching effect is progressively diminished. The speed of reaction seems to be constant at slightly over 40 m/s for silica layers over 1 μm. For substrate thickness greater than 500 nm, flame speeds as low as 2-5 m/sec could be achieved. It is also shown that heat dissipates less in photoresist than silica, so the flame speed in multilayer nanofilm with a photoresist substrate is much higher than silica, and

can reach up to 60 m/s. Length of the flame is also an important variable which relates the speed of flame and heat dissipation. Due to limited speed of flame in this study variation of length of flame is negligible so length of the flame considered being constant.

Among the analytical and numerical studies, one of the earlier models used was the sandwich theory [105]. Subsequent work by Weihs et al [56, 57] defined the reaction in multilayer thin film of energetic material based on the theory of atomic diffusion and thermal transport. They used the two-dimensional sandwich theory to predict the speed of reaction. This theory does not account for rapid reactions wherein the reactants and products may melt or vaporize prior to completion of the reaction. In reality, the flame dynamics depends on the substrate material and its thickness and other variables such as the stoichiometry, length and thickness of the nanofilms. The substrate acts as a heat sink and can control the extent of self-sustainability of the thin film reaction. The sandwich model used in the previous studies did not consider the effect of substrate on the flame and hence failed to explain the overall thermo-physical phenomena.

A second class of computational models uses a black box theory to analyze thin film materials [58, 59]. Unlike the sandwich theory, it simplifies the complex reaction processes in the thin film by introducing a control volume that moves with the flame front and encloses the region of the reaction front. The reactions within the black box are considered to occur in a stable steady state. The concept of the black box volume allows one to isolate the effects of the interaction of the control volume and the surroundings within the defined frame. The control volume moves with the flame speed along the reaction path and this flame speed is assumed to be constant. The black box model essentially takes into account the effect of the substrate on the flame and hence is more dynamic than the sandwich model. However, this method would require

a priori global analysis of the characteristic of the flame reaction to estimate the heat released by the control volume.
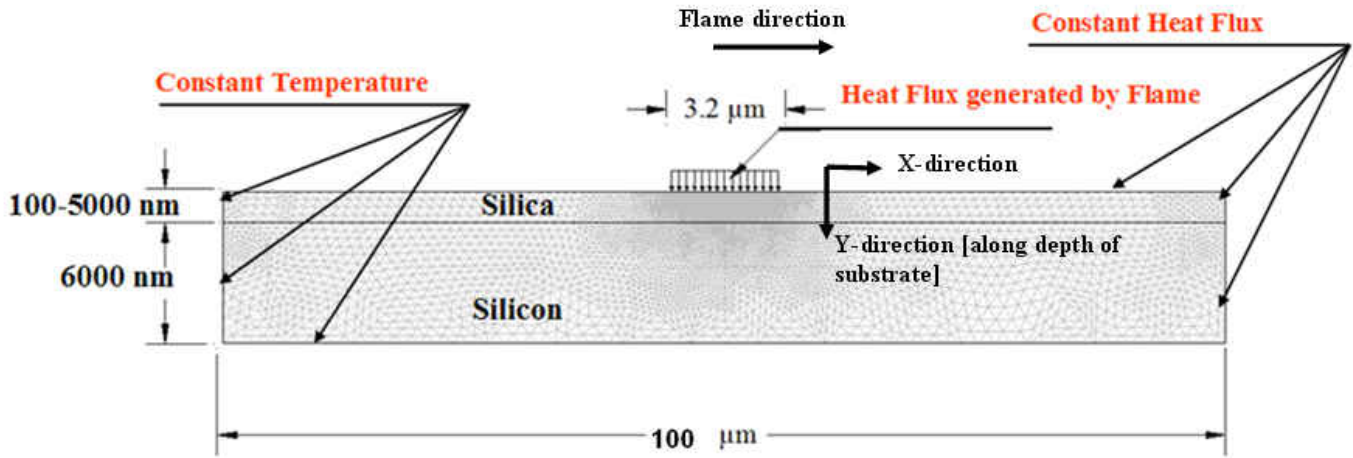
Fig. 3-1.Two-Dimensional computational domain with the flame propagating in the x-direction

It is clear from the literature that the sandwich model alone is insufficient to predict the overall thermal transport of multilayered thin films deposited on different substrates. On the other hand, the black box models alone would not successfully represent the flame heat release rate without considering the actual reaction in the flame front. Hence, it is important to integrate the two models supplemented by experimental results [103] to successfully analyze the heat transfer characteristics in the substrate of an energetic nanofilm. Thus, the objective of this paper is to determine the sustainability of the dense nanofilm reaction for different flame speeds (close to quenching points) and composite substrate thicknesses to aid in the physical understanding of limiting quenching conditions in nanofilms.

In the model considered in Fig. 1, the estimated width, ω, of 3.2 μm based on penetration depth of the flame front (described later) is taken on a substrate width of 100 μm. The heat source is a line source, and since all the heat goes into the substrate without any loss, the heat

30

flux needs to be carefully estimated as outlined in the following paragraph. The rest of the top surface of silica is insulated. The silica layer is a variable and the silicon layer below is taken as a constant at 6 μm. Constant temperature boundary condition is used on the left side of the domain and at bottom of the silicon layer

$$v_x^2 = \left(\sum_{n=odd} k_n \Big/ \alpha_n^3 \right)^{-1} \frac{\lambda^2 R T_f^2 A \delta}{E(T_f - T_0)} e^{\left(\frac{-E}{RT}\right)}$$
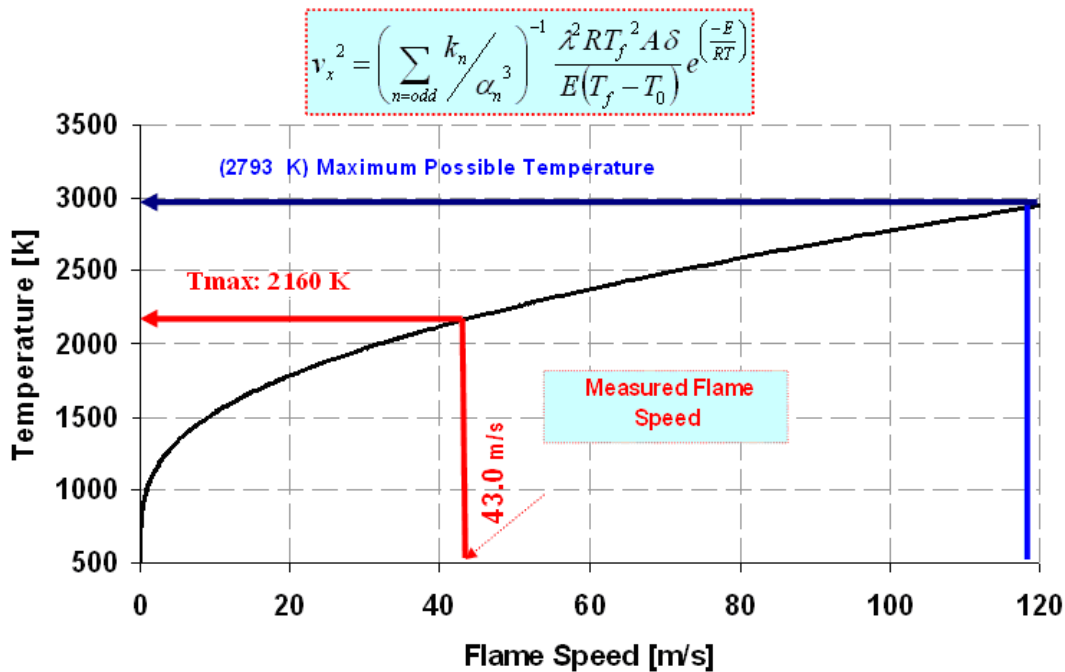
Fig. 3-2. Variation of maximum temperature with flame speed using sandwich theory.

Our numerical approach in this paper is to first use the sandwich theory (see section on Sandwich model) to predict the theoretical maximum temperature for flame speeds (from our recent experiments [105]) based on atomic diffusion and specific multilayer foils without the substrates. The total heat of reaction is subsequently computed from the chemical equilibrium calculations (see section on Stoichiometric calculations). This heat production can then be adjusted by comparing the maximum flame temperature in sandwich model with the black box (see section on black box model). Lastly, the correct heat flux is incorporated for a moving heat

31

source and the temperature profiles along the interface of the nanofilm and composite substrate can be predicted for a parametric variation of flame speeds and substrate thickness along with the determination of the corresponding limiting quenching conditions. The above events have been shown schematically in the flow chart given in Table 1.

Table 3-1. Flow chart of the numerical process
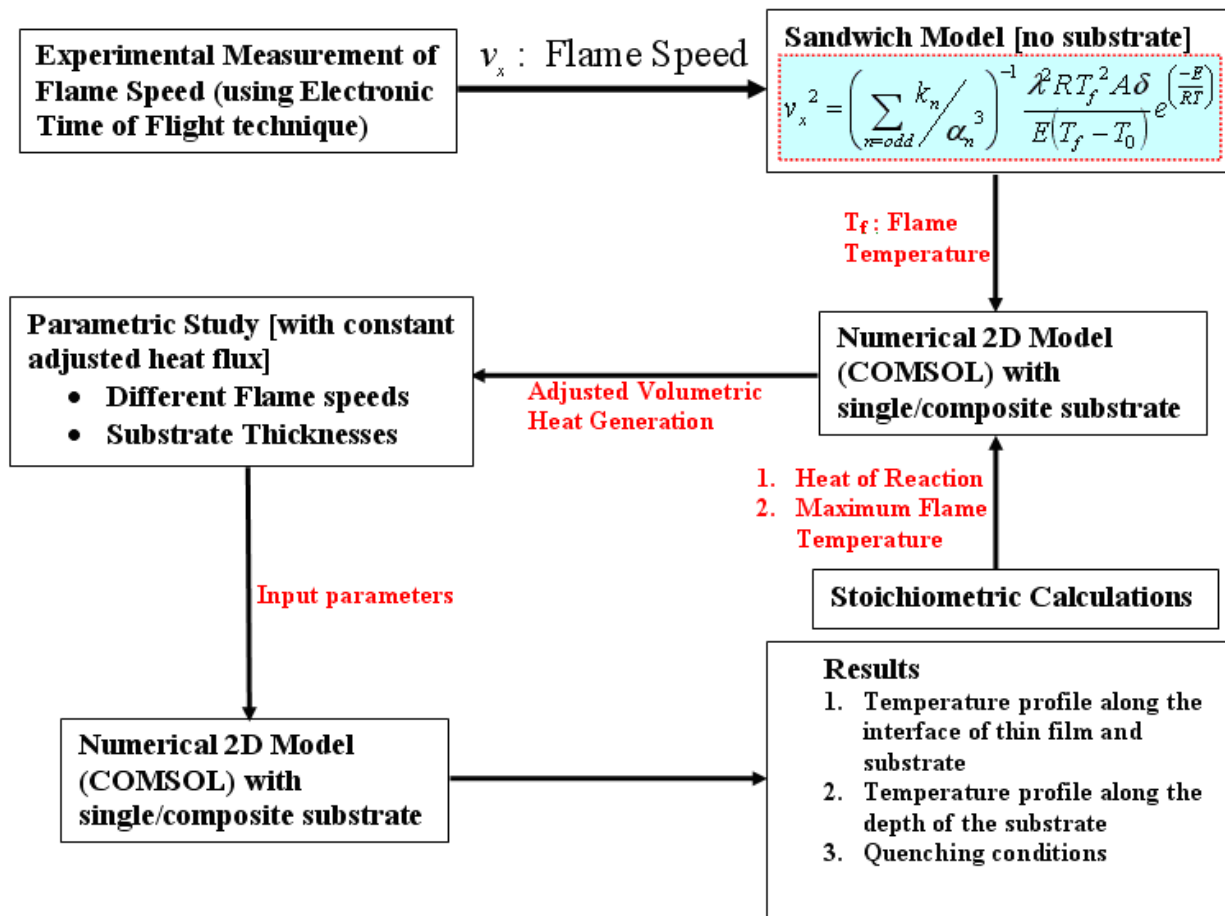
To support the modeling effort, samples of Al/CuO were prepared as multilayer thin film by vacuum deposition. The experimental effort was to study the kinetics of multilayer film reactions [106,107], using the flame speed as a measure of the reaction process. Layered Al/CuO having a total thickness of 3.2 μm was prepared by magnetron sputter deposition. An Al layer thickness

of 26 nm and CuO layer thickness of 54 nm were used to provide a single bi-layer of 80 nm for a standard sample configuration over different substrate, as illustrated in Fig. 3.

Sandwich Model

Mann et al. [57] developed a new model consisting of the so-called sandwich model of Armstrong and Koszykowski [105] by characterizing the rate of reaction for any multilayer pair of thin films. Based on the description of the bi-layer, the basic equation for atomic diffusion, and the general equation for thermal transport, and the speed of flame are calculated for multilayer using the Fourier series. This model is the classical approach to estimate the flame speed for a multilayer geometry in thin film. Additional details are available in appendix B of this document. Flame speed for multilayer thin film with linear interface can be calculated using the following equation.

$$
v_x{}^2 = \left(\sum_{n=odd} k_n \Big/ \alpha_n{}^3 \right)^{-1} \frac{\lambda^2 R T_f{}^2 A \delta}{E(T_f - T_0)} e^{\left(\frac{-E}{RT} \right)} \tag{1}
$$

Where δ is the thickness of each layer, E is the activation energy of the reaction [34], and T_0 and T_f are the initial and final temperature. The constants values were used to obtain the maximum temperature are available in Table 2. The relationship between flame speed, v_x, and maximum temperature is given in Fig. 2. The average flame speed measured for the silica-silicon substrate in our experimental work [103] is 43 m/s. Using this speed for the same substrate, the maximum temperature obtained from Fig. 2 is 2160 K. It is important to note that this reaction rate is based on the maximum energy released by the chemical reaction and does not consider any heat loss to the environment or substrate. Therefore, in order to obtain a realistic heat generated for the numerical model, we need to resort to the so-called black box model.

Table 3-2. Constants values were used to obtain the maximum temperature [34, 56, and103]

Variables	Values	Units
λ	7.42E-05	m^2/s
A	0.2	
T_0	300	K
E	9.80E+04	J/Mol

Black Box Model

The black box model [59] can be used to estimate the heat rate of reaction without considering the complexities of diffusion. In the actual flame condition, there would be heat loss not only to the substrate but also to the environment. But the idealized model given in Fig. 1 has all the heat dissipating to the substrate. Correct input of the heat generation, Q'_{gen} (Fig. 3), is hence required. The procedure for finding the corrected heat generation as explained briefly earlier is through finding the correct final temperature, and is given at the end of this section. Additional details are available in appendix C of this document.

Stoichiometric Calculations

Thin film reactions create an enormous amount of energy, which causes phase transformation throughout the reaction. The theoretical energy release of the reaction aluminum and copper oxide is 974.1 cal/g [29]. The reaction starts in the solid-solid phase, continues to liquid state, and ends up with a mixture of gas and liquid. The reaction of aluminum and copper oxide is

34

broken into 6 different stages, as given in Table 3 based on the melting and boiling point of each one of the reactants and products. Total amount of heat and the final temperature of a unit cell of aluminum and copper oxide[1] are calculated based on conservation of mass and energy. At any stage of the chemical reaction, total mass is constant, so the total loss of mass of reactants through the reaction is equal to the total amount of produced mass.

$$m = \sum m_{Al} + m_{cuo} = \sum m_{Al_2O_3} + \sum m_{Cu} \qquad (2)$$

The energy balance is given by

$$\sum E_{IN} + \sum E_{OUT} + \sum E_{GEN} = \sum E_{STOR} \qquad (3)$$

---
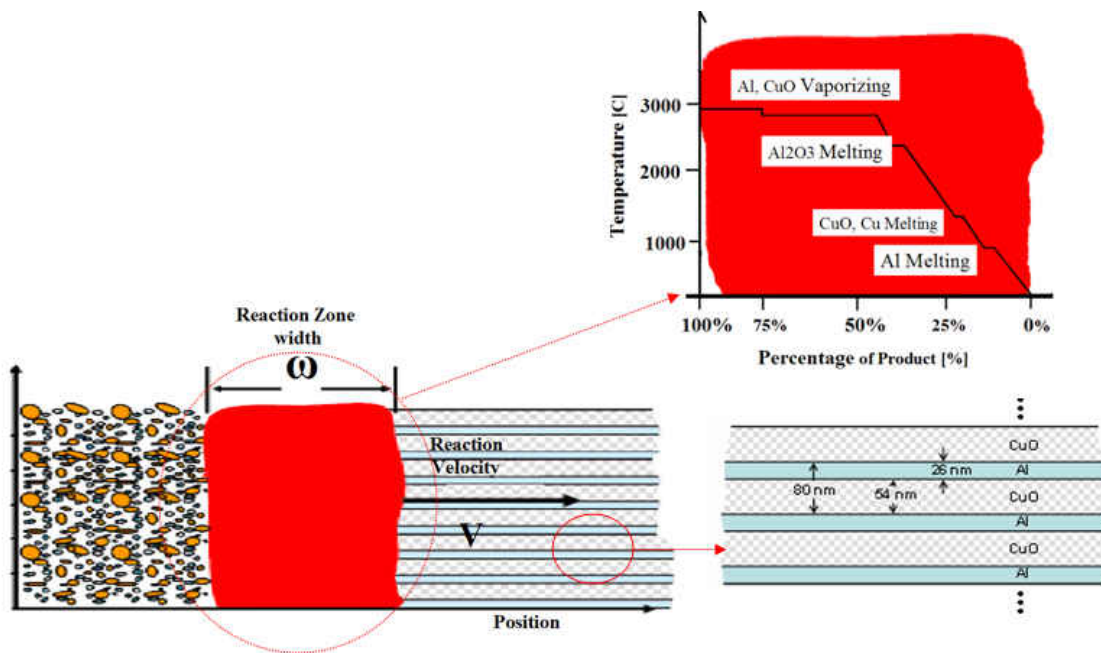
[1] CuO was used as a major reactant material. Due to the high temperature at reaction zone, majority of copper oxide, CuO_x dissociates to CuO [34, 103].
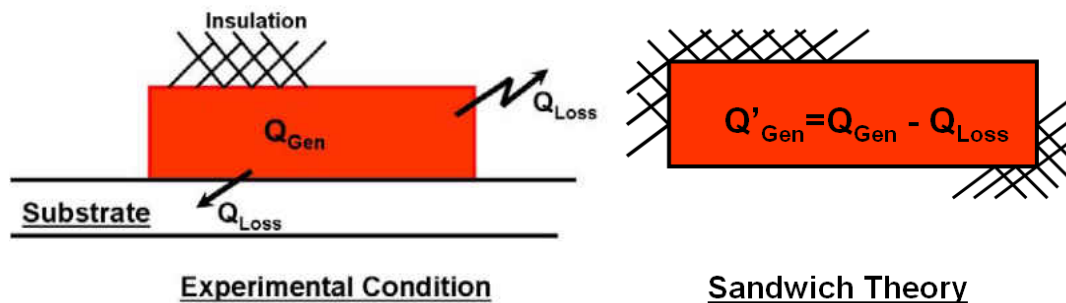
Fig. 3-3. Detailed schematic of the multilayer nano film

Fig. 4 shows the mass of reactants and products at each stage based on the simultaneous solution of equations (2) and (3). Feng [62] compared the various mathematical models that have been developed to simulate and predict instabilities in propagating combustion synthesis reactions. Mukasyan [108] had investigated high temperature combustion synthesis waves in the Ni and Al system. Reaction of aluminum and copper oxide in nanofilms exhibit similar mechanisms as in these studies. Temperature of the reaction in different phases ranges from 300K to 2793K. Before reaching 933 K, all materials are in solid phase and the reaction is limited to diffusion in solid-solid phase. Between 933 K and 1356 K, aluminum undergoes a phase change to liquid and the reaction is based on diffusion in solid–liquid phase. This is the temperature range at which ignition of the thin film is more likely to occur. As the temperature gets close to the melting point of copper oxide (1356 K), the possibility of reaction increases. Between 1358K and 2325 K reactants are in liquid phase and the reaction rate is based on the diffusion of liquid-liquid phase. The presence of alumina as a final product within the reaction zone can decrease the flame speed by reducing the contact area of the reactants. In between 2325K and 2723K, all the products and reactants are in pure liquid phase and reaction rate is

36

highest at this point. Above 2723K, reaction enters the gas phase of the reactants and the rate of reaction accelerates to its highest rate. Fig. 5 shows that the corresponding heat generation at this temperature of 2723K can be unrealistically high. Fisher [29] predicts the heat generation of aluminum and copper oxide reaction[2]. The numerical data points in Fig. 5 were generated by running the 2D model (Fig.1) iteratively for a substrate thickness of 300 nm for various heat fluxes. In this model, there is no heat loss to the environment and all the heat is dissipated to the substrate. For each heat flux and a flame temperature at flame speed of 43 m/s, the maximum flame temperature was obtained and plotted in Fig. 5. As seen earlier, in the sandwich model in Fig. 2, the final temperature that should be reached for a flame speed of 43 m/s is $2160 \pm 1.5\%$ K. Therefore the heat flux interpolated at this temperature is used as the constant heat flux boundary condition on the flame for all the numerical cases.

The justification for finding the heat flux given above is as follows. Although the estimated heat flux from the black box theory should ideally be ($Q_{gen} - Q_{loss}$) where no substrate is present, for numerical runs, this is not practical. Therefore, a thick enough substrate was chosen so that the heat lost through the substrate is minimized and the flame temperature of 2160 K approaches the flame temperature that would have been obtained without any substrate as in the sandwich theory. Secondly, the estimated heat flux is assumed to be the same across all flame speeds and substrate conditions as the reaction is still stoichiometric in nature and hence the total heat produced should be the same. In addition, the ambient is unaltered, and therefore, Q_{loss} to the surrounding is the same for all cases. Hence, the heat flux boundary condition as given by ($Q_{gen} - Q_{loss}$) is the appropriate boundary condition for all numerical simulations.

---

[2] Density, Cp, and some other physical properties of aluminum, copper, and copper oxide are available in "Binary Alloy Phase Diagrams" hand book even at high temperature [109]. Fisher, S. H., [29] also published properties of alumina and copper oxide in separate temperature zone.

Table 3-3. Six different stages for the unit cell temperature

Temperature range (K)		Phase change		Weight of reactants and products			
Start	End			CuO	Al	Al2O3	Cu
	300	AL + CuO	(Ignition)	79.6%	20.4%	0.0%	0.0%
300	933	Al	Melts	69.4%	18.1%	4.8%	7.6%
933	1356	CuO	Melts	61.7%	16.4%	7.6%	14.3%
1356	1358	Cu	Melts	61.3%	16.2%	7.8%	14.6%
1358	2325	Al2O3	Melts	46.5%	12.9%	14.1%	26.4%
2325	2723	Al	Vaporizes	15.1%	5.9%	27.5%	51.5%
2723	2793	Cu	Vaporizes	0.0%	0.0%	35.0%	64.6%
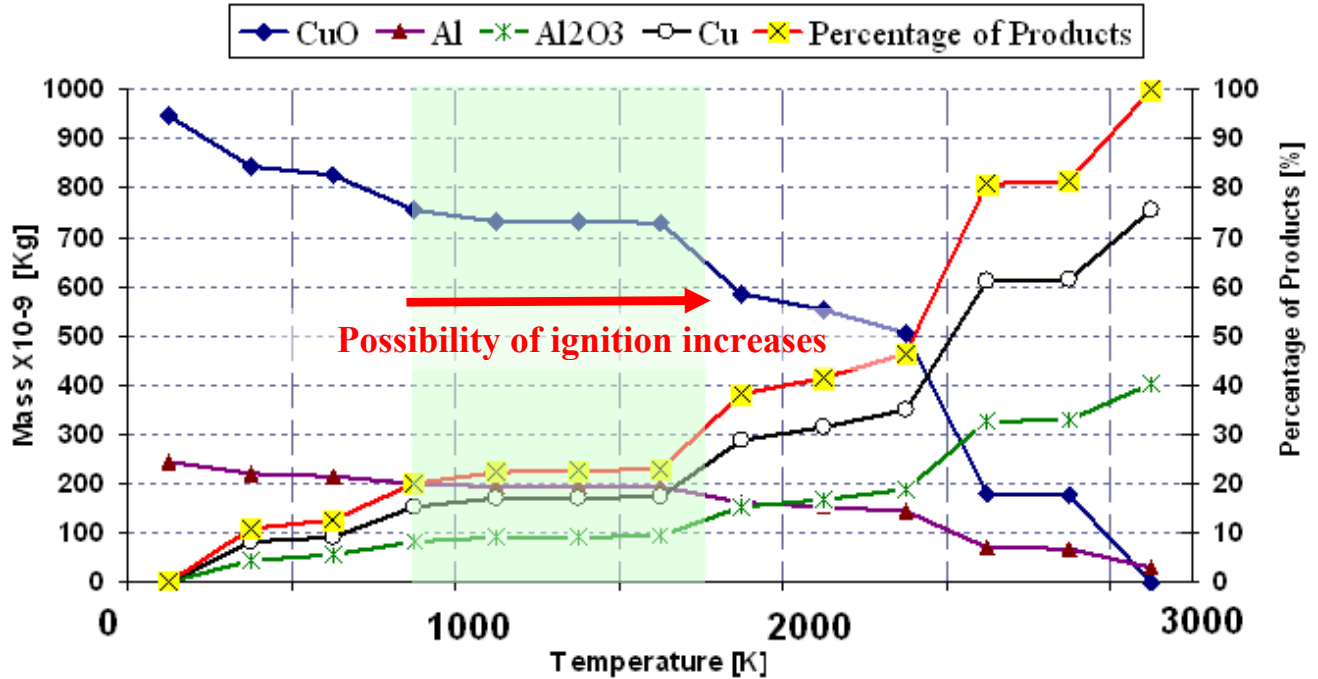
Fig. 3-4. Mass of reactants, products, and final temperature in stoichiometric reaction of aluminum and copper oxide

38
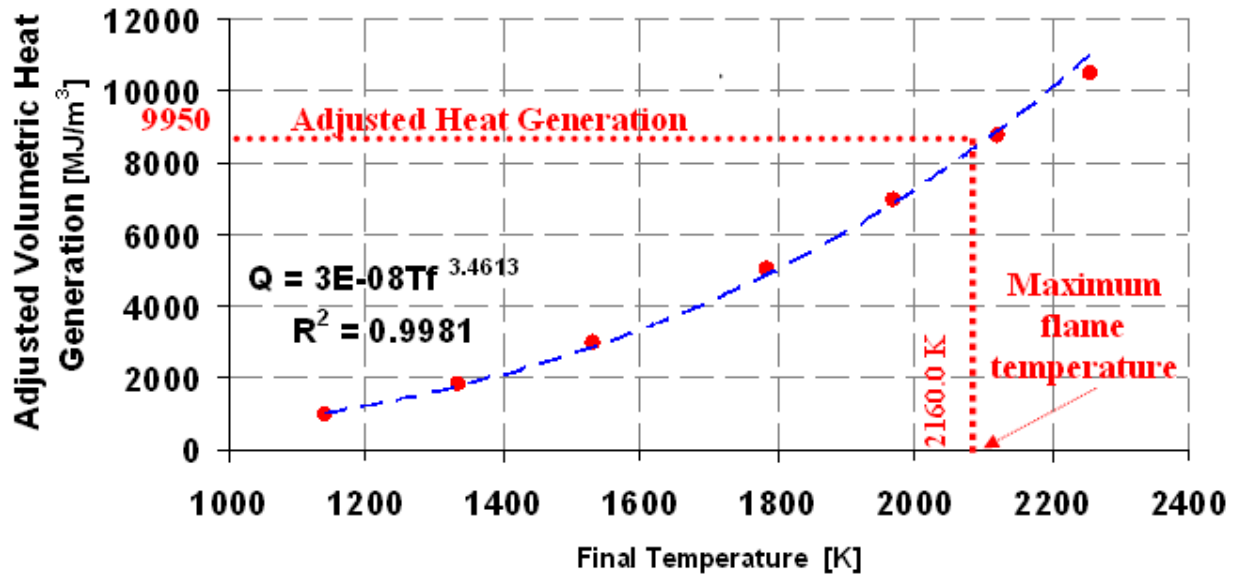
Fig. 3-5. Estimated volumetric heat generation as a function of final temperature based on numerical simulation and sandwich model

Numerical Procedure

Normally the numerical model is meant to simulate the actual samples of Al/CuO (40 bi-layers with each consisting of 26 nm of Al and 54 nm of CuO, totaling 3.2 µm) were prepared by vacuum deposition on a substrate. In this problem, this is considered the line heat source. A two-dimensional model using COMSOL, finite element software, which implements the finite element method, is used to simulate the temperature profiles and quenching characteristics of the flame as functions of substrate thickness and reaction rates. The thin reaction zone shows in Fig. 1. In the black box model, the flame is simulated as a finite width heat source with fixed coordinate moving over the substrate. From this heat source, heat dissipates into the substrate and there is no heat lost to the surrounding. As shown in the previous section, the heat flux was obtained from a combination of sandwich theory and black box model using stoichiometric calculations. The flame speed is assumed constant.

The computational domain shown in Fig. 1 is divided into three distinct segments, namely 1) the moving heat source with a uniform heat flux, 2) the silica substrate of varying thickness which serve as the heat sink and 3) the silicon substrate.

<u>Estimation of Flame Width</u>

One key input parameter apart from the corrected heat flux is the width of the flame front. Thermal penetration depth, δ, of the moving reaction front into the thermally grown SiO_2 surface layer was measured by varying the thickness, h_{SiO2}, of the layer. Our experiments [103] showed that the reaction was completely quenched for SiO_2 layer of less than or equal to 200 nm, and the flame speed was between 40 m/s and 45 m/s for SiO_2 layers of 1 μm and 2 μm.

In order to justify and provide a width of the flame front for the mathematical model, the following analysis is conducted. For the case of $h_{SiO2} > \delta$, the thermal penetration depth, the reaction velocity is expected to be similar to that of the bulk substrate. For $h_{SiO2} < \delta$, a reduced reaction velocity is expected due to the increased loss of the heat of the reaction into the higher thermal conductivity silicon. As a simple approximation, $\delta = \sqrt{4\alpha t}$, where α is the thermal diffusivity of SiO_2, then the time, t, may be estimated for reaction front as $t \sim 70$ ns, from which the effective width, ω, of 3.2 μm can be estimated for the averaged measured flame speed of 43 m/s (at t=70ns for a flame speed of 43 m/s, the flame length is calculated as ω =70e-9 x 43 =3.2 μm). Length of the flame changes as speed of flame changes but there is slight changing in length of flame within 40 to 50 m/s (quenching zone of the flame).Therefore, Length of flame in this area (40 to 50 m/s) is employed as a constant for all the cases reported in this paper.

Governing Equations and Boundary Conditions

The governing equation for the linear moving heat source [110], which is stretched along the x direction and moves in the same direction with constant speed of v_x over composite substrate shown in Fig. 2 are:

$$\frac{\partial^2 T}{\partial x^2} + \frac{\partial^2 T}{\partial y^2} = \frac{v_x}{\alpha_1}\frac{\partial T}{\partial x} \tag{4}$$

$$\frac{\partial^2 T}{\partial x^2} + \frac{\partial^2 T}{\partial y^2} = \frac{v_x}{\alpha_2}\frac{\partial T}{\partial x} \tag{5}$$

In this case, α_1 and α_2 are α_{SiO_2} and α_{Si} respectively, which are the thermal diffusion coefficient for silica and silicon relatively. Boundary conditions are similar for a single substrate:

$$\mathrm{T}(x = +\infty, y) \quad \begin{cases} q \cdot n = (\rho C_p vT) \cdot n \\ n.(-k\nabla T) = 0 \end{cases} \tag{6}$$

$$T(x = +\infty, y) = 300K \tag{7}$$

$$k\frac{\partial T}{\partial y}(x = \pm\omega/2, y = 0) = q \tag{8}$$

$$\frac{\partial T}{\partial y}(-\infty \le x \le -\omega/2 0, y = 0) = 0 \tag{9}$$

$$\frac{\partial T}{\partial y}(\omega/2 \le x \le +\infty, y = 0) = 0 \tag{10}$$

$$T(x, y = \infty) = 300\,\mathrm{K} \tag{11}$$

An explicit method was used to carry out the computations. Since the flame speed is constant, time is proportional to x direction of motion. Therefore forward differencing was used for x direction and central differencing was used for y direction. At the interface between silica

41

and silicon, as recommended by Patankar [113], a harmonic mean thermal conductivity, k_e, as the numerical value of heat conductivity at the interface of two materials.

$$k_e = \frac{k_{SiO_2} \cdot k_{Si}}{k_{SiO_2} + k_{Si}} \qquad (12)$$

where k_{SiO_2} and k_{Si} are the thermal conductivities of silica and silicon. The governing equations in discretized form were solved simultaneously using an iteration technique to obtain the temperature profiles. For most cases, a total of 175,000 to 200,000 elements seemed to be adequate to provide accurate calculations. The uncertainty was maintained within $\pm 0.5\%$.

Results and Discussion

Validation of Numerical Results

Weichert et al. [110] developed a closed form solution for a moving line source of width, w on a single substrate:

$$T - T_i = \left(\frac{q}{2\pi k}\right) \int_{-\omega/2}^{+\omega/2} K_0\left(\frac{v_x r}{2\alpha}\right) \exp(-v_x \xi / 2\alpha) d\xi \qquad (13)$$

where K_0 Is the Bessel function of the second kind and q, α, and k are heat flux, thermal diffusivity and conductivity respectively. In order to validate the model, non-dimensional profiles of temperature 100 nm below the heat source are generated for single substrates (SiO_2) of varying thickness as shown in Fig. 6. The maximum temperature for all the cases occurs at the leading edge of the heat source. As the substrate thickness increases, the temperature profiles become self-similar for h>1000 nm and compare well with the analytical solution given in equation 13. As h increases, the peak temperature increases. In addition, for the lower thicknesses, temperature reaches ambient temperature earlier in the direction of propagation.

42

Substrate Temperature Results

Fig. 7 shows the variation of the maximum temperature with substrate thickness. There is very little difference between a single substrate of silica and a composite Si-SiO₂ substrate. This shows the effectiveness of the composite substrate. As the substrate thickness increases, the maximum temperature increases up to about 1 μm. Beyond 1μm, the maximum temperature becomes a constant for both single and composite substrate.

Fig. 8 shows the temperature profiles in the X-direction at the interface of the substrate and the moving heat flux (nanofilm) for different reaction rates and substrate thickness of 50 nm. The shaded portion signifies temperatures above 933K where Al melts and the possibility of ignition increases. In order for the reaction to self-sustain, the temperature at the preheat zone must remain above the melting point of one of the reactants, i.e. aluminum [108]. For flame speeds in range 40-50 m/s, the maximum temperature is below this minimum temperature of 933 K needed to sustain the flame. Below the grey shaded zone in Fig. 8, flame cannot be sustained for a 50 nm silica substrate. The heat generated by the flame front through the chemical reaction is quickly dissipated by the thin substrate resulting in the quenching of the flame. In the same thin film with thicker silica substrate, the lower heat dissipation lead to higher maximum temperature in flame zone with the same speeds range (40-50). As flame temperature rises to the gray zone (over 933 k) self-sustainability of the flame is more likely.

Fig. 9-12 show details of the temperature profiles at the interface (substrate and moving line source) for substrate thicknesses of 75, 100, 300 and 500 nm respectively. It is observed that with increase in substrate thickness, the quenching effect is progressively diminished. These results are consistent with the observations in our experiments [103]. Flame speeds of 40 m/s to

45 m/s (average is taken as 43 m/s) were obtained on thin films on Si substrates having a thick intervening layer of SiO_2 to provide thermal isolation. In thin films deposited directly on a Si substrate without a thermal isolation layer, no self-propagating reaction was observed, i.e. the reaction was effectively quenched. As seen in the experiments, the numerical results show that the average speed and quenching of flames depend on the thickness of SiO_2 substrate. Thus, it is inferred from the current computations that the flame speeds and the temperature profiles can be controlled in thin film energetic materials by a careful choice of the substrate. Fig.s 8-12 also show that the peak temperature increases initially as the substrate thickness is increased from 50 nm to 300 nm for this flame speed range, but attains a constant value as the substrate thickness is increased to 500 nm. In the current model, the total heat responsible for the temperature rise is the difference between the heat released and the heat dissipated. An increase in silica thickness augments the insulation effect resulting in lower heat dissipation, up to 500 nm.

The temperature profiles along the depth of the substrate thickness are shown as a function of flame speed in Figures 13-17. Fig. 13 and 14 show almost a linear decay in temperature for all flame speeds. It can be seen that at the interface between silica and silicon substrates, the temperatures drop to about 60 % of the ignition temperature of 933 K. In fact, it is clearly seen that the higher the flame speed sharper is the decay in the temperature profile.

44
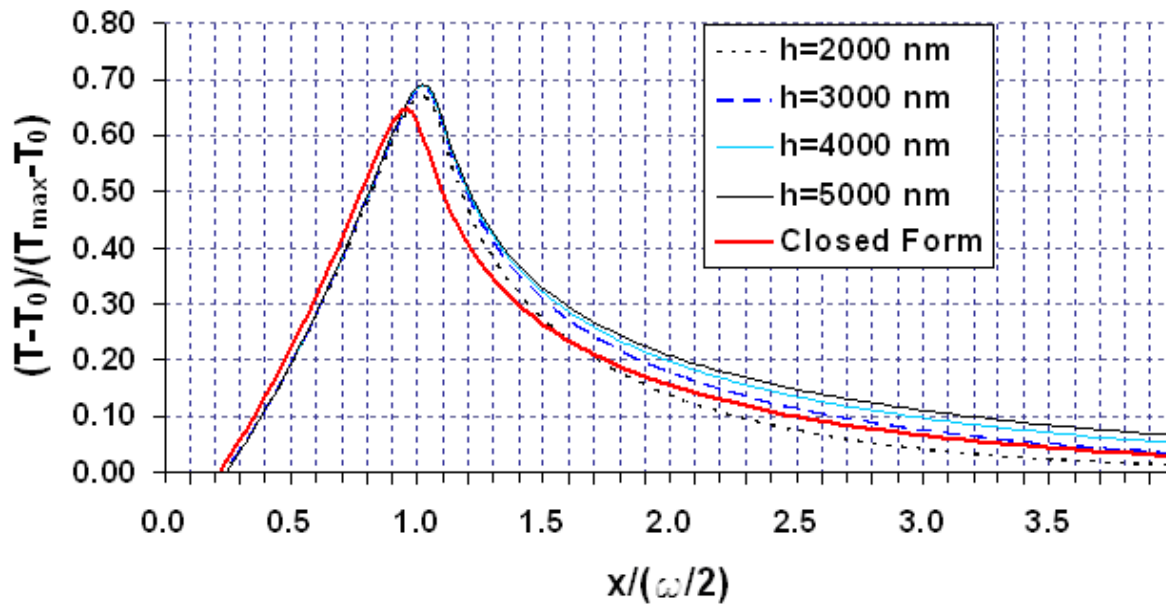
Fig. 3-6.Temperature distribution 100 nm below the heat source for various substrate thicknesses, h. The curve in red is the analytical solution
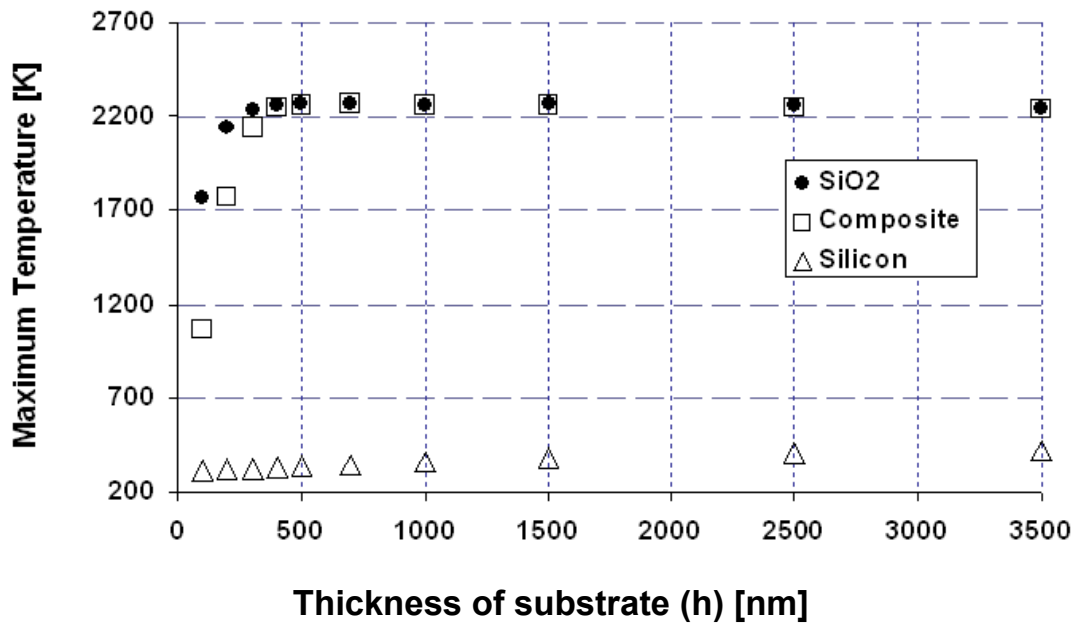
Fig. 3-7. Maximum Temperature at 100 nm below the flame front for simple and composite substrate in various thicknesses

45
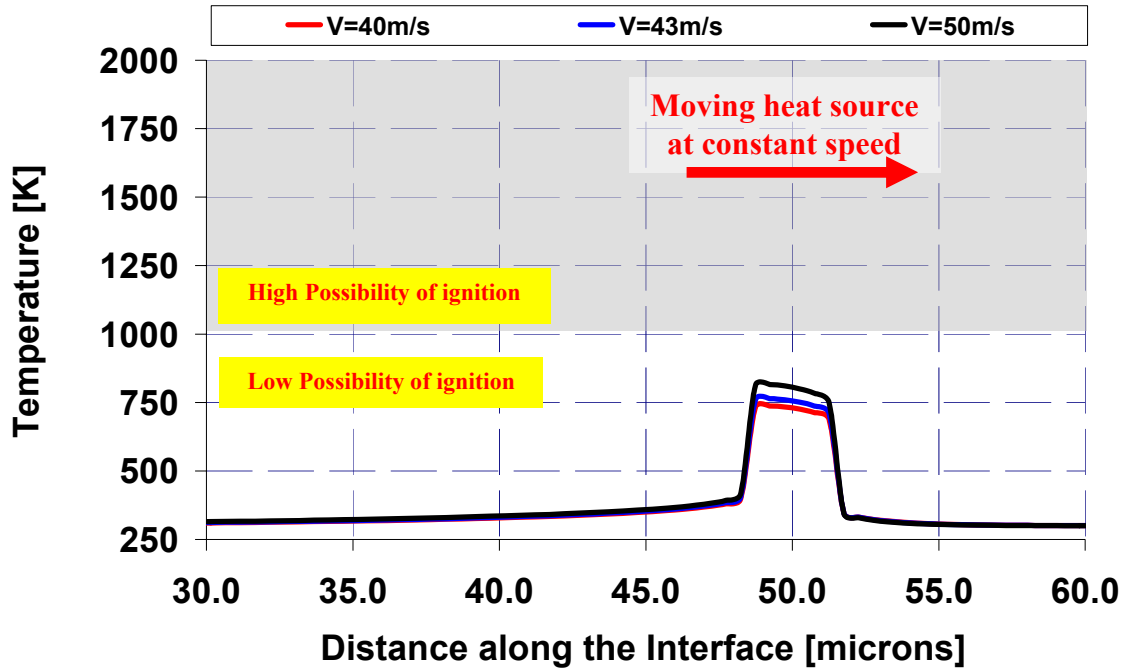
Fig. 3-8.Temperature profile along the interface of the moving heat source and a 50 nm thick immediate substrate.
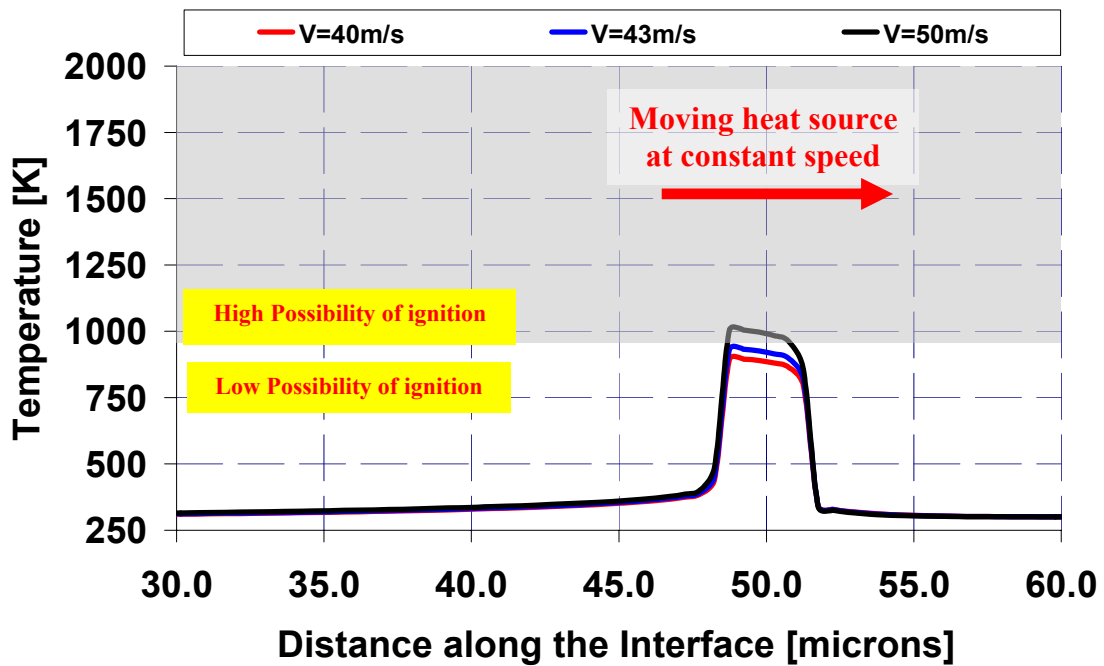
Fig. 3-9.Temperature profile along the interface of the moving heat source and a 75 nm thick immediate substrate.
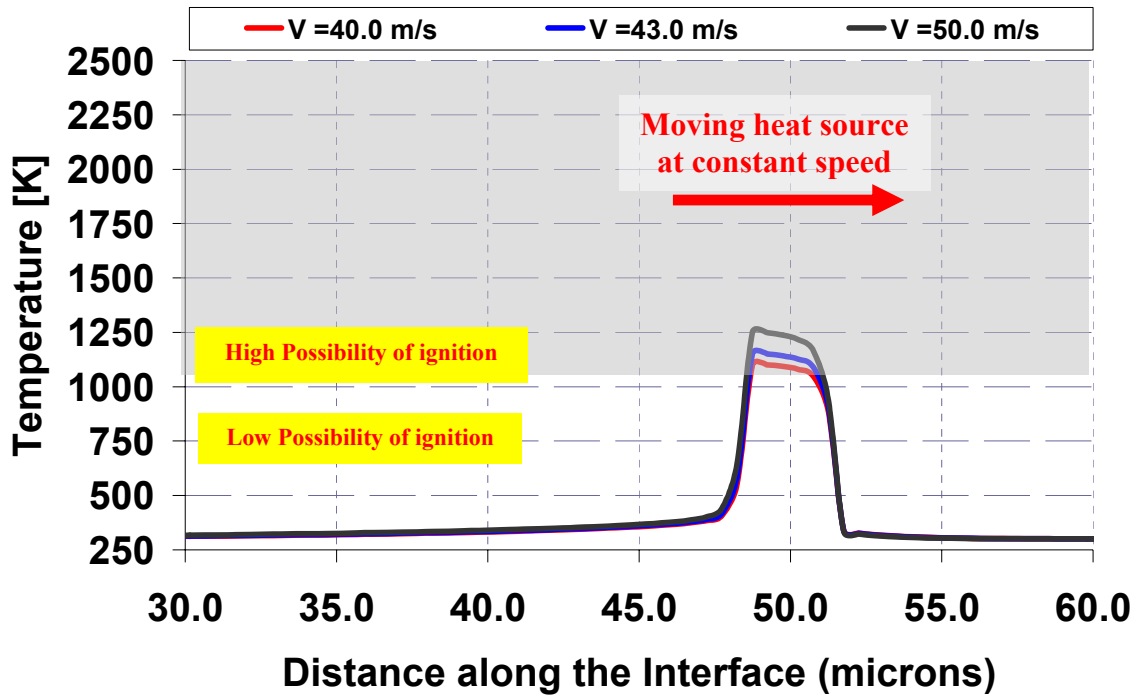
Fig. 3-10.Temperature profile along the interface of the moving heat source and a 100 nm thick immediate substrate.
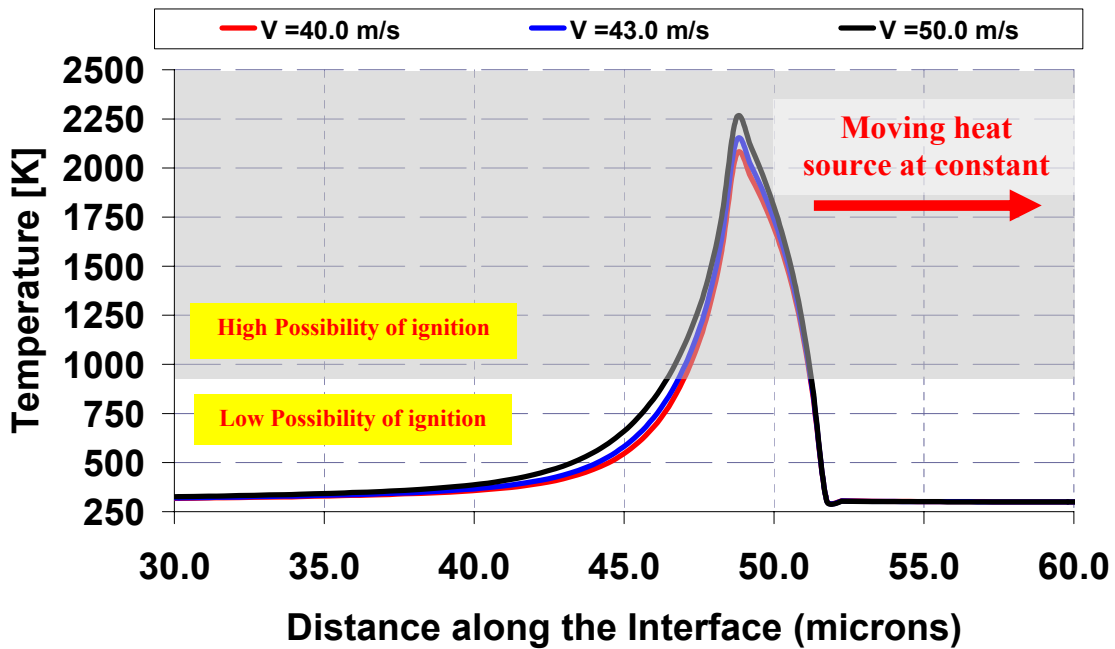
Fig. 3-11.Temperature profile along the interface of the moving heat source and a 300 nm thick immediate substrate.
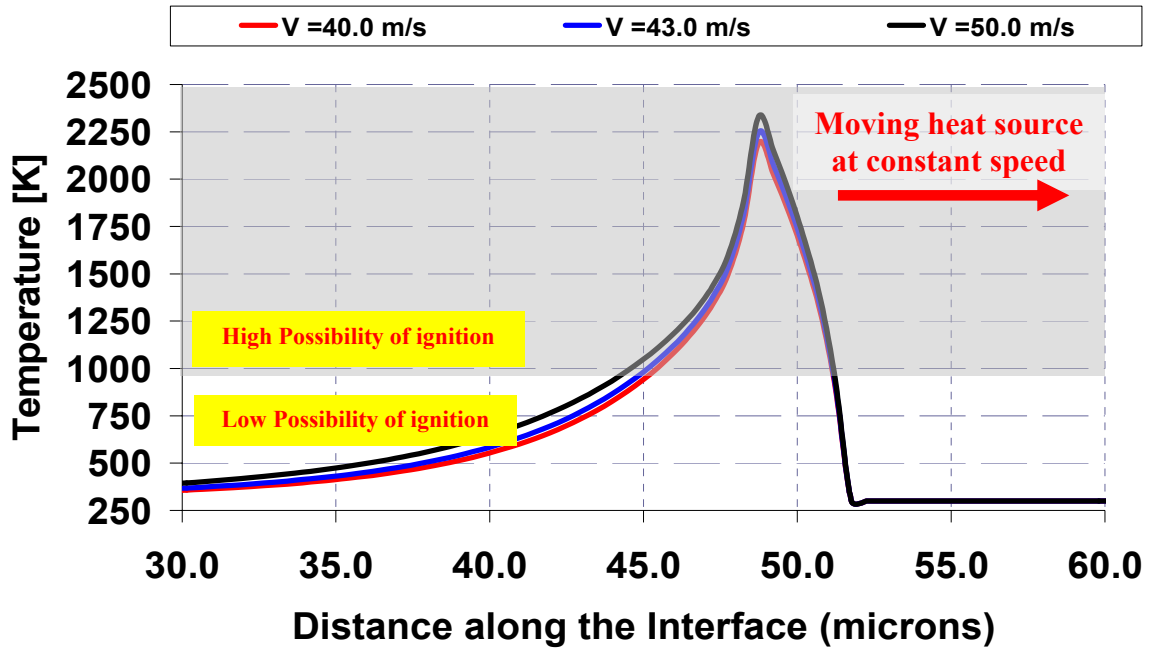
Fig. 3-12.Temperature profile along the interface of the moving heat source and a 500 nm thick immediate substrate.
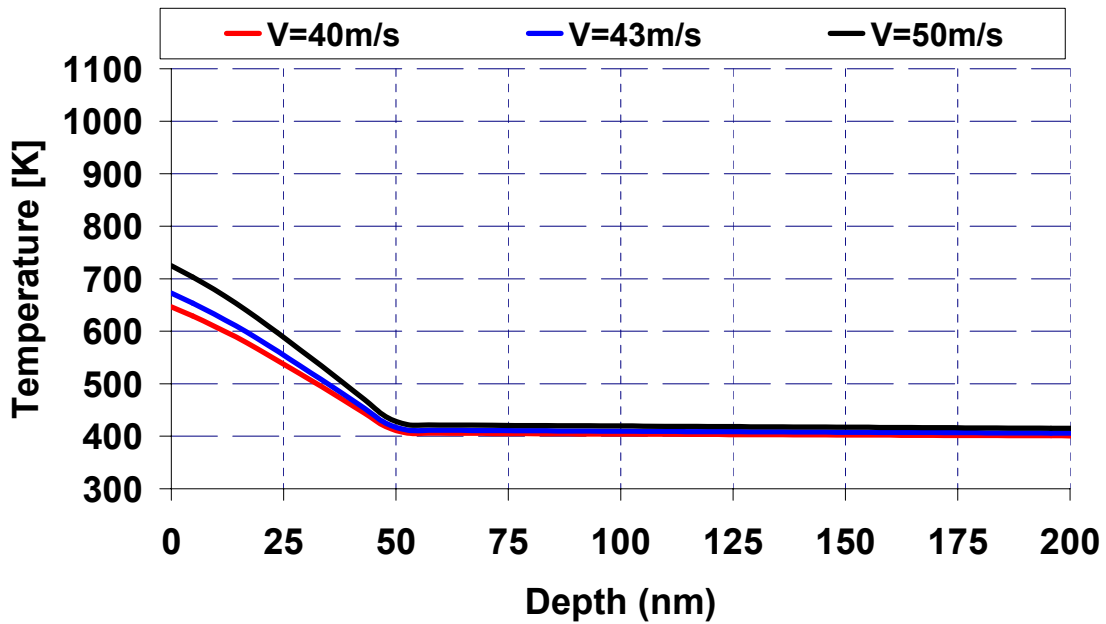
Fig. 3-13. Temperature profile along the depth of a 50 nm thick immediate substrate at the flux front.
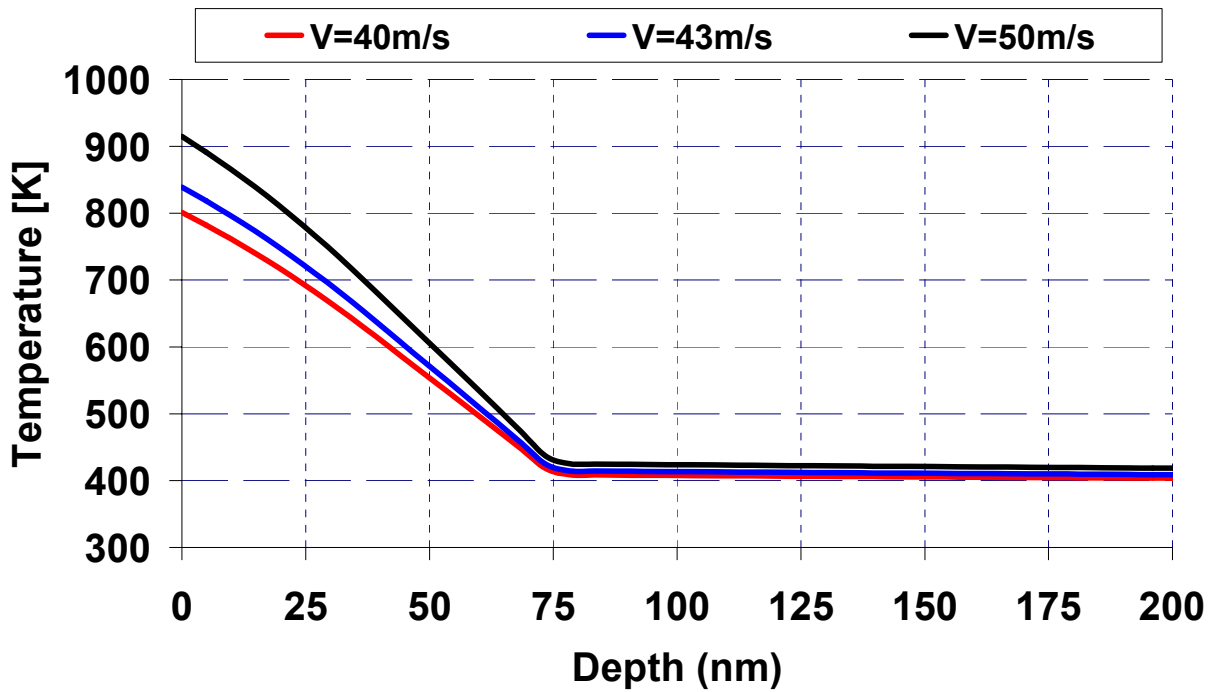
Fig. 3-14. Temperature profile along the depth of a 75 nm thick immediate substrate at the flux front.
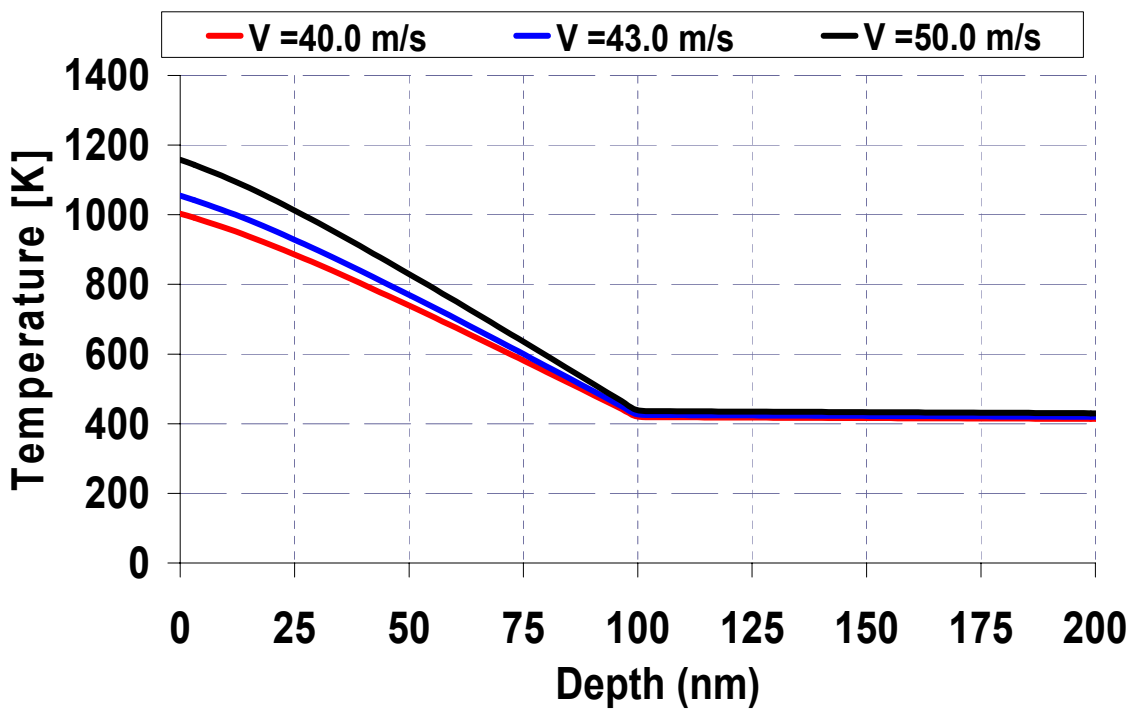
Fig. 3-15. Temperature profile along the depth of a 100 nm thick immediate substrate at the flux front.

49
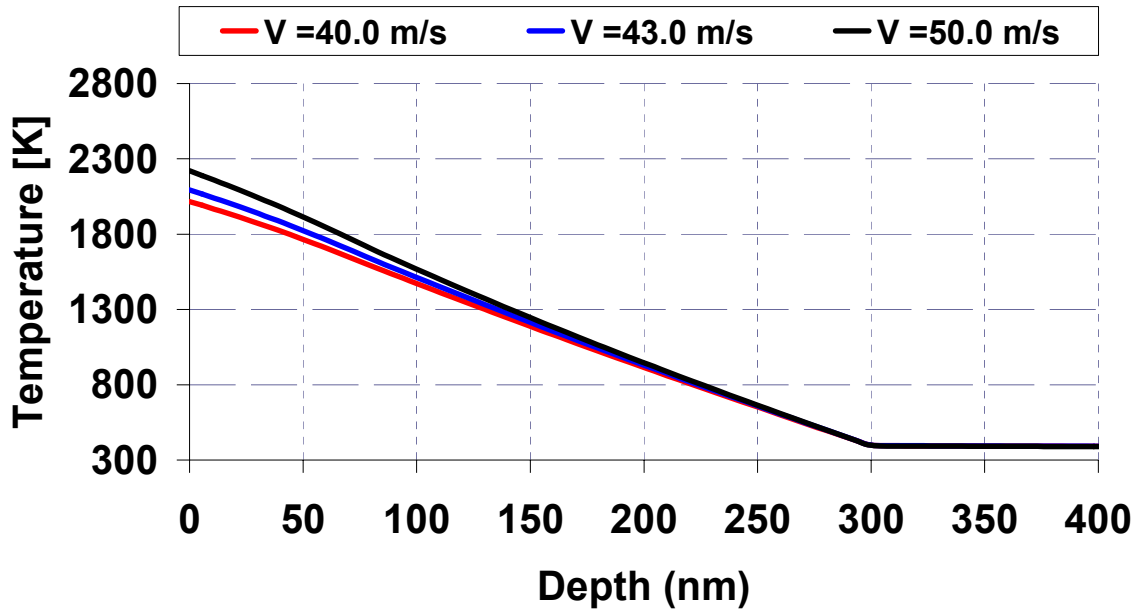
Fig. 3-16. Temperature profile along the depth of a 300 nm thick immediate substrate at the flux front.
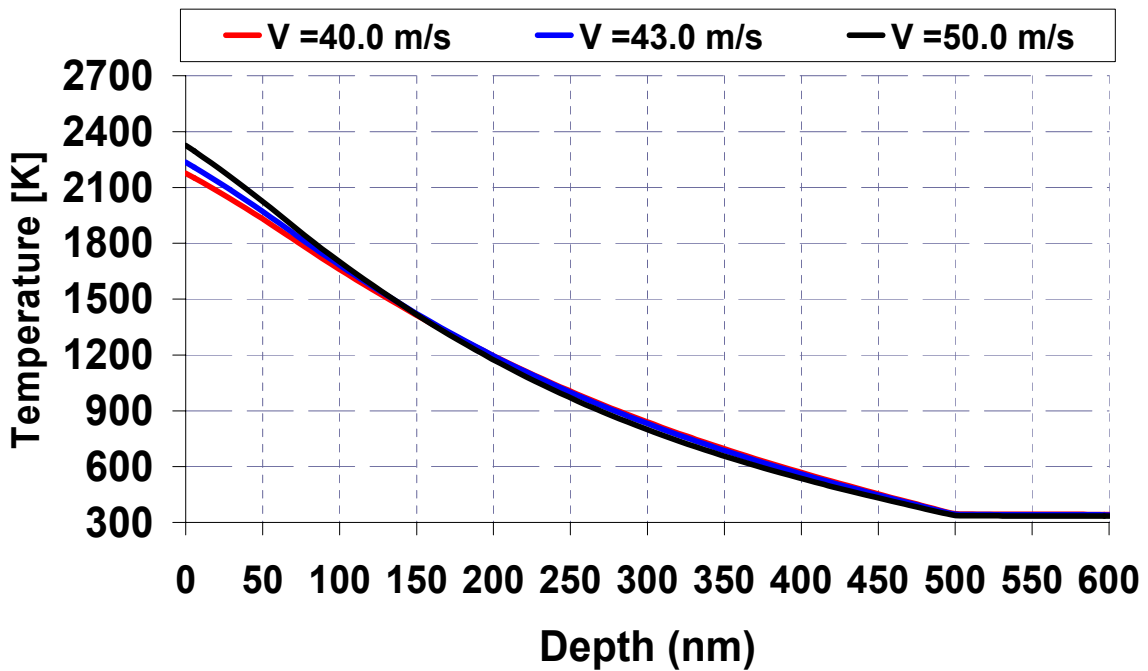
Fig. 3-17. Temperature profile along the depth of a 500 nm thick immediate substrate at the flux front.

50

Summary

The problem of thermal transport of a multilayer nanofilm of Aluminum and Copper oxide has been analyzed for varying substrate material and thicknesses. A numerical analysis of the thermal transport of the reacting film deposited on the substrate combined a hybrid approach in which a traditional two-dimensional black box theory was used in conjunction with the sandwich model to estimate the appropriate heat flux on the heat sources accounting for the heat loss to the surroundings. A procedure to estimate this heat flux using stoichiometric calculations is provided. By plotting the temperature profiles in the substrate, possibilities of ignition and quenching have been explored for certain range of flame speeds.

This work highlights two important findings. One is that there is very little difference in the temperature profiles between a single substrate of silica and a composite substrate of silicon-silica substrate. Secondly, with increase in substrate thickness, the quenching effect is progressively diminished at given speed. The results show that for small substrate thicknesses of 50 nm, flames cannot be sustained. However, for a high substrate silica layer thickness of 300 to 500 nm, flame is self-propagate with expected speed range 40 to 50 m/s. These results are consistent with the experimental observations for multilayer films of Al/CuO.

These findings show that the composite substrate is effective and that the average speed and quenching of flames depend on the thickness of the silica substrate, and can be controlled by a careful choice of the substrate.

51

CHAPTER 4
CHARACTERISTICS OF THE FLAME FOR REACTION OF MULTILAYER NANO THIN FILM OVER SUBSTRATE

Introduction

Self–propagating high temperature reaction in compact nano film typically includes multilayer vapor deposition of a transition metal and an element. Reactants deposit in bi-layer with even thickness. Flame temperature and speed of flame front are two distinctive characters of nano thin film reaction. A number of variables such as deposition temperature, density, thermo conductivity of the material, and the rate of heat loss impact the combustion temperature and the speed of the flame during the reaction. In the same deposition process and steady reaction, indicated variables can be reduced to the enthalpy of the final products and the heat loss value during the reaction. Similarly, speed of flame front relates to the maximum flame temperature, the diffusion distance (length of flame), and the rate of heat loss during the reaction [61-63,113-115].

Multilayer nano film Reaction is considered in a self-propagating mode; therefore, four important temperature values affect the reaction process. The reactants at initial temperature T_0 (1) should be heated up to the ignition temperature T_{ig} (2) which the reaction initiates. After the ignition, sufficient heat is released by the reaction, and temperature at the flame zone exceeds to the maximum combustion temperature T_c (3) in order to self-sustain the reaction. Combustion temperature T_c is much lower than the maximum combustion temperature under adiabatic condition T_{ad} (4). Combustion temperature can change from one reaction environment to the other; however, in order for the reaction to remain in self-sustain propagating mode, combustion temperature should

remain above certain level. Sufficient heat $\Delta H(T_{ig})$ is necessary to keep the temperature at preheated zone above ignition temperature.

$$\Delta H(T_{ig}) = -[H(R) + H(P)] \quad (1)$$

Excessive $\Delta H(T_{ig})$ heat in the flame area has to balance with the required heat for the preheated zone, phase transformation, and heat loss through the substrate. $H(R)$ and $H(P)$ are heat of reactants and the products.

In adiabatic reaction, maximum temperature is achieved based on the following function (eq. 2). It can also get more complicated if the total heat is affected by additional heat loss through its surroundings (eq.3).

$$H(P) = \int_{t(T_{ig})}^{T_{ab}(T_0)} \sum n_i C_P(P_j) dT + \sum_{T_{ig} \approx T_{ab}(T_0)} n_i L(P_j) \quad (2)$$

$$H(P) = \int_{t(T_{ig})}^{T_c(T_0)} \sum n_i C_P(P_j) dT + \sum_{T_{ig} \approx T_c(T_0)} n_i L(P_j) + [heat_{loss}] \quad (3)$$

Where n_i, $C_P(P_j)$, and $L(P_j)$ are the reaction stoichiometry coefficients, heat capacity , and phase transformation enthalpies for the products.

Therefore, the heat dissipation through the substrate directly impacted the maximum combustion temperature. Speed of the flame front (the second distinctive characteristic in this study) is impacted by the heat loss as a result of a change in maximum temperature.

53

Analytical models were developed to estimate the reaction velocity in multilayered film by solving atomic diffusion (eq. 4) [116] and thermal transport (eq. 5)

$$\frac{dC}{dt} = \nabla.(D\nabla C) \qquad (4)$$

$$\frac{dQ}{dt} = C_P \frac{dT}{dt} - C_P \lambda \nabla^2 T \qquad (5)$$

Where t is time, C is the composition, and D is the average coefficient of atomic diffusion. C_P is the average heat capacity, λ is the average thermal diffusivity, T is the temperature, Q is the total heat in a unit volume of the system, and dQ/dt is the rate of the heat generation. These equations are coupled by assuming that the rate at which heat is generated (dQ/dt) is proportional to the rate at which the composition of the thin film changes (dC/dt).

Armstrong [52-53] solved the coupled equations by using the sandwich theory assuming that a linear relationship exists between the composition and the energy released. In the simplest case considering the above assumption, the following relationship was obtained [51].

$$v_x^2 = \frac{3A \exp\left(-E/RT_{max}\right) RT_{max}^2 \lambda^2}{\delta^2 E(T_{max} - T_0)} \qquad (6)$$

where A is an Arrhenius refractor, E is the activation energy for mass diffusion, R is the gas constant, δ is 1/4 of the bi-layer thickness (the sum of the A and B layer thicknesses); and T_0 is the initial temperature. T_{max} is the maximum temperature obtained during steady-state propagation.

Mann et al. [57] expanded on Armstrong and Koszykowski's model by including the effect of an intermixed region. In one simple case, they assumed that the intermixed region consisted of the final phase with full reaction, and the composition profile was a step function.

$$v_x{}^2 = \frac{RT_{max}^2 A\lambda^2 \delta}{E(T_a - T_0)} \exp(-E/RT_{max}) \quad (7)$$

Maximum combustion flame temperature is clearly related to the speed of flame front and the heat loss (eq.7). In order to find the actual relation between the speed of flame front and maximum combustion temperature with additional heat loss, the current model is not sufficient. To add the impact of the heat loss though the substrate, reaction should be analyzed based on fundamental combustion phenomena by using the black box theory. This theory simplifies the complex reaction process of thin film by introducing a control volume that moves with the flame front and encloses the region of the reaction front. The reactions within the black box are considered to occur in a steady state mode. The concept of the black box theory allows one to isolate the effects of the interaction of the control volume and the surroundings within the defined frame. The control volume moves with the speed of the flame along with the reaction path, and this speed is assumed to be constant. A controllable heat absorber (composite substrate) was added as a substrate of multilayer thin film reaction to capture the additional heat loss through the surrounding. The black box models alone would not successfully represent the flame heat release rate without considering the actual reaction in the flame area. Hence, it is important to integrate the two models (sandwich and black box) supplemented by

www.manaraa.com

experimental results [34] to successfully analyze the reaction for maximum combustion temperature at a certain speed.

Carslaw and Juger [95] introduced the moving heat source model. Rosenthal's [96] solved it with the semi-infinite body subjected to an instant point heat source, line heat source, or surface heat source. These solutions can be used to predict the temperature field at a distance far from the heat source but fail to predict the temperature in the vicinity of the heat source. Eagar and Tsai [97] modified Rosenthal theory to include a two-dimensional (2-D) surface. Gaussian distributed the heat source with a constant distribution parameter and found an analytical solution for the temperature of a semi-infinite body subjected to this moving heat source. Jeong and Cho [98] used the conformal mapping technique and they successfully transformed the solution of the temperature field in the plate of a finite thickness to the fillet welded joint [28-30].

In this study, two theories (sandwich and black box) were integrated along with the experimental results to estimate the maximum flame temperature and the other flame characteristics. Composite substrate was used as a mechanism to control the heat loss during the reaction. Numerical model was developed based on moving heat source for multilayer thin film of aluminum and copper oxide over composite substrate of silica\silicon [117]. The maximum combustion flame temperature corresponding to speed of flame front is the main target of this model. Thickness of the substrate, length of flame front, and density of product were utilized for the standard multilayer thin film with 43 m/s flame front speed. The calculated heat penetration depth in this case was compared to the experimental result for the same flame front speed. Numerical model also was used to estimate three major variables for a range of 30-60 m/s. In fact, the maximum combustion

56

flame temperature that corresponds to speed along with the length of the flame, density of the product behind the flame, and maximum penetration depth in steady reaction were calculated.

Material and methods

In previous study, maximum combustion temperature was calculated with limited heat loss of the thin film; hence maximum combustion temperature should be modified if reactions have significant heat loss through the environment. Due to the additional heat loss through the substrate, using the sandwich model alone to estimate the flame temperature reaction of aluminum and copper oxide over the substrate is not sufficient. Using the black box theory, a moving heat source model would be an appropriate alternative to represent the heat transfer simulation. The black box model alone would not successfully represent the actual diffusion process within the reaction zone. Hence, it is vital to integrate the two theories supplemented by experimental results [103] to successfully relate the speed of flame front and the heat loss to the maximum flame temperature. A numerical model of moving heat source was developed based on the black box theory with four different variables to calculate the maximum flame temperature.

Length of flame represents the certain amount of multilayer thin film which is participating in the reaction at any instant.

Reaction Heat loss is controlled by thickness of silica within composite substrate. As thickness of silica increases, more heat flow is blocked by silica which causes maximum flame temperature to rise. Excessive heat loss thought the substrate can be adjusted by changing the thickness of the silica.

Density of the product behind the flame is reduced during the reaction. The porosity of the product can be adjusted by the properties of the materials, and it impacts the heat loss and the flame temperature.

Speed of flame front would impact the flame temperature and it is specified as a variable within a numerical model. Fig. 1 demonstrates the physical aspect of each variable in a projected model of the reaction. In the following sections, each one of these variables is presented with more details.
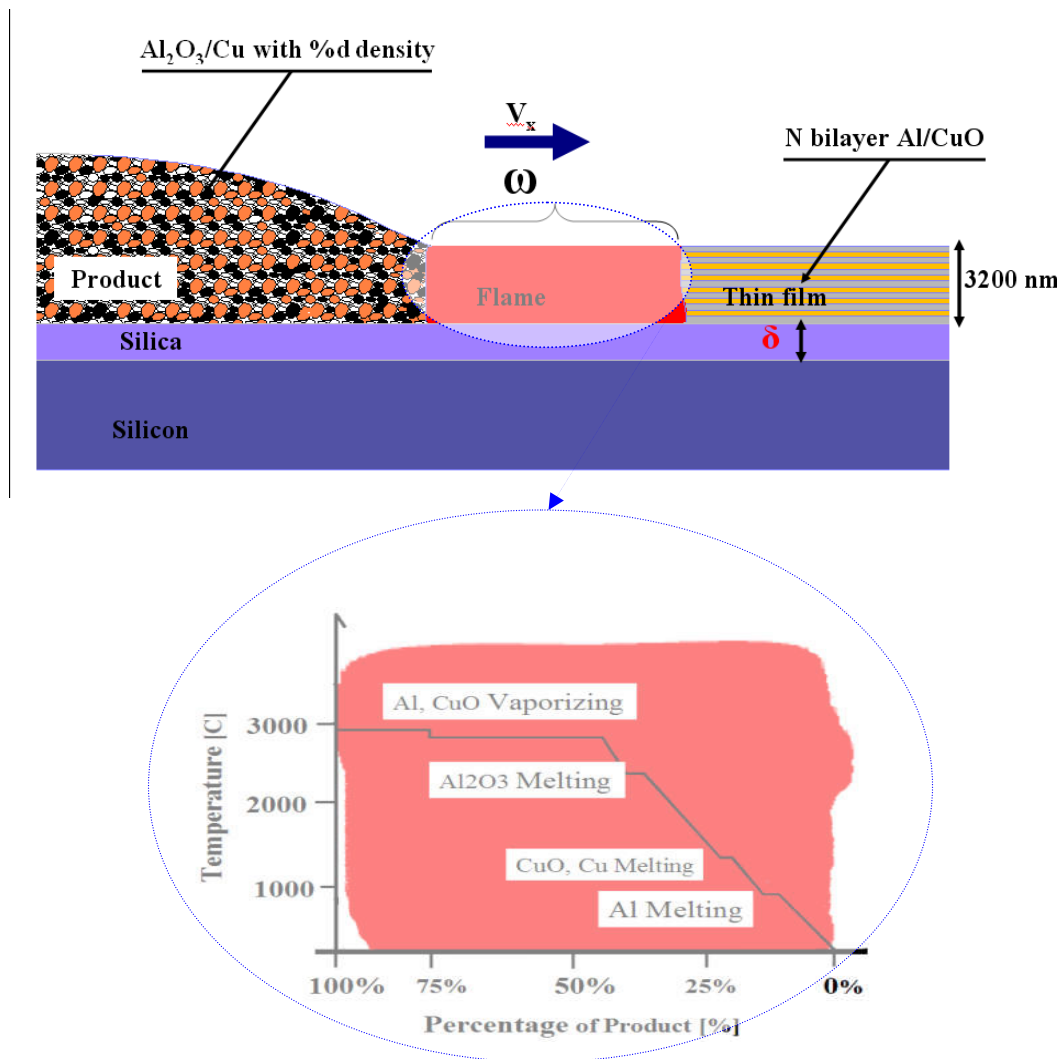
Fig. 4-1.Schematic multilayer thin film reaction over composite substrate

<u>Maximum flame temperature</u>

Thin film reactions create an enormous amount of energy, which causes the phase transformation of the reactants and the products through the reaction. Fisher [36] predicted the heat generation of the aluminum and copper oxide reaction[3]. The theoretical energy release of the aluminum and copper oxide reaction is 974.1 cal/g [29]. The reaction starts in the solid-solid phase, continues to liquid state, and ends up with a mixture of gas and liquid. Based on the melting and boiling point of each one of the reactants and products, the reaction of aluminum and copper oxide is broken into 6 different stages, as shown in Fig. 1. Total amount of heat and the final temperature of a unit cell of aluminum and copper oxide[4] are calculated based on conservation of the mass and energy. At any stage of the chemical reaction, total mass is constant, so the total loss of mass of reactants through the reaction is equal to the total amount of produced mass.

$$m = \sum m_{Al} + m_{cuo} = \sum m_{Al_2O_3} + \sum m_{Cu} \qquad (8)$$

The energy balance is given by

$$\sum E_{IN} + \sum E_{OUT} + \sum E_{GEN} = \sum E_{STOR} \qquad (9)$$

Figure1 shows the mass of reactants and products at each stage based on the simultaneous solution of equations (8) and (9). Feng [61] compared the various mathematical models that have been developed to simulate and predict instabilities in propagating combustion synthesis reactions. Mukasyan [108] had investigated high temperature combustion synthesis waves in the Ni and Al system. Reaction of aluminum and copper oxide in nanofilm is demonstrated with a similar mechanism in these studies.

---

[3] Density, Cp, and some other physical properties of aluminum, copper, and copper oxide are available in "Binary Alloy Phase Diagrams" hand

[4] CuO was used as a major reactant material. Due to the high temperature at reaction zone, majority of copper oxide, CuO_x dissociates to CuO [121, 34].

Temperature of the reaction in different phases ranges from 300 K to 2793 K. Before reaching 933 K, all materials are in solid phase, and the reaction is limited to diffusion in the solid-solid phase. Between 933 K and 1356 K, aluminum undergoes a phase change to liquid and the reaction is based on diffusion in solid–liquid phase. This is the temperature range at which ignition of the thin film is more likely to occur. As the temperature gets close to the melting point of copper oxide (1356 K), the possibility of reaction increases. Between 1358 K and 2325 K reactants are in liquid phase, and the reaction rate is based on the diffusion of liquid-liquid phase. The presence of alumina as a final product within the reaction zone can decrease the flame speed by reducing the contact area of the reactants. In between 2325 K and 2723 K, all the products and reactants are in pure liquid phase, and the reaction rate is highest at this point. Above 2723 K, the reaction enters the gas phase which causes the rate of reaction to accelerate.

Estimation of the maximum combustion temperature is more complex than the adiabatic temperature due to a numbers of involved variables. In the multilayer thin film reaction [102,105], heat loss was limited through the products and reactants. Also, the additional heat loss was dismissed through its surroundings. In this study, heat loss through the substrate is significant, and it should be addressed by the reduction of the heat generation ($Q_{gen} - Q_{loss}$) value within the flame area. The justification for finding the corrected heat generation is based on the conjunction of two theories and experimental result. The adiabatic heat generation was reduced accordingly, and the corrected heat generation was used in the numerical model to estimate the actual flame temperature when the substrate is present. Although the estimated heat flux from the black box theory should ideally be ($Q_{gen} - Q_{loss}$) where no substrate is present simulation this is not

practical for numerical. Therefore, a composite substrate of silicon/silica was chosen to control the heat loss. As heat loss balances, the speed of the flame front should reach the steady state. As captured in the experimental result, the speed of the flame front jumps to this stable state as soon as the heat loss approaches to the balance point (thickness of silica substrate reaches to the maximum heat penetration. For instance, in standard thin film reaction, the flame front jumps from almost zero to average 43 m/s when thickness of the silica reaches more than 500 nm. The speed flame front remains similar as the thickness of silica increases up to 2000 nm (Fig. 2).
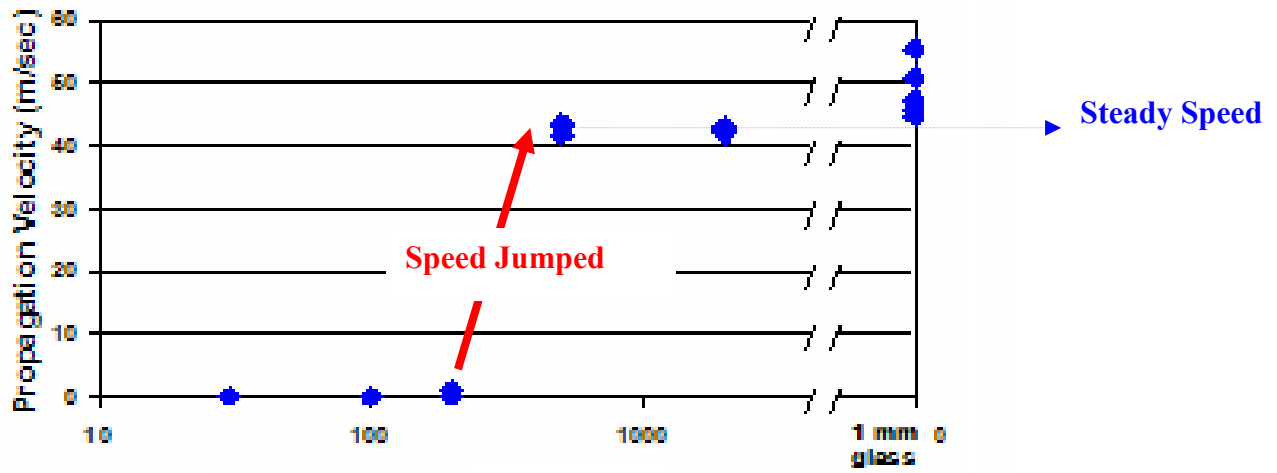
Fig. 4-2. Experimental result of speed of flame front for standard thin film over composite substrate

In order to control the heat loss through the substrate and capture the similar phenomena in the numerical model, standard thin film configuration was calculated for a number of cases. As the thickness of silica increases, combustion flame temperature increases to 2160 K as the thickness of silica surpasses 500 nm. The maximum flame temperature would hold even if the thickness of silica increases further. Similarly, heat

61

generation correction was applied to the other speed of flame front and the maximum flame temperature was captured and demonstrated in the following plots (Fig. 3).
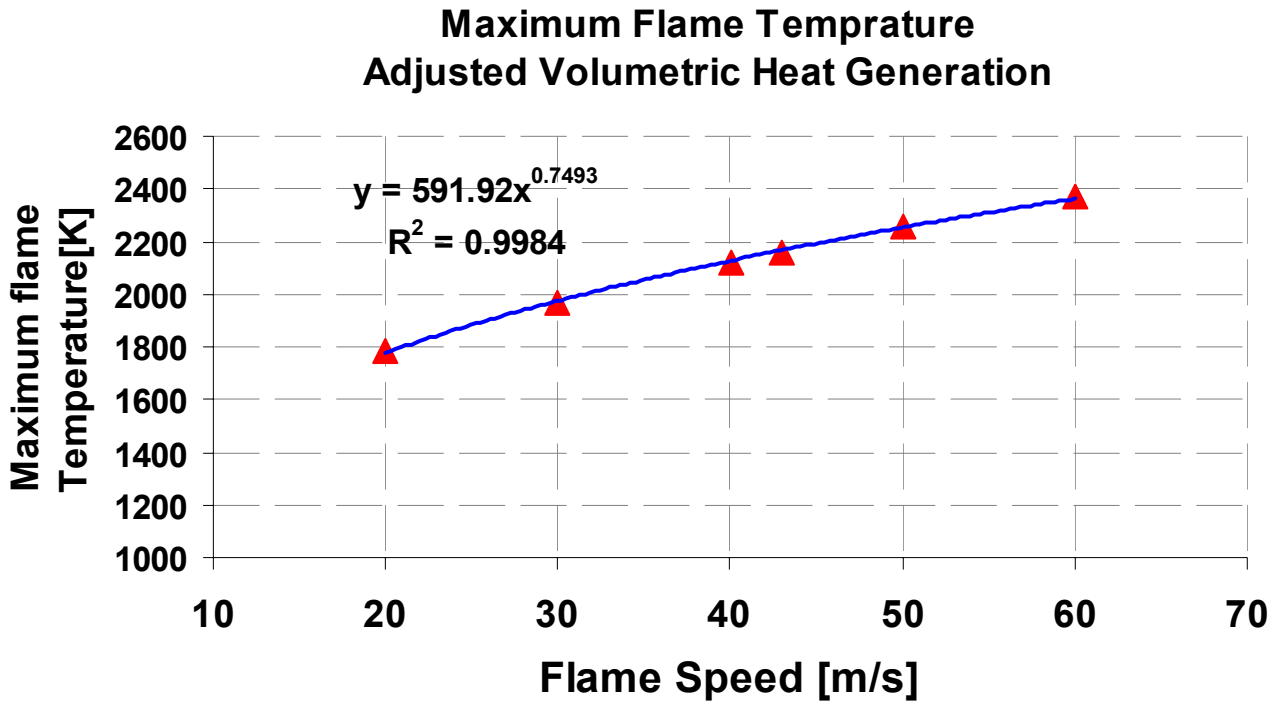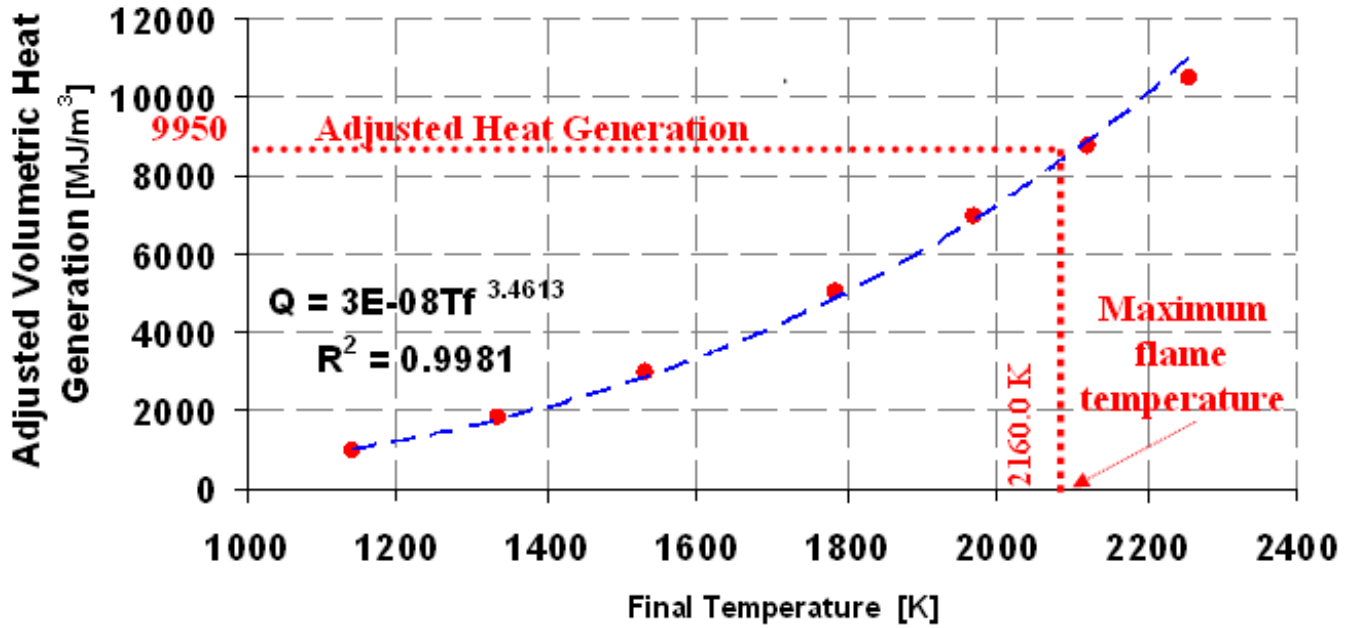
Fig. 4-3. Adjustment of heat generation due to heat loss through the substrate

The speed of the flame front, the heat loss through the substrate, and the density of the product impact the maximum temperature of the flame front. Thin film with a different number of bi-layer but the same total thickness can have a different flame front speed. The maximum combustion temperature can change as the number of bi-layer is increased. As flame travels faster over the substrate, the instantaneous amount of thin film that reacts (length of flame) should be adjusted as well as the density of the product behind the flame. Also in order to have a steady flame, the heat loss should be stable and in an acceptable range. Unstable or over range heat loss can quench the flame. To control the heat loss, the thickness of silica must reach its maximum heat penetration depth which also prevents the huge heat loss through the silicon. To find this maximum heat penetration depth, the thickness of silica should be increased until the maximum calculated temperature becomes independent from the thinness of the silica. Fig. 4 compares the impact of the following four variables; the number of bi-layers, the length of the flame, the thickness of silica, and the speed of the flame front. Thin film with a higher number of bi-layers but the same total thickness has a higher flame front speed with less concentration of products. Flame with a higher speed loses less heat through the substrate as well as the product, thus less material (a shorter flame) should be consumed to keep the flame in self-sustained mode. Due to the less heat loss through the substrate, the heat penetration depth is smaller, so the flame should be steady with a smaller silica thickness.
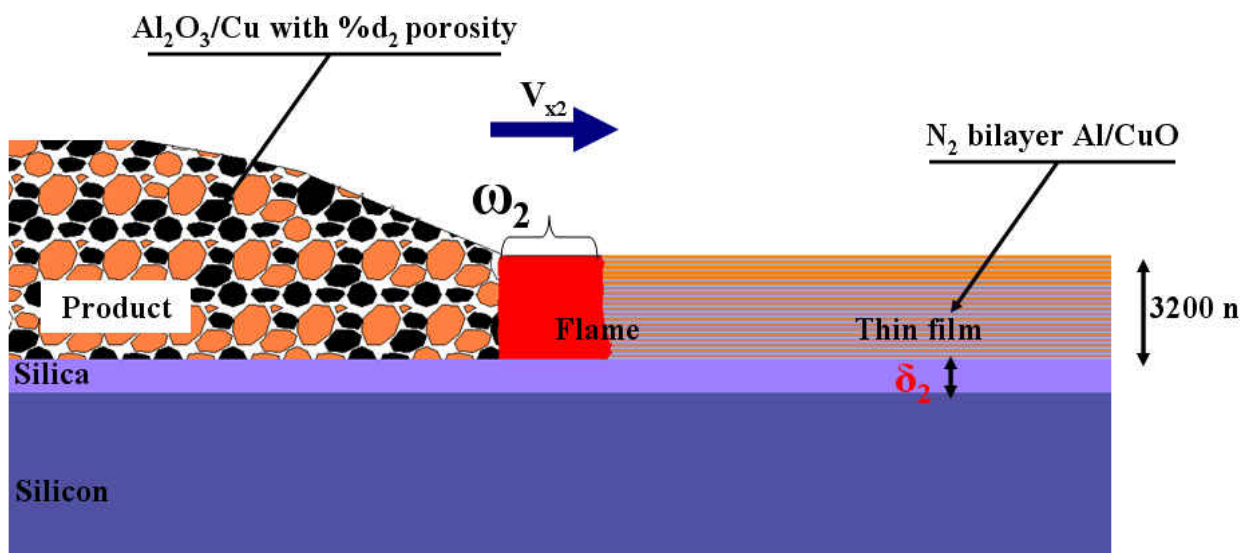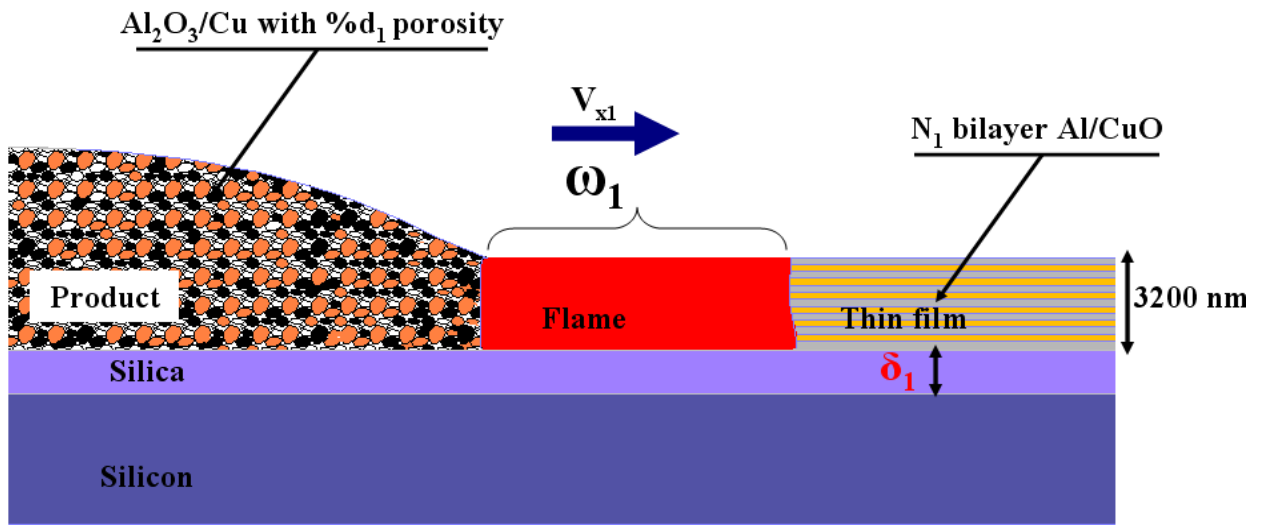
Fig. 4-4. Compare the flame characters in high and low speed

$$N_2 \geq N_1 \begin{cases} V_2 \geq V_1 \\ \omega_1 \geq \omega_2 \\ d_1 \geq d_2 \\ \delta_2 \leq \delta_1 \end{cases}$$

<u>Reaction heat loss (thickness of silica substrate)</u>

It is possible to control the heat at the flame front by placing a substrate underneath the heat source. Absorbing the heat that is generated in the flame can reduce the speed of the flame and quench the reaction [35]. The substrate can absorb a significant amount of heat at the front of the flame. Using different materials with high to low thermal conductivity can reduce the speed of the flame or even stop it. Poor conductive material absorbs less heat, boosts the speed of the flame, and causes reaction at a higher rate. On the other hand, highly conductive materials have opposite effects on the speed of the flame. In some experiments with high conductive substrates, heat loss through the substrate is relatively high, so the flame cannot remain in self-sustained mode, and the reaction takes place only on a few top layers of the thin film.

Heat loss to the substrate has a main role in determining the speed of the flame. The heat becomes a control variable by utilizing different heat sinks for the flame. Part of the generated heat can be absorbed by the substrate if a thin layer of material with low conductivity (silica) is deposited over a high conductive material (silicon). Thickness of deposition can be varied and affects the speed of the flame.   As the thickness of silica increases, the amount of heat that is dissipated through the silicon decreases due to the low conductivity of silica. Extra heat transfers through the silica and increases the maximum flame temperature.

Fig. 5 profiles the temperature at the interface of the thin film and a substrate. These profiles become similar, while the silica thickness increases. As this thickness passes the maximum heat penetration depth, there is no extra heat available to raise the temperature.

www.manaraa.com

Therefore, the temperature distribution within the substrate becomes stable. Penetration depth is the maximum distance that heat travels through the substrate (Fig. 5).
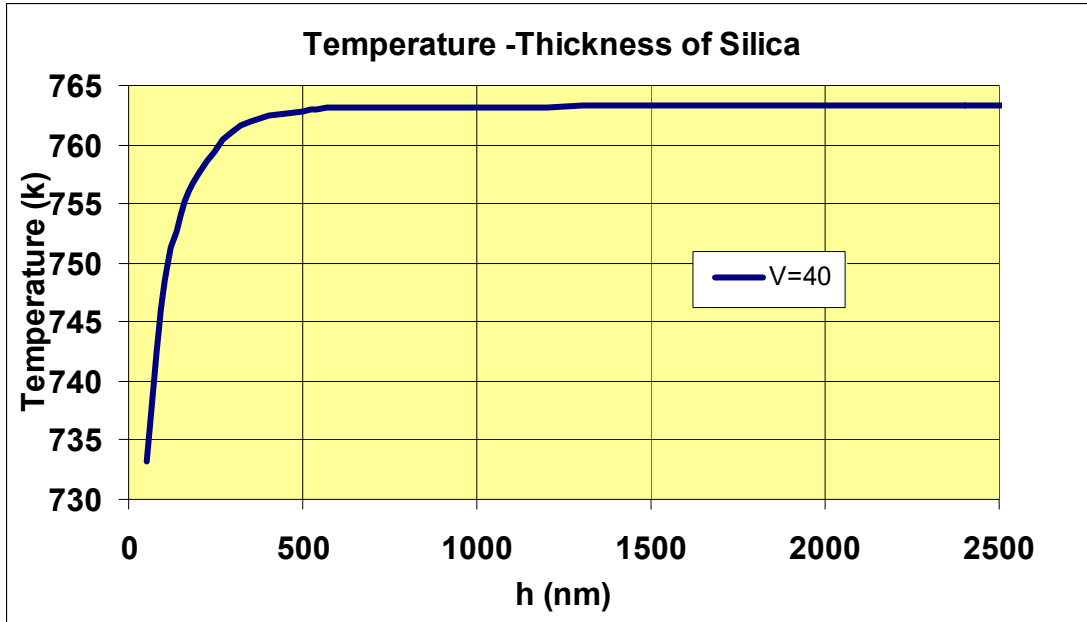
Fig. 4-5. Calculated temperature within penetration depth of substrate

In order to find the flame in a steady state mode, the model should be solved with maximum penetration depth. Thickness of the silica is increased until the maximum temperature becomes independent from this thickness. Fig. 5 compares the maximum temperature distribution within the computational domain, while the thickness of the substrate is increased.

66

<u>Speed of flame front</u>

Speed of flame front is another distinctive characteristic of the thin film reaction. In this study, speed of flame front is considered constant across the sample after the thin film is fully ignited, which is proved by a number of experimental measurements [103]. Speed of flame front has a major role in the experimental evaluation. It is practically impossible to capture the combustion temperature due to the high speed of the reaction. This speed is a measurable value and it can be used to evaluate and compare the temperature result for different cases. Numerical and experimental evaluations also suggest that speed of flame can represent the stability of the flame and heat loss through the substrate. Consequently, controlling the heat loss can directly impact the speed of flame front. Flame should be considered stable within $100\% \pm 0.5\%$ maximum flame temperature as the thickness of silica approaches to the maximum penetration depth. In numerical model, thickness of silica was increased for any given speed of flame front until maximum calculated temperature reaches to the balance point. It is expected that the maximum thickness of silica would be equivalent to maximum penetration depth for any nominated speed. The stability of flame front speed can be used as an indicator of the final combustion temperatures of the reaction, making it unnecessary to measure the temperature value.

<u>Length of flame</u>

Length of the flame is an indicator of the self-sustainability of the reaction. In order for the flame to remain in self-sustain mode, its temperature should stay at a certain level above ignition temperature. Energy within the flame zone should also balance along with the mass and species according to the black box theory. In any situation, length of the flame should satisfy these two conditions. Chemical reaction is the source of heat

67

generation within the flame area. Product, substrate, and preheated area are three major sources of the heat loss in the flame zone. In stationary situation, heat loss always balances the total energy within the flame area without changing the dimensions of the flame zone, but this can not be true when the flame zone is moving based on the rate of chemical reaction. Fast movement of the flame is caused by higher chemical energy generation. Also, the reaction zone loses less energy to the surroundings due to the faster movement of the flame. In order to keep the temperature at self-sustain level, length of the flame should be reduced. In other extreme case, if the chemical reaction is slowed down, the speed of the flame will be reduced, and the flame zone lose more energy. To maintain the flame temperature at a certain level, length of the flame should be increased. This type of balancing is part of the nature of the flame, and it should be defined in numerical model.

Volumetric heat generation can be represented by volume of thin film which reacts at any instant. In two-dimensional models, this volume is presented as length of the flame. The length of flame is specified within geometry of the model for any nominated flame front speed, and it is gradually adjusted until maximum combustion temperature meets the expected value. This adjustment must be accompanied by appropriate thickness of silica substrate. Length of flame for each nominated speed is calculated by comparing the penetration depth:

$$\delta_i = K\sqrt{4\alpha t} \quad (10)$$

$$\omega_i = v_i.t = v_i.\frac{\delta_i^2}{4K.\alpha} \quad (11)$$

Length of flame for 43 m/s ($\omega_{@43m/s}$) was calculated based on measured penetration depth in 43 m/s flame speed [115]. Length of flame for other nominated speeds can be calculated based on the following function:

$$\frac{\omega_i}{\omega_j} = \frac{v_i}{v_j} \cdot \frac{\delta_i^{\,2}}{\delta_j^{\,2}} \quad (12)$$

<u>Product concentration</u>

The medium that is surrounded the flame zone should not have any influence on the reaction of dense multilayer aluminum and copper oxide. In the bulk reaction, oxygen has a major impact on this type of oxidation-reduction reaction, while dense multilayer film is independent of any influences. Weihs et al. [34] investigated a number of aluminum and copper oxide reactions under the isolated chamber without the presence of air (noble gas such as argon was used). The results indicate that the reaction is taken place with the presence of neither air nor oxygen.

The surrounding medium (air) has an influence on the product side of the reaction. Significant temperature gradient between the loose products (mixture of solid, liquid phase) and the sounding environment is a proper condition to force medium (air) to move into the product zone. Fig. 6 shows a simple image of air movement within the product side which is the source for the porosity of the products. In this figure, the height of the material is gradually elevated directly proportional to the air volume that is entering the product side. Close to the reaction zone, the height increase of the material is relatively negligible, and it would be noticeable far down the stream.

69
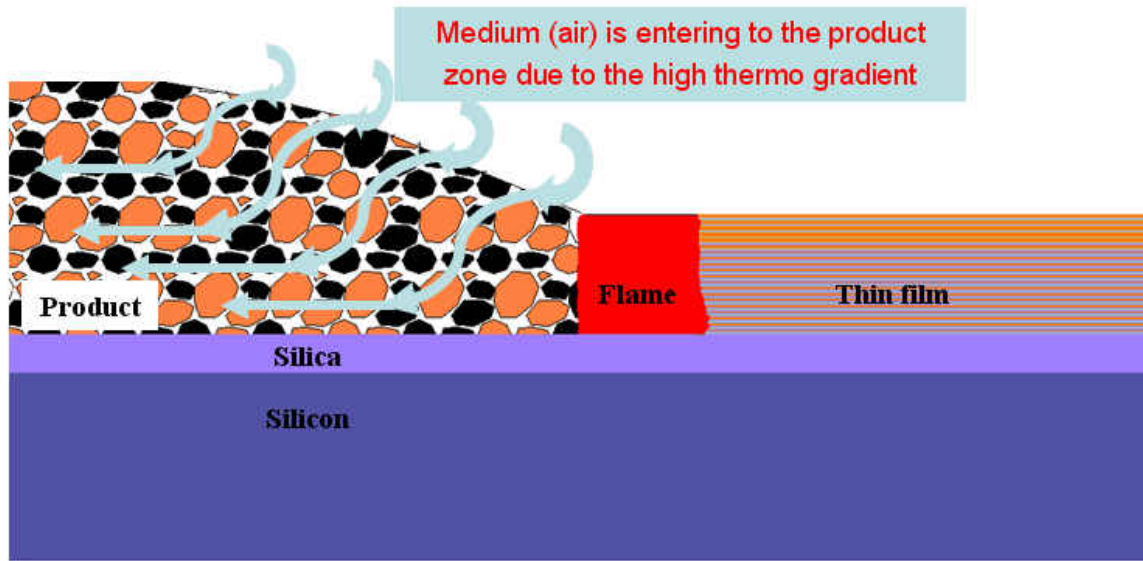
Fig. 4-6. Schematic path for air movement within the product area

John J Moore et al. [61] closely monitored a number of combustion synthesis of advance material in thin film. Their experimental observations suggested that the product porosity is a part of characteristic of the flame, and it would vary based on flame front speed [121-122]. These studies show the porosity of the product behind the flame is related to the curvature of flame speed. Numerical study shows that the Maximum flame temperature reaction zone is impacted by the porosity of the product behind the flame. Porosity can be manipulated by adjusting the properties of product behind the reaction zone. In this case, density of the product was reduced by adding air as a replacement for the product.

$$\alpha \cdot \rho_{product} + (1-\alpha)\rho_{air} = \rho_{com} \quad (13)$$

Since the second term in the above function is relatively negligible, the function is reduced to the following:

70

$$\alpha \cdot \rho_{product} = \rho_{com} \quad (14)$$

The Maximum flame temperature is used as a target to estimate the density of the product for different flame front speed. The final density of the product must be correlated to the curvature of flame front speed. To validate the final result, the density of the product should be inversely proportional to the second power of flame speed.

$$\rho_{product} \propto \frac{1}{v^2} \quad (15)$$

Heat transfer in micro and nanoscale geometry

Heat flows within the solid by carrying energy with electrons in metals and lattice vibration phonons, in insulator and semiconductor. Mean free path of electrons' and phonons' have an important role in the rate of heat transfer within the solid and across the interfaces. As geometry of the object shrinks to micro and nanoscale, electrons' and phonons' movements are limited to these low scale geometries as well as the heat rate. The difference may be negligible in low temperature due to limitation on electrons and phonons movements, but it would be significant in high temperature [82-84]. The same study also shows transient heat transfer is more sensitive to low scale geometry than steady state cases. In order to use Fourier law as a reliable function in micro and nanoscale objects, heat conductivity of the material should be modified. The following is the typical definition for thermal conductivity of the material (Rohsenow and Choi, 1961).

$$k = \frac{1}{3} C \cdot v \cdot \Lambda$$

For thermo conductivity of metals C is the specific heat, v is the Fermi velocity, and Λ is mean free path of electron. For thermo conductivity of dielectrics and semiconductors C is the specific heat of phonon, v is the average speed of sound, and Λ is the phonon mean free path. Reduction in mean free path of electrons and phonons in high temperature environments directly impacts the thermo conductivity of low scale material. Cahill et al. [86, 87] investigates the impact of the low scale heat transfer on a number of different materials such as aluminum, copper, silicon, silicon oxide, and diamond. Final results show that the scaling impact is not similar in all the materials, and it would be different for each case.

The heat transfer properties of martial in this numerical model are in micro and nanoscale zone, and it should be slightly different than the macroscale properties. The majority of material properties that are used in this model are based on the existing experimental values in the literature search. There are still some gray areas in this field of study, and mitigation risks should be considered for this type of numerical simulation.

Heat transfer across the interfaces is the second concern in the heat transfer study in micro and nanoscale geometry. Types of materials, quality of contact surfaces, and quality of materials are the major factors impacting the heat transfer across the interfaces. Study shows [86] that organic materials are more sensitive to heat transfer across the interfaces relative to none organic materials. Cahill et al. presented their experiences with multilayer micro and nanoscale organic and none organic materials. Conductivity of none

organic material is independent of the dimension and the thickness of materials. Thin films with a perfect surface contact are less sensitive to heat transfer rate at the cross interface in micro and nano scale objects. In this study all materials are none organic, and quality and surface contact between materials are assumed to be perfect so no additional correction is necessary for heat transfer across the different interfaces in this numerical model.

Numerical model

<u>Two-dimensional model of a moving heat source over a composite substrate</u>

A moving heat source is simulated similarly to the friction stir welding concept presented by M. Song and R. Kovacevic model [123]. In a welding process, the tool that moves along the weld join can be considered a moving heat source over the plate. Similarly, in this study, the flame moving along the substrate through complex chemical and physical mechanism can simply be modeled as a moving heat source. The coordinate of the computation domain is attached to the moving control volume. This coordinate transformation changes the heat transfer problem to a stationary convection-conduction problem (Fig. 6).
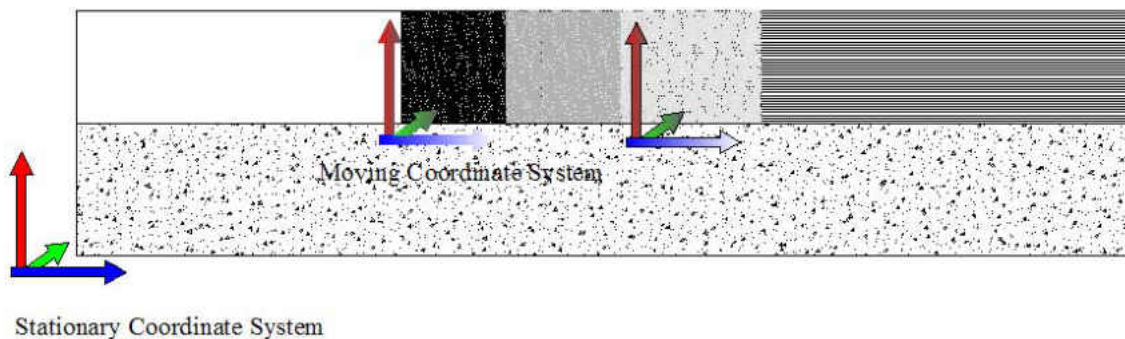
Fig. 4-7. Moving the frame of reference

This model includes some simplifications; the coordinate transformation assumes the thin film and substrate to be infinitely long in the direction of flame propagation. However, this analysis does not take into account the edge effects at the start and end of the plate. Furthermore, the model does not include any variation of concentration profile within the flame. A general model is developed based on energy equation 16.

$$\rho \cdot c_p \left[\frac{\partial T}{\partial t} + V \cdot \nabla T \right] = Q + \nabla \cdot (k\nabla T) - \frac{2}{3}\mu(\nabla \cdot V)^2 + 2\mu S : S + \beta T \frac{Dp}{Dt} \quad (16)$$

Pressure during the reaction of non-organic material such as aluminum and copper oxide is considered constant. This further simplifies the main equation to the following:

$$\rho \cdot c_p \left[\frac{\partial T}{\partial t} + V \cdot \nabla T \right] = Q + \nabla \cdot (k\nabla T) - \frac{2}{3}\mu(\nabla \cdot V)^2 + 2\mu S : S \quad (17)$$

Velocity is constant during reaction so equation (3-2) can be simplified as:

$$\rho \cdot c_p \left[\frac{\partial T}{\partial t} + V \cdot \nabla T \right] = Q + \nabla \cdot (k\nabla T) \quad (18)$$

The reaction is considered to be a steady process and the model is not time dependent, therefore:

$$\rho \cdot c_p (V \cdot \nabla T) = Q + \nabla \cdot (k\nabla T) \quad (19)$$

The general equation includes the conduction and convection terms.

$$Q - \rho \cdot c_p (V \cdot \nabla T) = \nabla \cdot (-k\nabla T) \quad (20)$$

$$V(x, y, z) = u\hat{i} + v\hat{j} + w\hat{k} \quad (21A)$$

$$Q - \rho \cdot c_p \left(u\frac{\partial T}{\partial x} + v\frac{\partial T}{\partial y} + w\frac{\partial T}{\partial z} \right) = \nabla \cdot \left(-k\left(\frac{\partial T}{\partial x}\hat{i} + \frac{\partial T}{\partial y}\hat{j} + \frac{\partial T}{\partial z}\hat{k} \right) \right) \quad (21)$$

$$Q - \rho \cdot c_p \left(u \frac{\partial T}{\partial x} + v \frac{\partial T}{\partial y} + w \frac{\partial T}{\partial z} \right) = \left(-k \left(\frac{\partial^2 T}{\partial x^2} + \frac{\partial^2 T}{\partial y^2} + \frac{\partial^2 T}{\partial z^2} \right) \right) \quad (22)$$

The third dimension (z) is negligible due to the existing symmetry. The governing

equation can be further simplified as:

$$Q - \rho \cdot c_p \left(u \frac{\partial T}{\partial x} + v \frac{\partial T}{\partial y} \right) = \left(-k \left(\frac{\partial^2 T}{\partial x^2} + \frac{\partial^2 T}{\partial y^2} \right) \right) \quad (23)$$

Material moves through the flame only along the x axis in the moving reference frame;

therefore velocity vector, $V(x,y,z) = u\hat{i} + v\hat{j} + w\hat{k}$, can be simplified to $V(x,y,z) = u\hat{i}$,

and the main equation is simplified to:

$$Q - \rho \cdot c_p \left(u \frac{\partial T}{\partial x} \right) = \left(-k \left(\frac{\partial^2 T}{\partial x^2} + \frac{\partial^2 T}{\partial y^2} \right) \right) \quad (24)$$

Q is calculated based on the heat generation which is produced during the chemical

reactions within the flame. S.H. Fischer [29] tabulated volumetric heat generation of

aluminum and copper oxide. Density (ρ) and coefficient (c_p) are considered constant

based on a concentration profile within flame. Fig. 3-6 shows the typical geometry of the

thin film and substrate model. The velocity is considered to have a constant magnitude,

in which the material moves toward the negative side of the x-axis.

Boundary conditions should be specified at 10 different interfaces of the model. Fig. 7

shows the computational domain for the two-dimensional model.
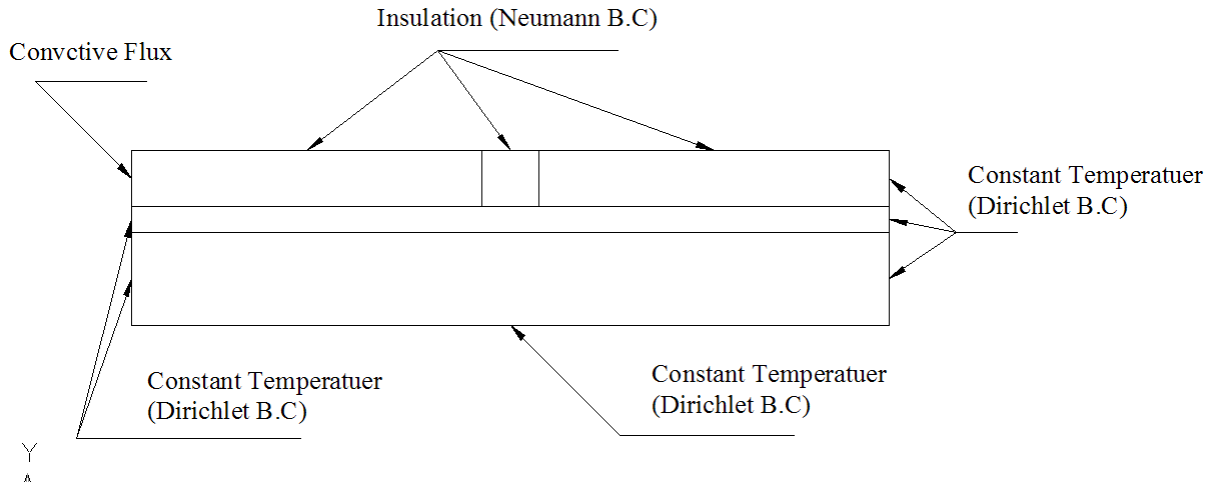
Fig. 4-8. Boundary conditions for two-dimensional model of moving heat source

$$T(x = -\infty, -3.2nm > y > 3.2 + h) = 300K \text{ (25)}$$

$$T(x = -\infty, -3.2nm + h > y > -\infty) = 300K \text{ (26)}$$

$$K\frac{\partial T}{\partial x}(x = -\infty, 0 > y > 3.2nm) = h(T - T_{IN}) \text{ (27)}$$

$$k\frac{\partial T}{\partial y}(x = \pm\omega/2, y = 0) = 0 \text{ (28)}$$

$$\frac{\partial T}{\partial y}(-\infty \le x \le -\omega/2, y = 0) = 0 \text{ (29)}$$

$$\frac{\partial T}{\partial y}(\omega/2 \le x \le +\infty, y = 0) = 0 \text{ (30)}$$

$$T(x = +\infty, y) = 300K \text{ (31)}$$

$$T(x, y = \infty) = 300K \quad \text{(32)}$$
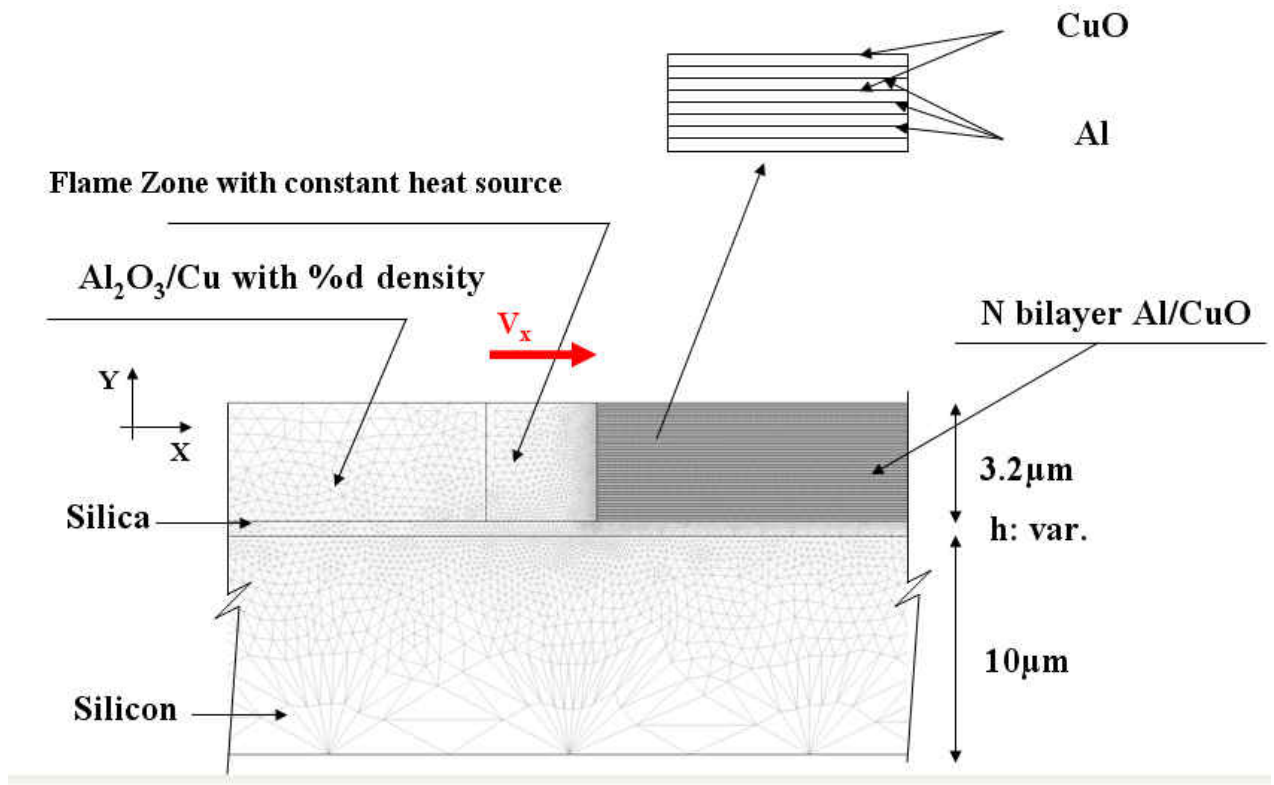
Fig. 4-9. Computational domain for a standard thin film over composite substrate

Numerical procedure

Numerical solution is the only approach for solving the two-dimensional moving flame problems. The thin film and substrate is moved through the flame with constant speed, and the temperature profile is taken to be steady. The heat generation within the flame area increases with the rising temperature of the materials within the flame and preheat zone. Heat penetrates inside the substrate along the path of the motion (x-axis). Heat lost due to radiation can be neglected because of significant differences between the length of the flame and surface contact. This two-dimensional conduction-convection model cannot be solved analytically. Therefore, a numerical approach based on the finite element method is adopted using commercial software, COMSOL. A two-dimensional moving heat sources with composite substrate model was solved numerically.

COMSOL is developed based on FEMLAB. It is a powerful, interactive environment for modeling and solving scientific and engineering problems based on partial differential equations. It can easily extend the conventional models that address one branch of physics to the state-of-the art. Multiphysics module relates multiple branches of science and engineering such as chemical, and heat transfer. These Models are built simply by defining the relevant physical quantities rather than defining the equations directly. FEMLAB then internally compiles a set of PDEs representing the problem. FEMLAB is also capable of creating equation-based models. Besides providing these multiple modeling approaches, FEMLAB offers multiple ways to harness this power, either through a flexible self-contained graphical user interface or from the MATLAB prompts.

<u>Governing equation and Boundary conditions</u>

The governing equations for the flame over the composite substrate which is moving along the x direction are as follows:

Governing equation within flame is

$$Q - \rho_0 \cdot c_{p0}\left(u\frac{\partial T}{\partial x}\right) = \left(-k_0\left(\frac{\partial^2 T}{\partial x^2} + \frac{\partial^2 T}{\partial y^2}\right)\right) \quad (33)$$

Governing equation inside the flame front is

$$\frac{\partial^2 T}{\partial x^2} + \frac{\partial^2 T}{\partial y^2} = \frac{u}{\alpha_1}\frac{\partial T}{\partial x} \quad (34)$$

Governing equation behind the flame is

$$\frac{\partial^2 T}{\partial x^2} + \frac{\partial^2 T}{\partial y^2} = \frac{u}{\alpha_2}\frac{\partial T}{\partial x} \quad (35)$$

Governing equation within immediate substrate is

$$\frac{\partial^2 T}{\partial x^2} + \frac{\partial^2 T}{\partial y^2} = \frac{u}{\alpha_3}\frac{\partial T}{\partial x} \quad (36)$$

Governing equation within second substrate is

$$\frac{\partial^2 T}{\partial x^2} + \frac{\partial^2 T}{\partial y^2} = \frac{u}{\alpha_4}\frac{\partial T}{\partial x} \quad (37)$$

ρ_0, c_{p_0}, k_0 represent the properties of the reactant and product with constant concentration. Q is volumetric heat generation of aluminum and copper oxide [29]. α_1 and α_2 are thermal diffusivity coefficients for the reactant and product with constant

79

concentration within the flame front and behind the flame. α_3 and α_4 are thermal diffusion coefficients of the composite substrate. In this study, these values relatively correspond to the silica (α_{SiO_2}) and silicon (α_{Si}). Boundary conditions are defined similarly to the case of friction stir welding in composite substrates.

Variable mesh was used in this model and the number of elements was increased along the interface and flame zone. Appropriate space discretization can improve both the accuracy and stability of the solutions. In the following chapter, the discretization and final geometry of the model is described in more details.

Implicit Method

The implicit method was used to carry out the computations. Since the flame speed is constant, time is proportional to the x coordinate of motion. Therefore, forward differencing was used for the x direction and central differencing was used for the y direction.

$$\frac{\partial T}{\partial x} = \frac{T_{i+1} - T_i}{\Delta x} + O(\Delta x) \qquad \text{(Forward differencing) (38)}$$

$$\frac{\partial^2 T}{\partial y^2} = \frac{T_{i+1} - T_i + T_{i-1}}{\Delta y^2} + O(\Delta y^2) \quad \text{(Central differencing) (39)}$$

$$\frac{\partial^2 T}{\partial x^2} = \frac{T_{i+2} + T_i - 2T_{i+1}}{\Delta x^2} + O(\Delta x^2) \quad \text{(Forward differencing) (40)}$$

The finite difference form of the differential equation within flame zone is

$$\frac{Q}{k_0} - \frac{u}{\alpha}\left(\frac{T_{i+1} - T_i}{\Delta x}\right) = \frac{T_{i+1} - T_i + T_{i-1}}{\Delta y^2} + \frac{T_{i+2} + T_i - 2T_{i+1}}{\Delta x^2} + O(\Delta y^2, \Delta x) \quad (41)$$

Differential equation within flame and within substrate is:

$$\frac{u}{\alpha}\left(\frac{T_{i+1} - T_i}{\Delta x}\right) = \frac{T_{i+1} - T_i + T_{i-1}}{\Delta y^2} + \frac{T_{i+2} + T_i - 2T_{i+1}}{\Delta x^2} + O(\Delta y^2, \Delta x) \quad (42)$$

At the interface between flame zone and substrate, Pletcher [108] recommended a harmonic mean thermal conductivity, k_e. For instance, the harmonic mean of thermal conductivity for the interface between silica and silicon is calculated as follows:

$$k_e = \frac{k_{SiO_2} \cdot k_{Si}}{k_{SiO_2} + k_{Si}} \quad (43)$$

k_{SiO_2} and k_{Si} is thermal conductivity of silica and silicon, respectively.

$$\frac{v}{\alpha_{SiO_2}}\left(\frac{T_{i+1} - T_i}{\Delta x}\right) = \frac{T_{i+1} - T_i + T_{i-1}}{\Delta y^2} + \frac{T_{i+2} + T_i - 2T_{i+1}}{\Delta x^2} \quad (44)$$

$$\frac{v}{\alpha_{Si}}\left(\frac{T_{i+1} - T_i}{\Delta x}\right) = \frac{T_{i+1} - T_i + T_{i-1}}{\Delta y^2} + \frac{T_{i+2} + T_i - 2T_{i+1}}{\Delta x^2} \quad (45)$$

$$\frac{v}{\alpha_e}\left(\frac{T_{i+1} - T_i}{\Delta x}\right) = \frac{T_{i+1} - T_i + T_{i-1}}{\Delta y^2} + \frac{T_{i+2} + T_i - 2T_{i+1}}{\Delta x^2} \quad (46)$$

α_e is the harmonic mean of the thermal diffusion coefficient, k_e, for elements at the interface of silica and silicon.
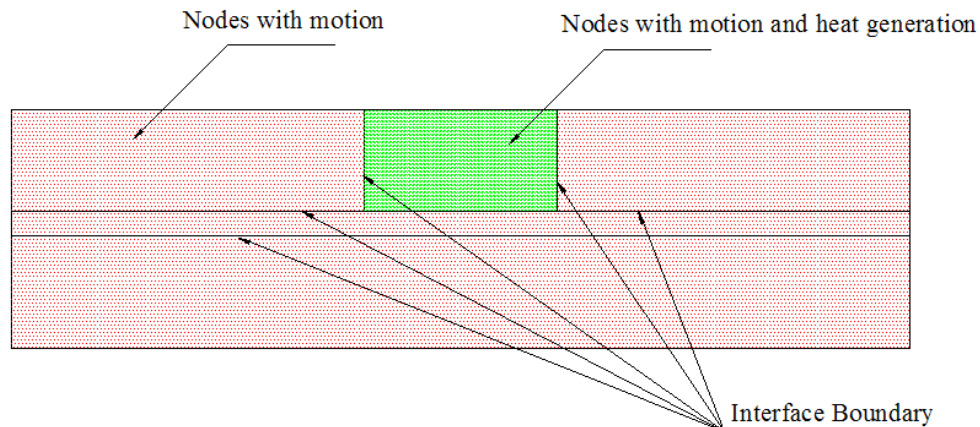
Fig. 4-10. Interfaces within computational domain

Equation 44, 45, and 46 were solved simultaneously using an iteration technique to obtain the temperature profiles. To reduce the uncertainty and increase the accuracy of numerical solutions, the geometry of the substrate is extended to the point that the heat flux on each side of the substrate approaches zero.

A study [99] show that the heat distribution within the flame area based on chemical reaction or any other driven function does not increase the accuracy of the temperature distribution. Even though the heat generation in the flame area is driven based on chemical reaction, heat was distributed uniformly in the numerical model to avoid any unnecessary complexity.   To find the appropriate number of elements in the computational domain, a random number of elements were picked, and the maximum temperature in the exact same geometry was compared. The temperature gets more accurate by increasing the number of elements in the same geometry. Beyond a certain limit (100000-150000 elements) inaccuracy increases due to the truncation error and limitation on computational processing. A 100000-150000 range of elements was chosen

for these calculations. In fact, the uncertainty within the heat transfer model is kept below 0.5%.

Experimental model

Tappan [67] used different types of thin film geometry to create a controllable environment to measure the characteristics of the flame in microscale. Controlling some of these characteristics such, as speed and length of the flame, are necessary to create a comparable controlled environment. Rossi [68] used different types of thin film geometry to create a similar environment. This geometry is used in many micro thin film materials as mechanical and electric devices.

Multilayer Al/CuO, having a total thickness of 3.2 μm, was prepared by magnetron sputter deposition. An Al layer thickness of 26 nm and CuO layer thickness of 54 nm were used to provide a bi-layer period of 80 nm for a standard sample configuration, as illustrated in Fig. 10.
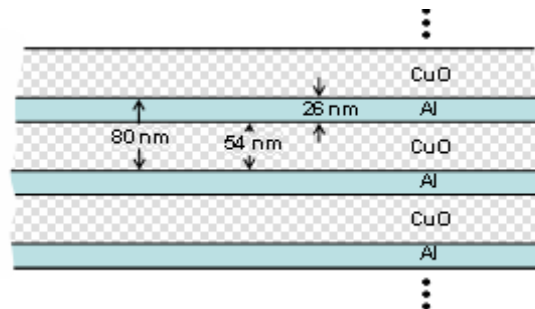
Fig. 4-11. Standard multilayer Al and CuO

An electronic time-of-flight technique was developed using patterned strips of layered multilayer thin film on a substrate , wherein the passage of the reaction front passes through copper contacts spaced along the length of the strip. As the flame ignites on one side of the thin filmstrip, it can propagate with a constant speed across the sample. The

flame can burn each copper strip in equal time increments. This configuration produced a stepwise change voltage, which was digitally acquired and analyzed to determine the propagation velocity. Each copper probe is connected to a series of resistances in the circuit; voltage output can drop at the instant that the flame passes across the copper probes. Several types of substrates for multilayer thin film were examined. Single substrate samples were prepared on glass, photo resist, and silica. In order to control and capture the heat loss from the flame area, a composite substrate of silicon with thick layer of silica was used as the standard substrate. For a typical multilayer thin film (40 bi-layers with 80 nm thickness) over the standard substrate, the speed of flame front jumps up to 43 m/s as the thickness of silica is reached to maximum heat penetration.

Numerical procedure to estimate the characteristics of the flame

In order to utilize the temperature of flame, length of diffusivity, and density of the product, with minimum heat loss for any nominated speed, the following steps were taken.

1. Adiabatic temperature of the flame was calculated as an individual unit cell of the reactants (Al/CuO). Maximum calculated flame temperature should be less than adiabatic flame temperature.

2. Maximum combustion temperature of the reaction Al/CuO, without considering the heat loss through the substrate, was calculated for several nominated speed based on sandwich theory.

3. Actual speed of flame front for a standard multilayer thin film over composite substrate was measured accurately in order to estimate the penetration depth at 43 m/s.

4. In order to justify the accuracy of the numerical model, maximum penetration depth was calculated using numerical model at 43 m/s.

5. Volumetric heat generation corresponding to 43 m/s was corrected in order to match the maximum flame temperature with the expected value in this speed (Correction in sandwich theory due to heat loss through the substrate).

6. Maximum heat generation for the other nominated speed was corrected accordingly

7. Maximum flame temperature for the reaction over the substrate, with a maximum penetration depth thickness of silica, was calculated for all nominated speed using the corrected heat generation in numerical model. The maximum flame temperature should be used as a reference for the other numerical procedure.

Model of moving heat source was used to estimate the length of the flame and the concentration of the product behind the flame.

8. Model was used with initial estimation of the flame length and the nominated density of the product. Maximum penetration depth was calculated by increasing the thickness of the silica and comparing the results. The maximum flame temperature gradually increases in each case until the maximum temperature difference between each two

consecutive temperatures drops below 0.5% (accuracy of the measurement). Thickness of the silica is the maximum penetration depth, and the maximum temperature should match with the temperature at the reference point. If the temperature does not match the reference, the calculation process should be repeated with slightly different flame length. Density of the product behind the flame should be adjusted as well.

9. Process 6 and 7 should be repeated for the other nominated speed.

Chart 12 demonstrates a sample of above process for any nominated speed.
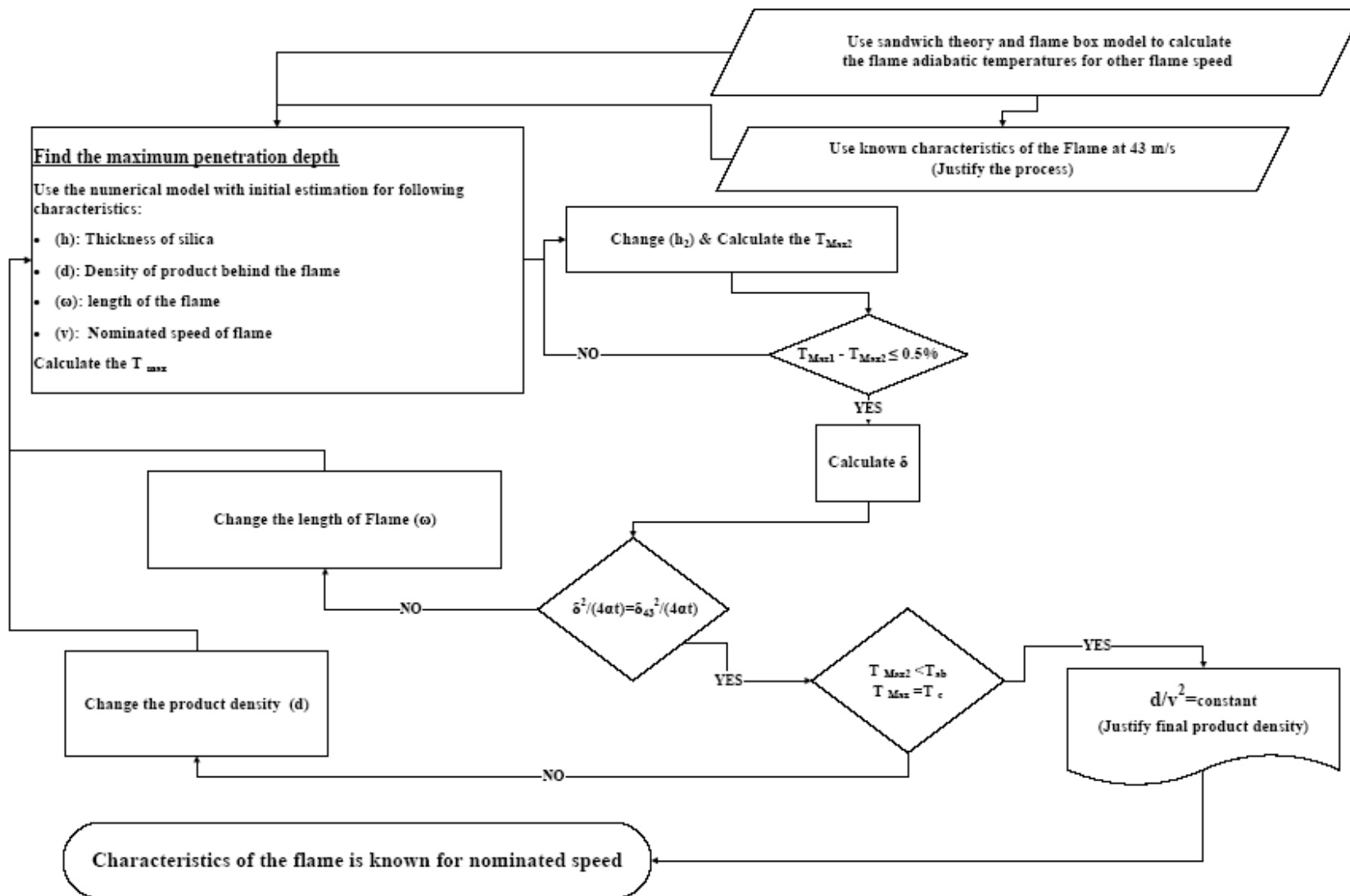
Fig. 4-12.Numerical procedure to estimate the characteristics of the flame

www.manaraa.com

Result

<u>Numerical model result</u>

Numerical approach was used to relate the maximum temperature and speed flame front to three other characteristics of the flame: penetration depth, length of the flame, and concentration of the product behind the flame. Heat loss through the substrate plays an important role in comparing different cases. Composite substrate (silicon\silica) creates a comparable heat loss; therefore, all the characteristics of the flame can be linked to one another for different flame front speed. Generated heat within the reaction zone of the immediate substrate (Silica) is dissipated through the second substrate (Silicon). The heat flow decreases as the thickness of the silica increases, the length of the flame shrinks, and the density of the product reduces.

In this section, numerical model was used to investigate the impact of each characteristic on heat loss and maximum flame temperature. The standard thin film configuration, along with a premeasured speed of flame front (43 m/s), was used as the baseline. Final calculated value for maximum heat penetration was also used as a comparable value to justify the numerical result with experimental observation. While each characteristic of the flame was deviated from the actual value, the baseline configuration was applied to investigate the impact of each individual characteristic on the temperature profile. This comparison helps to find the actual characteristics of the flame for different speed.

Actual length of the flame and density of the product behind the flame corresponding to different flame front speeds (30-70 m/s) were calculated as an ultimate goal of this study.

The calculation details for one additional speed of flame front (50 m/s) and the final result for other speeds are presented.

Characteristics of standard thin film reaction with 43 m/s speed of flame front

The numerical model was used for standard thin film geometry with constant speed of 43 m/s. Maximum flame temperature stabilized as thickness of the silica was reached over 570 nm (table 1). Calculated penetration depth, based on measured speed of flame, also suggests that the speed of flame stabilizes when the silica thickness reaches 500 nm or more.

Calculated maximum flame temperature is much lower than the expected ($2160\pm0.5\%$ K) flame temperature in Fig. 3, so density of the product behind the flame should be adjusted until the flame temperature matches with the expected value. When the density of the product behind the flame was dropped to 69%, the maximum flame temperature rises to 2160 K(the expected value). In fact, 31% air will be mixed with product during this reaction. Table (1) demonstrates all the steps in detail as the density of the product drops from 100 to 69%. In summary, speed of flame front for standard multilayer thin film over the composite substrate reaches to $43+1.5\%$ m/s as the thickness of silica gets close to 500 nm. The calculated length of the flame is 3200 nm, and the product contains 31% air mixture. Also, maximum estimated flame temperature for this reaction is $2160+0.5\%$ K.

Table 4-1. Calculation of characteristic of flame for speed V=43 m/s

	V [m/s]	Peneration Depth [nm]	W [nm]	T [K]	W (Model)	Density of product [%]	h	T @ 43m/s	% delta (Local)	% delta	Error [0.5%]
	43	569.3	3200	2160	3200						
Case 1	43	569.3	3200	2160	3200	100	400	1597.1		26.06018519	0.5000
Case 2	43	569.3	3200	2160	3200	100	500	1605.6	0.52939711	25.66666667	0.5000
Case 3	43	569.3	3200	2160	3200	100	570	1608.73	0.194563413	25.52175926	0.5000
Case 4	43	569.3	3200	2160	3200	75	570	2035.6	20.97022991	5.759259259	0.5000
Case 5	43	569.3	3200	2160	3200	70	570	2147	5.188635305	0.601851852	0.5000
Case 6	43	569.3	3200	2160	3200	65	570	2271	5.460149714	-5.138888889	0.5000
Case 7	43	569.3	3200	2160	3200	66	570	2245	-1.158129176	-3.935185185	0.5000
Case 8	43	569.3	3200	2160	3200	67	570	2219.8	-1.135237409	-2.768518519	0.5000
Case 9	43	569.3	3200	2160	3200	68	570	2195	-1.129840547	-1.62037037	0.5000
Case 10	43	569.3	3200	2160	3200	69	570	2171	-1.105481345	-0.509259259	0.5000

In order to investigate the impact of each character of the flame on maximum flame temperature, final values of each character were deviated from the actual value individually. The numerical model was used to find the maximum temperature value for each case and to compare them. None of the deviated value represents the real flame characteristic and the deviation is only for numerical comparison.

<u>Thickness of silica substrate</u>

In order to investigate the impact of the heat loss through the substrate on the maximum temperature profile, the thickness of silica substrate was increased (between 100 nm and 1500 nm) for the baseline configuration. The maximum flame temperature rises exponentially (Fig. 12) until it reaches to the peak value (2160 K) and it stabilizes. Thickness of silica reaches the maximum penetration depth at $570 \pm 0.5\%$ nm. Temperature profile (Fig. 13) for individual cases shows the impact of silica thickness on the heat loss. The temperature profile for the cross-section of both directions of thin film reveals more details regarding heat flow. The temperature profile at the interface of thin film and the substrate (Fig. 14) shows that the maximum temperature profile becomes self-similar as soon as the thickness of silica reaches the maximum heat penetration (570 nm). Also the temperature at the cross-sectional area of the flame shows (Fig. 15) how the heat flow drops and temperature at the interface of silicon and silica reduces as thickness of the silica gets close to the maximum heat penetration of 570 nm.

Impact of Thickness of Silica Substrate on Maximum Flame Temperature

$(V=43 \text{ m/s}, d=69 \%, \omega=3200 \text{ nm})$
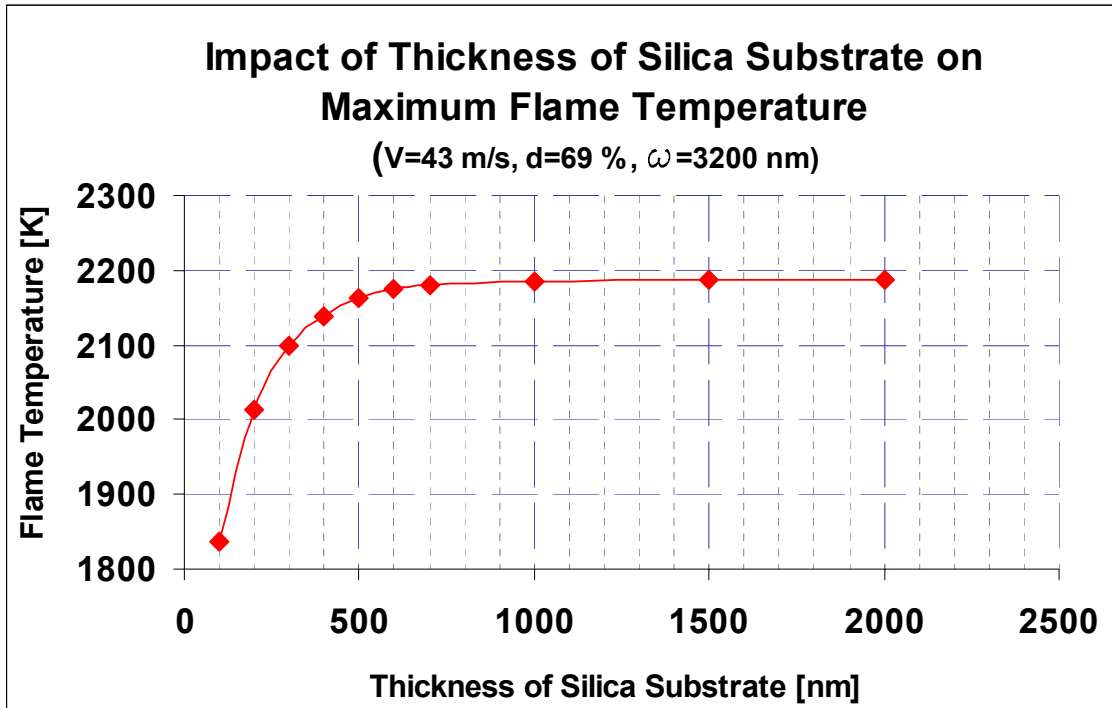
Fig. 4-13. Calculated temperature within penetration depth of substrate

Case 16: h $_{silica}$=100nm, V =43m/s, ω=3200nm, d=69%

Case 15: h $_{silica}$=200nm, V =43m/s, ω=3200nm, d=69%

Case 13: h $_{silica}$=400nm, V =43m/s, ω=3200nm, d=69%
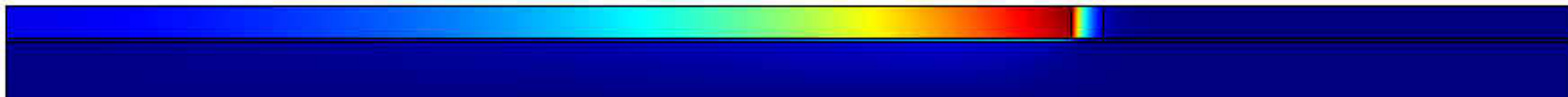
Case 11: h $_{silica}$=600nm, V =43m/s, ω=3200nm, d=69%
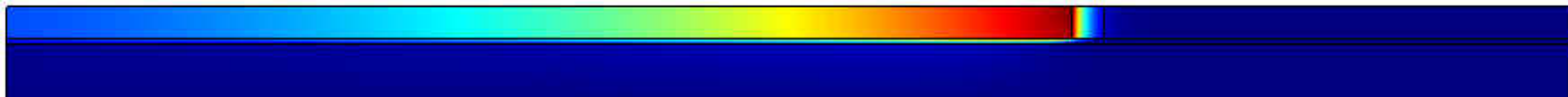
Case 11B: h $_{silica}$=1000nm, V =43m/s, ω=3200nm, d=69%

Case 11C: h $_{silica}$=1500nm, V =43m/s, ω=3200nm, d=69%
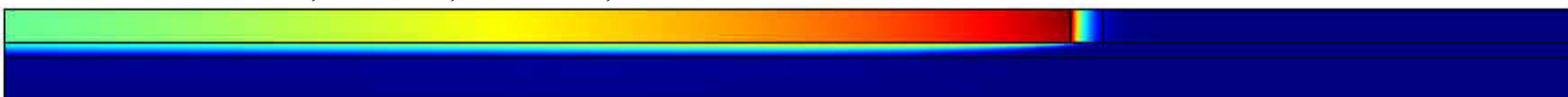
Case 11D: h $_{silica}$=2000nm, V =43m/s, ω=3200nm, d=69%

400   600   800   1000   1200   1400   1600   1800   2000 K

Fig. 4-14. Temperature distribution within computational domain

Fig. 4-15.Temperature profile at the interface of thin film and silica substrate
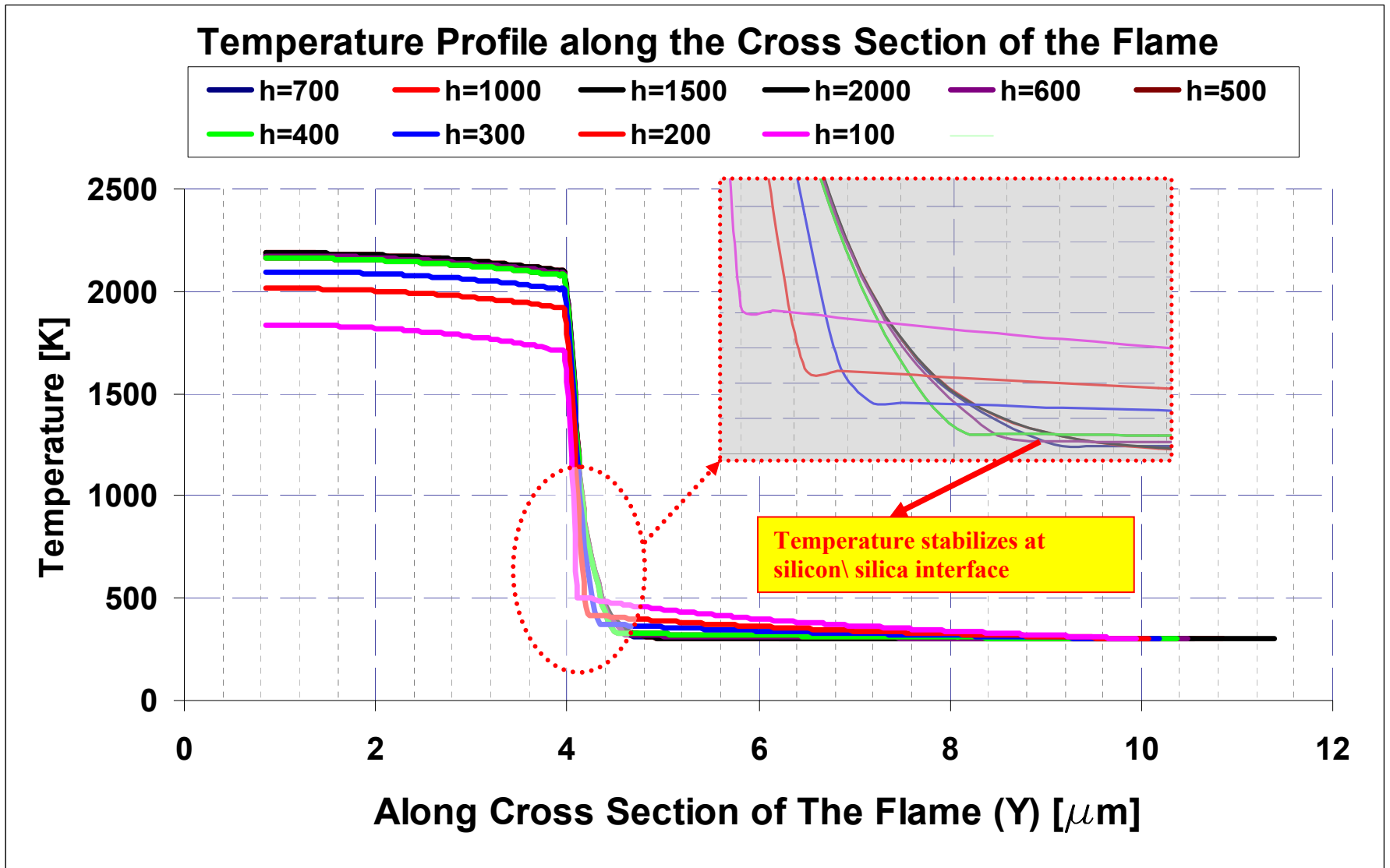
Fig. 4-16. Temperature profile at the cross-section of flame and the substrate

Fig. 16 compares the maximum temperature distribution within the computational domain while the length of the flame increases from 2000 nm to 5000 nm in standard configuration. As the length of the flame increases, more thin film material participates in the reaction and more heat is generated within the flame area however the contact surface area extends. Numerical results (Fig. 16) show that the maximum flame temperature is almost linearly increased as the length of the flame increases. Temperature profile at the interface of thin film (Fig. 17-19) and the substrate shows that the maximum temperature profile does not impact the temperature distribution and maximum heat penetration.
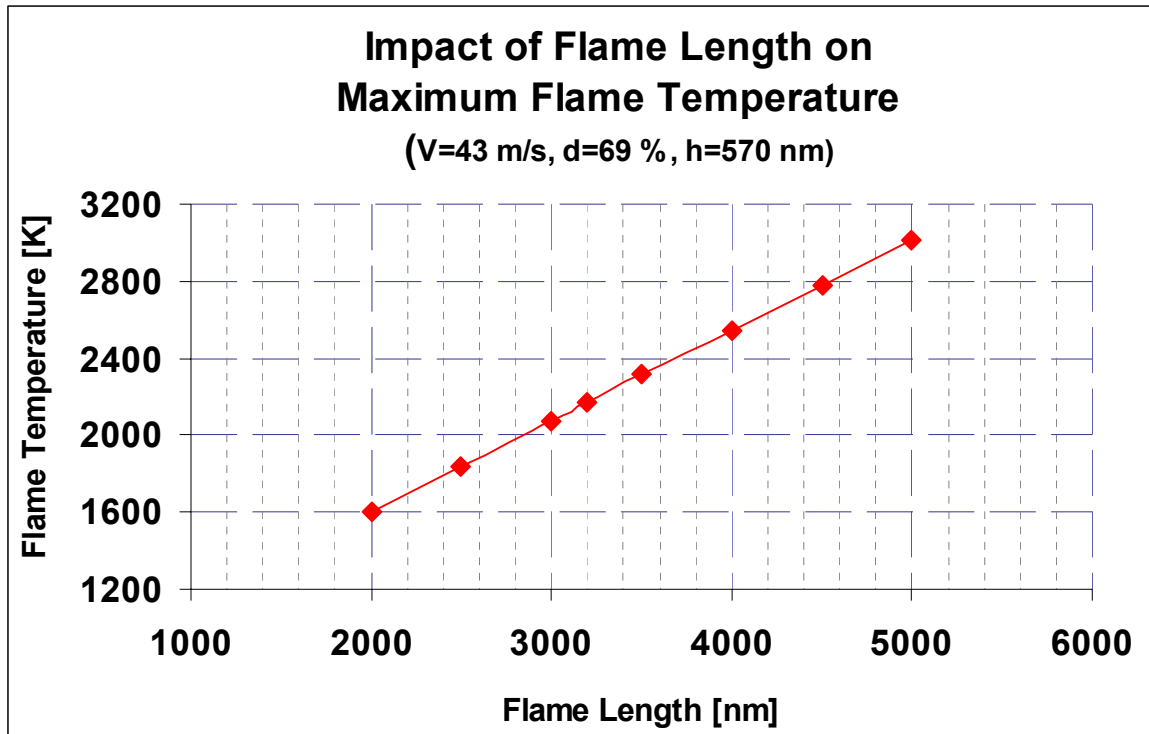
Fig. 4-17.Calculated temperature within penetration depth of substrate

Case 24: h $_{silica}$=570nm, V =43m/s, ω=5000nm, d=69%   T$_{max}$=3017 K

Case 25: h $_{silica}$=570nm, V =43m/s, ω=4500nm, d=69%   T$_{max}$=3070 K

Case 26: h $_{silica}$=570nm, V =43m/s, ω=4000nm, d=69%   T$_{max}$=3070 K

Case 27: h $_{silica}$=570nm, V =43m/s, ω=3500nm, d=69%   T$_{max}$=3070 K

Case 29: h $_{silica}$=570nm, V =43m/s, ω=3000nm, d=69%   T$_{max}$=3070 K

Case 30: h $_{silica}$=570nm, V =43m/s, ω=2500nm, d=69%   T$_{max}$=1839 K

Case 31: h $_{silica}$=570nm, V =43m/s, ω=2000nm, d=69%   T$_{max}$=1602 K

400   T$_{max}$

Fig. 4-18. Temperature profile at the interface of thin film and silica substrate

97

Fig. 4-19. Temperature profile at the interface of thin film and silica substrate
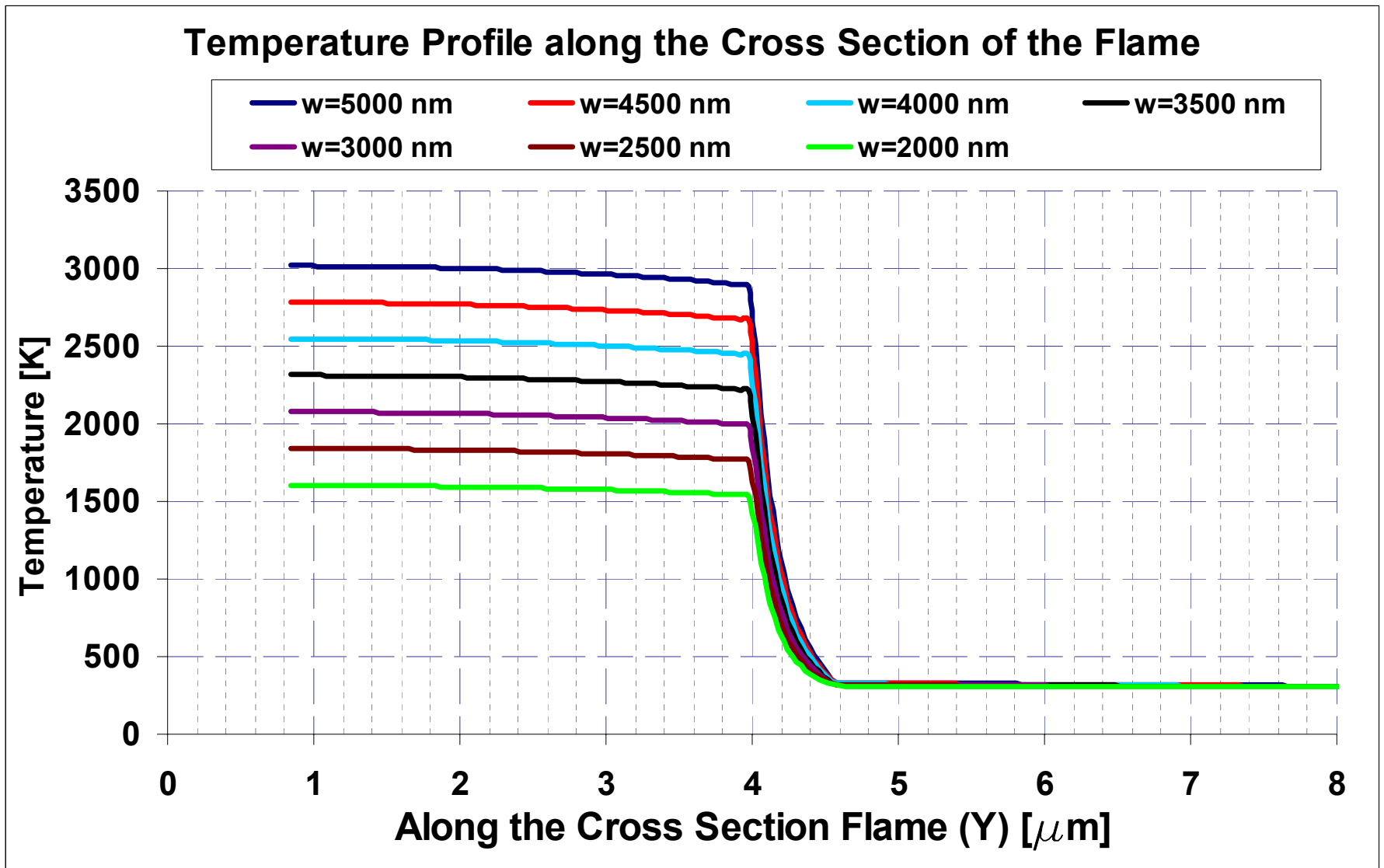
Fig. 4-20. Temperature profile at the cross-section of flame and the substrate

<u>Density product behind the flame</u>

Fig. 21 compares the heat distribution within the computational domain while the density of the product reduces from 100% to 50%. As the density of the product behind the flame decreases, less heat should transfer to the product side, and the excessive heat in the flame area causes the maximum flame temperature to boost. Numerical results (Fig. 20) show that the maximum flame temperature almost linearly increases as density of the product decreases. Temperature profile (Fig. 22-23) at the interface of the thin film and the substrate shows the maximum temperature profile directly offset from the baseline in each case, so the density of the product should not impact the maximum heat penetration depth.
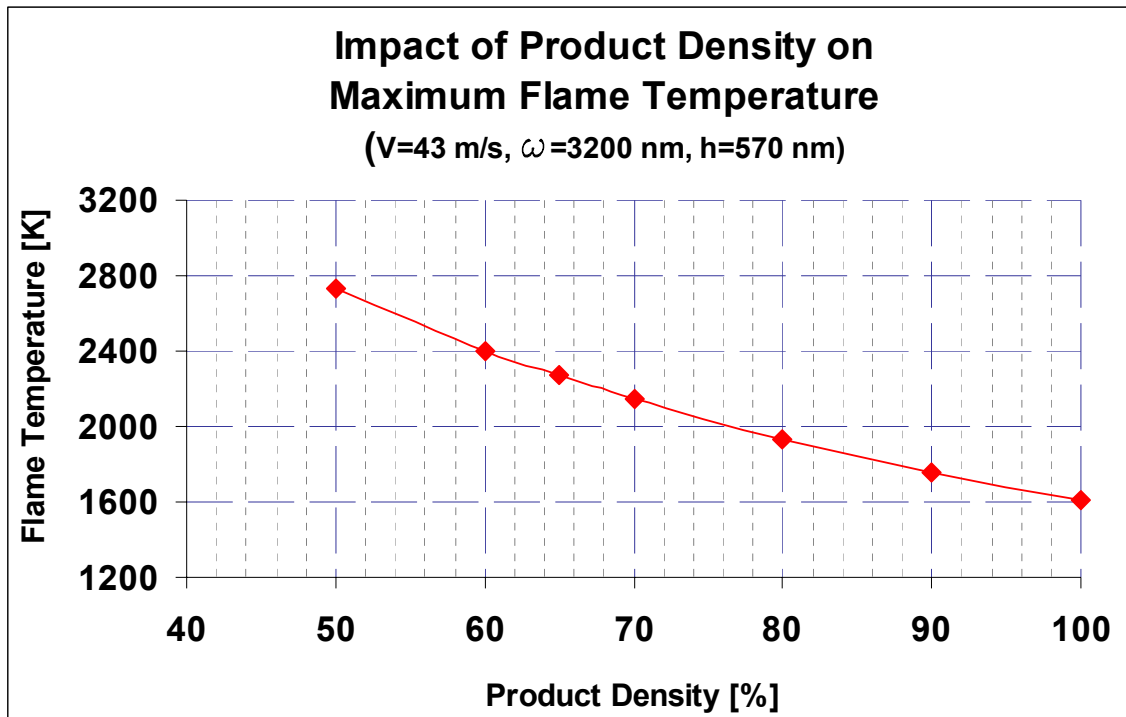
Fig. 4-21. Calculated temperature within penetration depth of substrate

Case 17: h $_{silica}$=570nm, V =43m/s, ω=5000nm, d=100%   T$_{max}$=1608 K

Case 18: h $_{silica}$=570nm, V =43m/s, ω=4500nm, d=90%   T$_{max}$=1757 K

Case 19: h $_{silica}$=570nm, V =43m/s, ω=4000nm, d=80%   T$_{max}$=1934 K

Case 20: h $_{silica}$=570nm, V =43m/s, ω=3500nm, d=70%   T$_{max}$=2147 K

Case 21: h $_{silica}$=570nm, V =43m/s, ω=3000nm, d=65%   T$_{max}$=2271 K

Case 22: h $_{silica}$=570nm, V =43m/s, ω=2500nm, d=60%   T$_{max}$=2404 K

Case 23: h $_{silica}$=570nm, V =43m/s, ω=2000nm, d=50%   T$_{max}$=2731 K

400   T$_{max}$
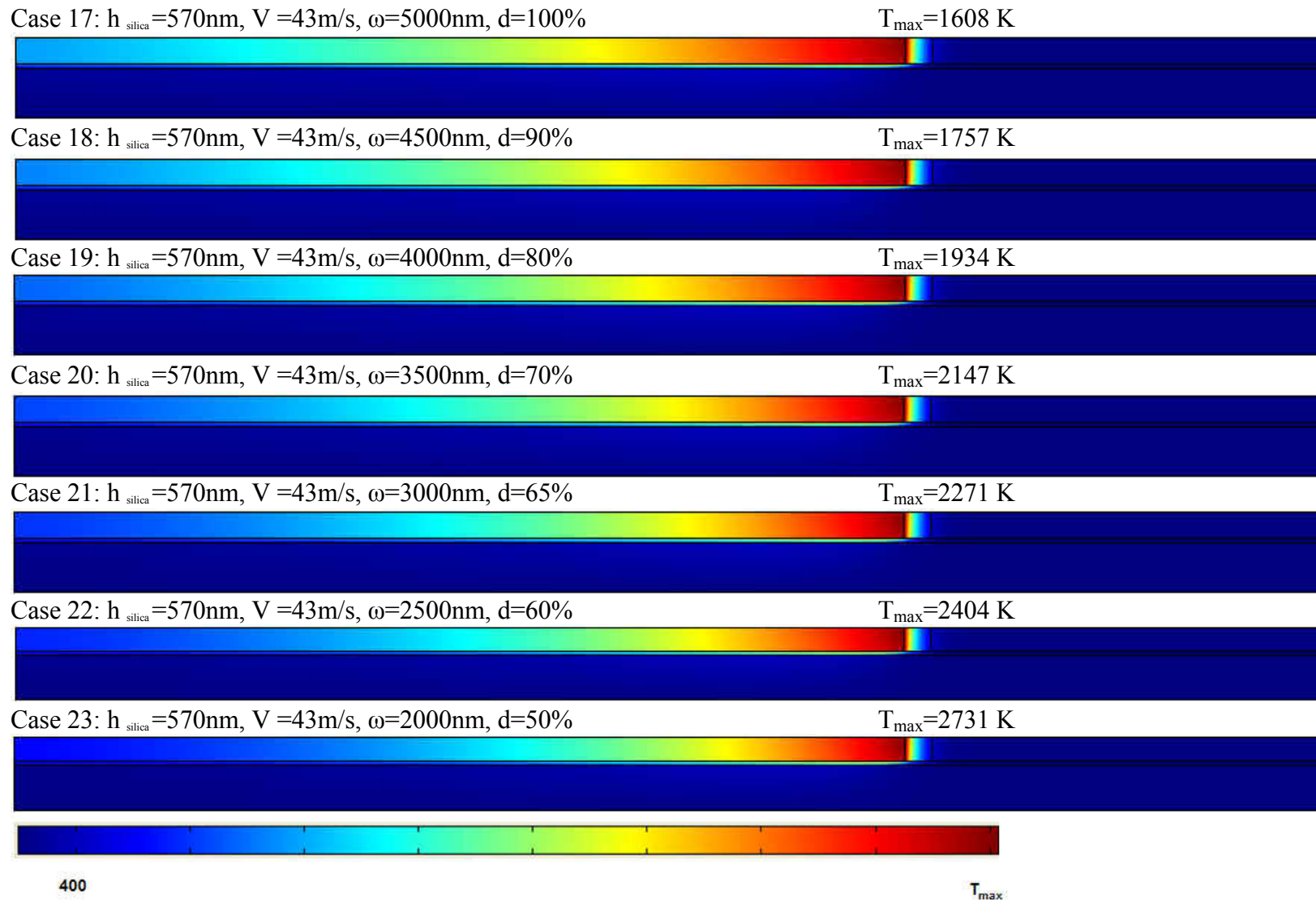
Fig. 4-22. Temperature distribution within computational domain
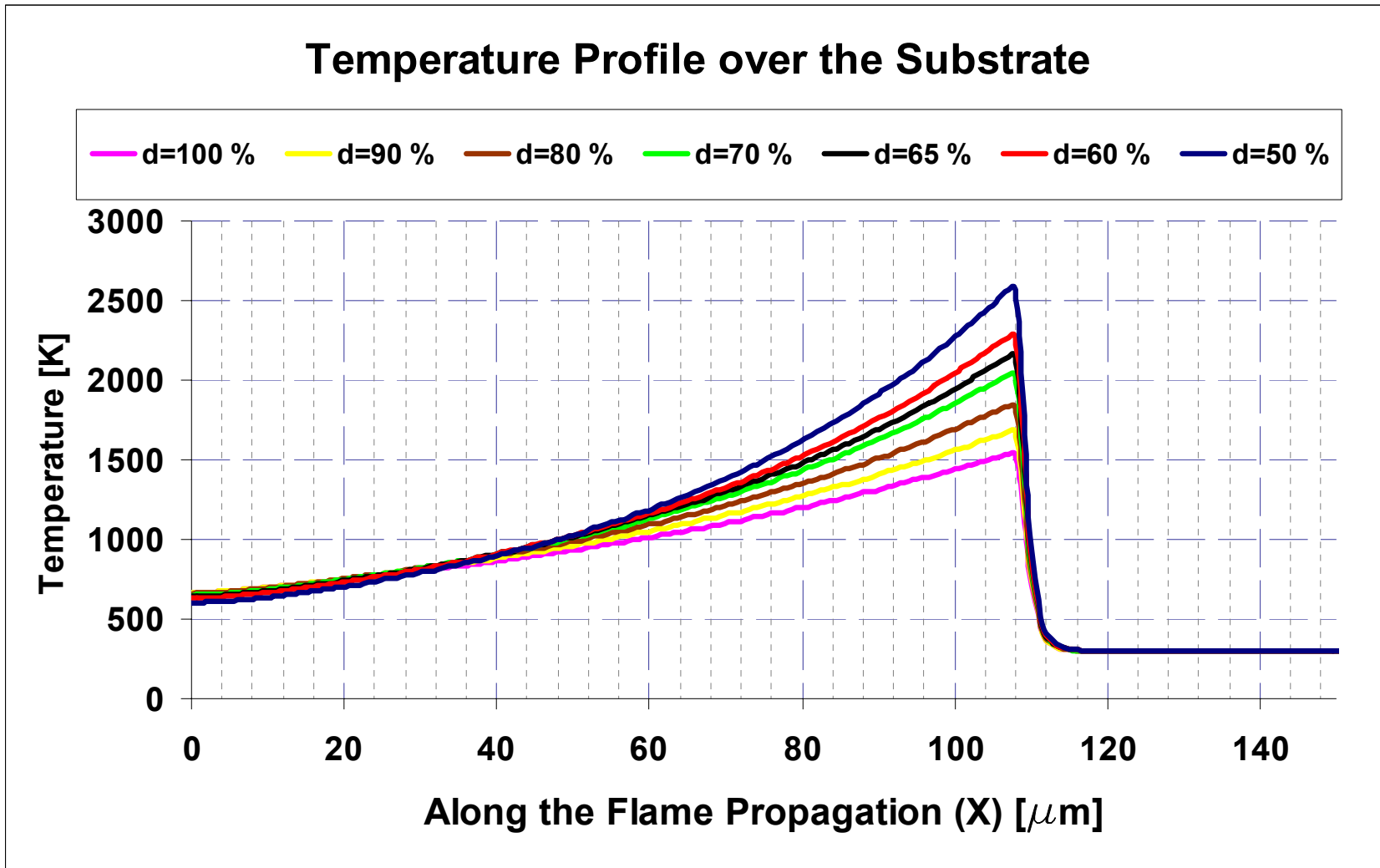
Fig. 4-23. Temperature profile at the interface of thin film and silica substrate
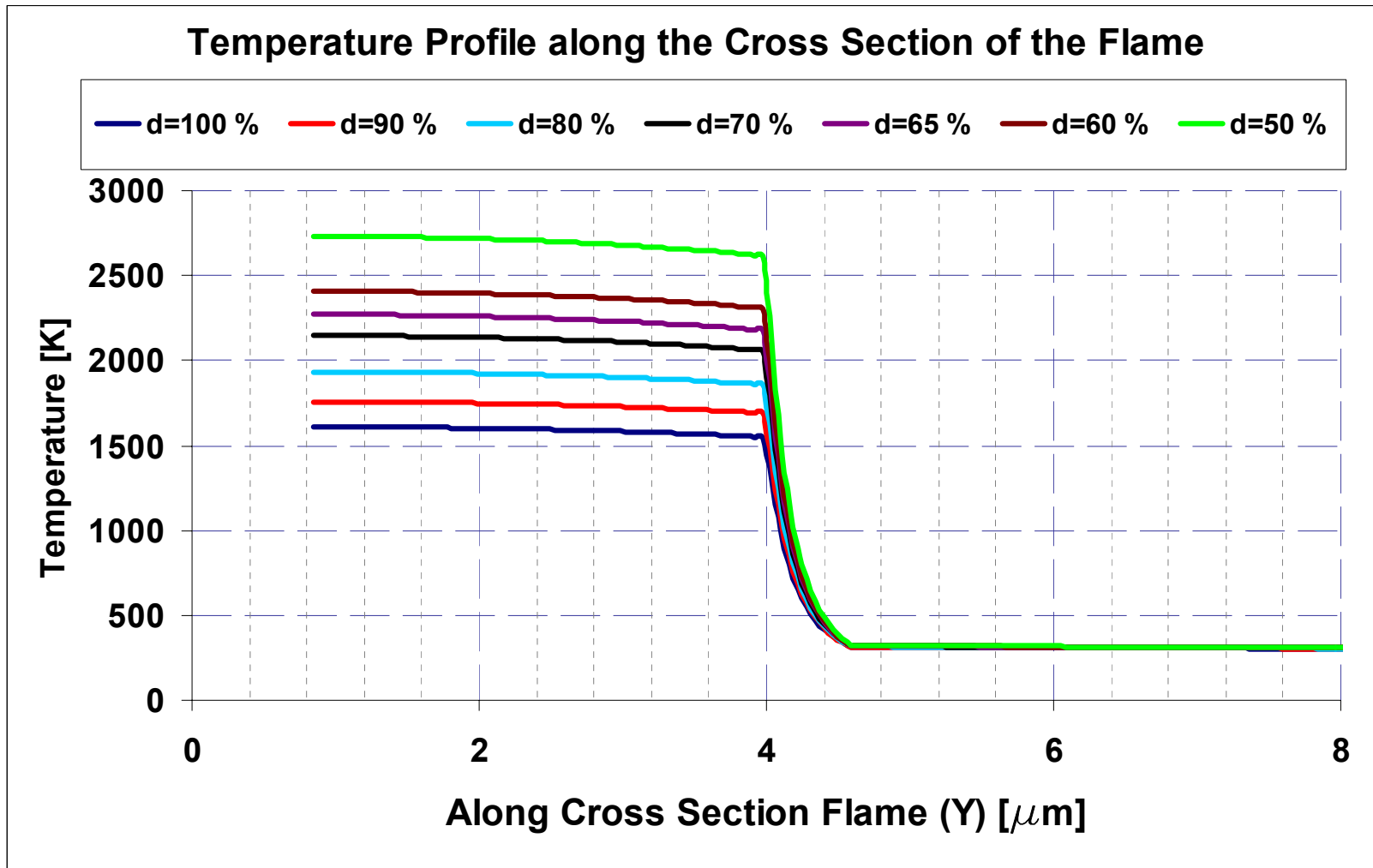
Fig. 4-24. Temperature profile at the cross-section of flame and the substrate

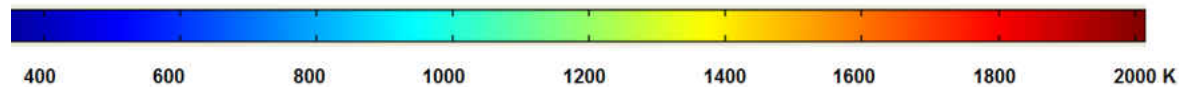Fig. 25 compares the temperature distribution within the computational domain while the speed of the flame front increases form 30 to 70 m/s in standard configuration. As the speed of the flame front increases, less heat transfers to the substrate, and additional heat raises the maximum flame temperature. Numerical results (Fig. 24) show that maximum flame temperature almost linearly decreases as the speed of flame front increases. The temperature profile at the interface of the thin film and the substrate shows how the speed of flame front impacts on the temperature distribution and maximum heat penetration.

Impact of Speed of Flame Front on Maximum Flame Temperature
(d=69%, ω=3200 nm, h=570 nm)

Fig. 4-25. Calculated temperature within penetration depth of substrate

Case 33: h $_{silica}$=570nm, V =60m/s, ω=5000nm, d=69%   T$_{max}$=1830 K

Case 34: h $_{silica}$=570nm, V =50m/s, ω=4500nm, d=69%   T$_{max}$=2009 K

Case 35: h $_{silica}$=570nm, V =43m/s, ω=4000nm, d=69%   T$_{max}$=2171 K

Case 36: h $_{silica}$=570nm, V =40m/s, ω=3500nm, d=69%   T$_{max}$=2252 K

Case 37: h $_{silica}$=570nm, V =30m/s, ω=3000nm, d=69%   T$_{max}$=2594 K

Case 38: h $_{silica}$=570nm, V =20m/s, ω=2500nm, d=69%   T$_{max}$=3069 K

400   T$_{max}$
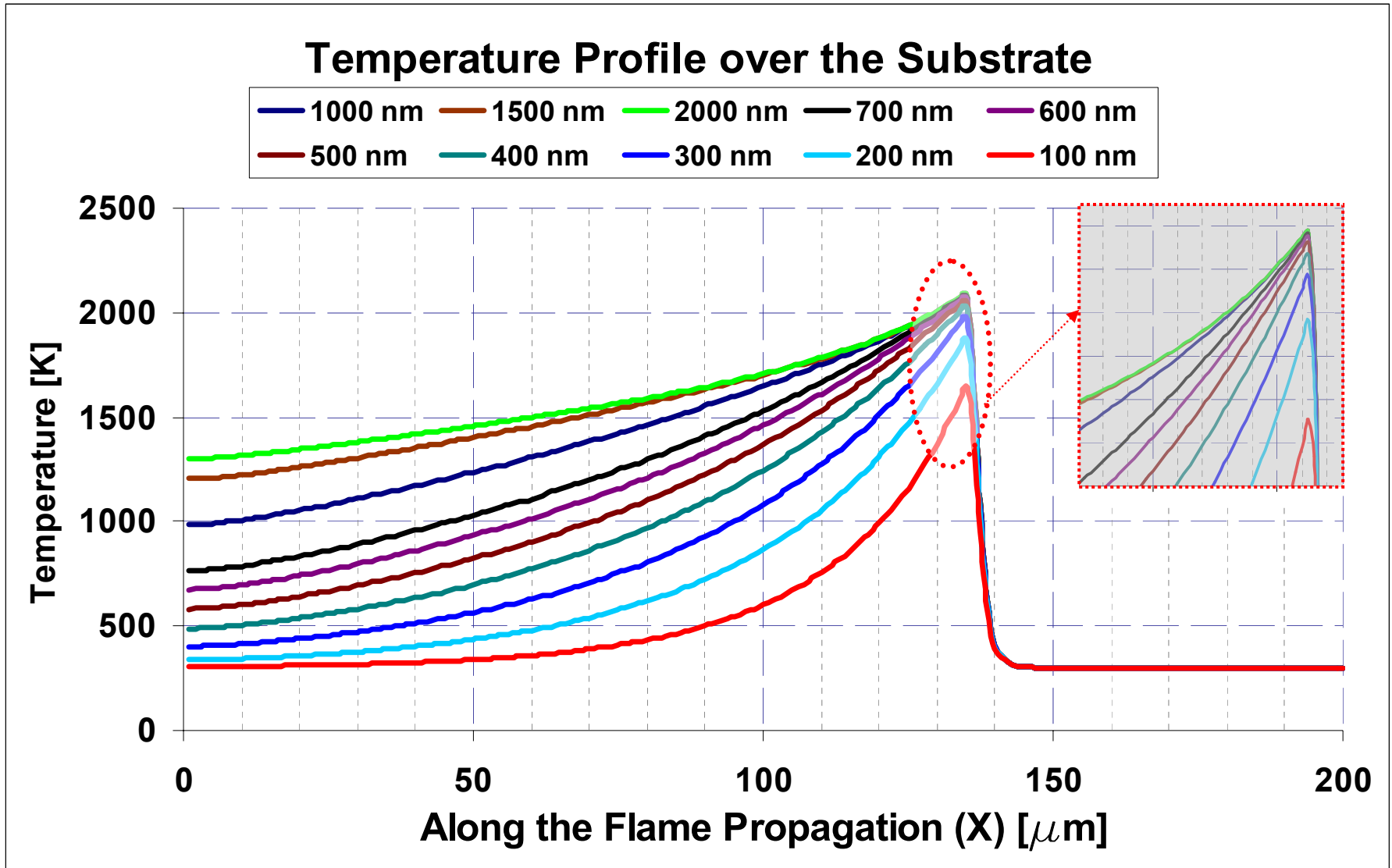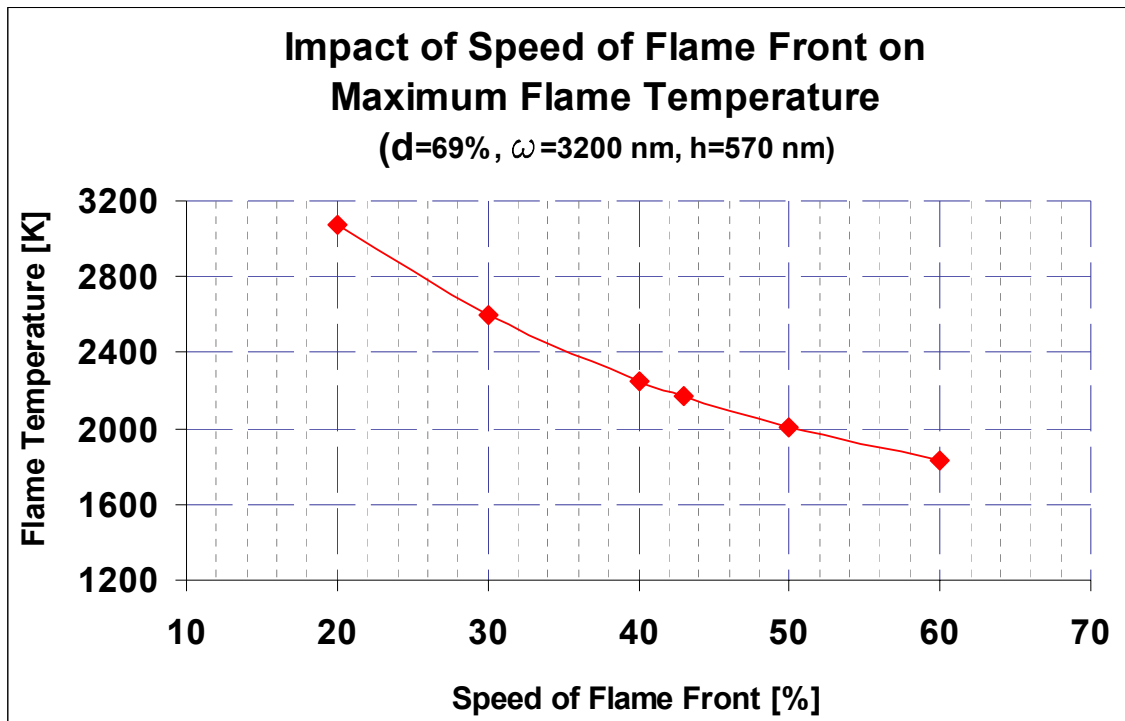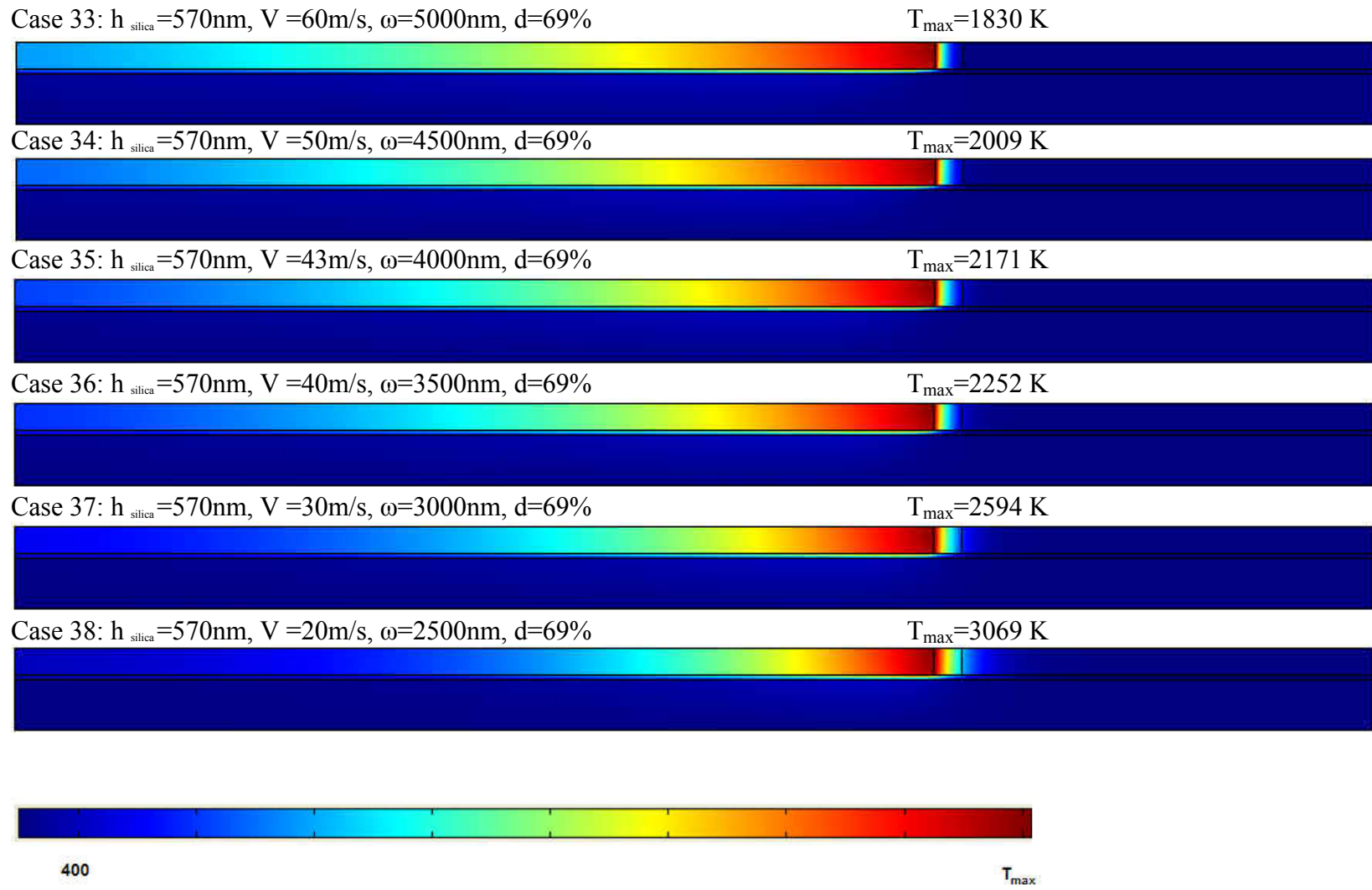
Fig. 4-26. Temperature distribution within computational domain

105
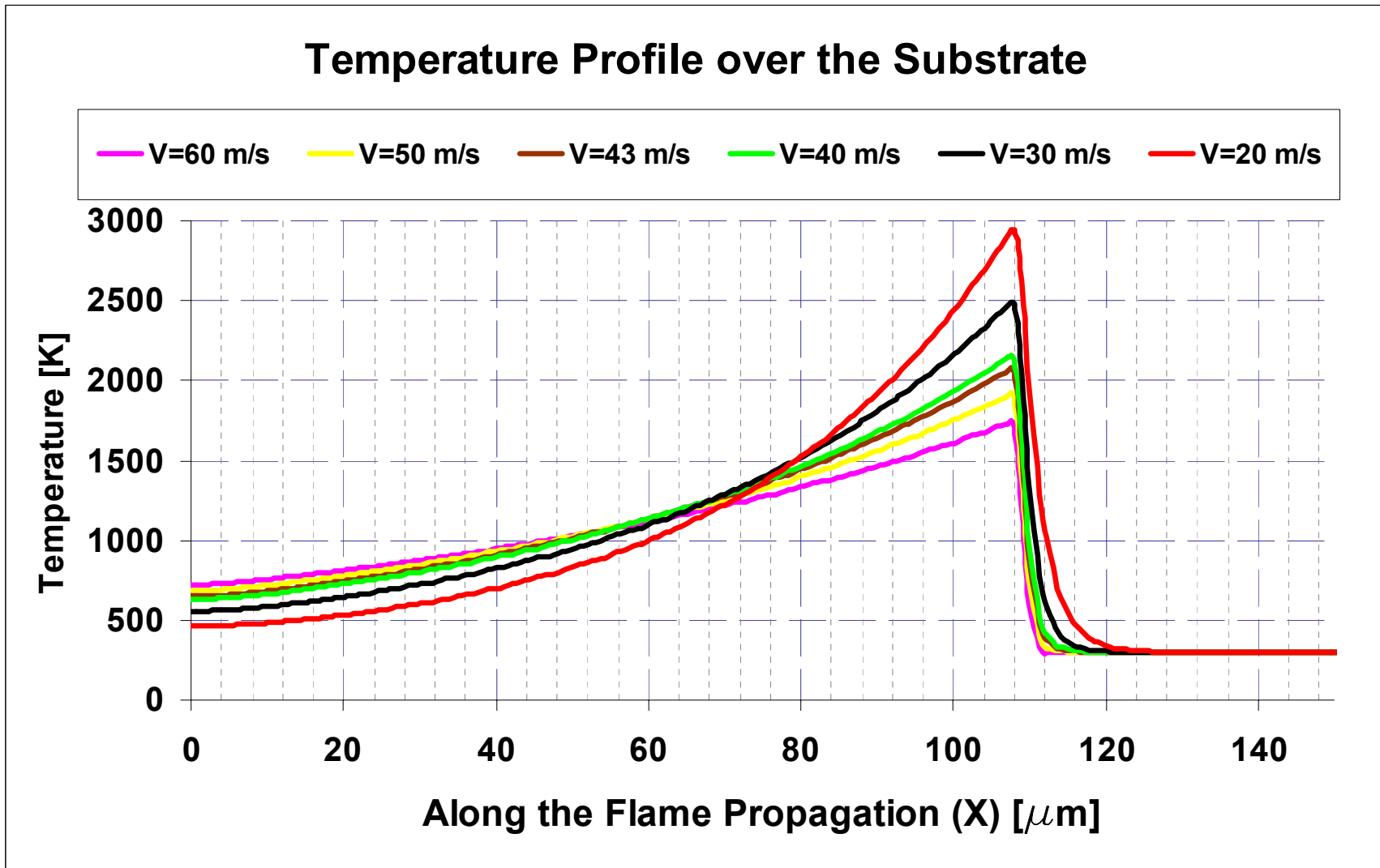
Fig. 4-27. Temperature profile at the interface of thin film and silica substrate
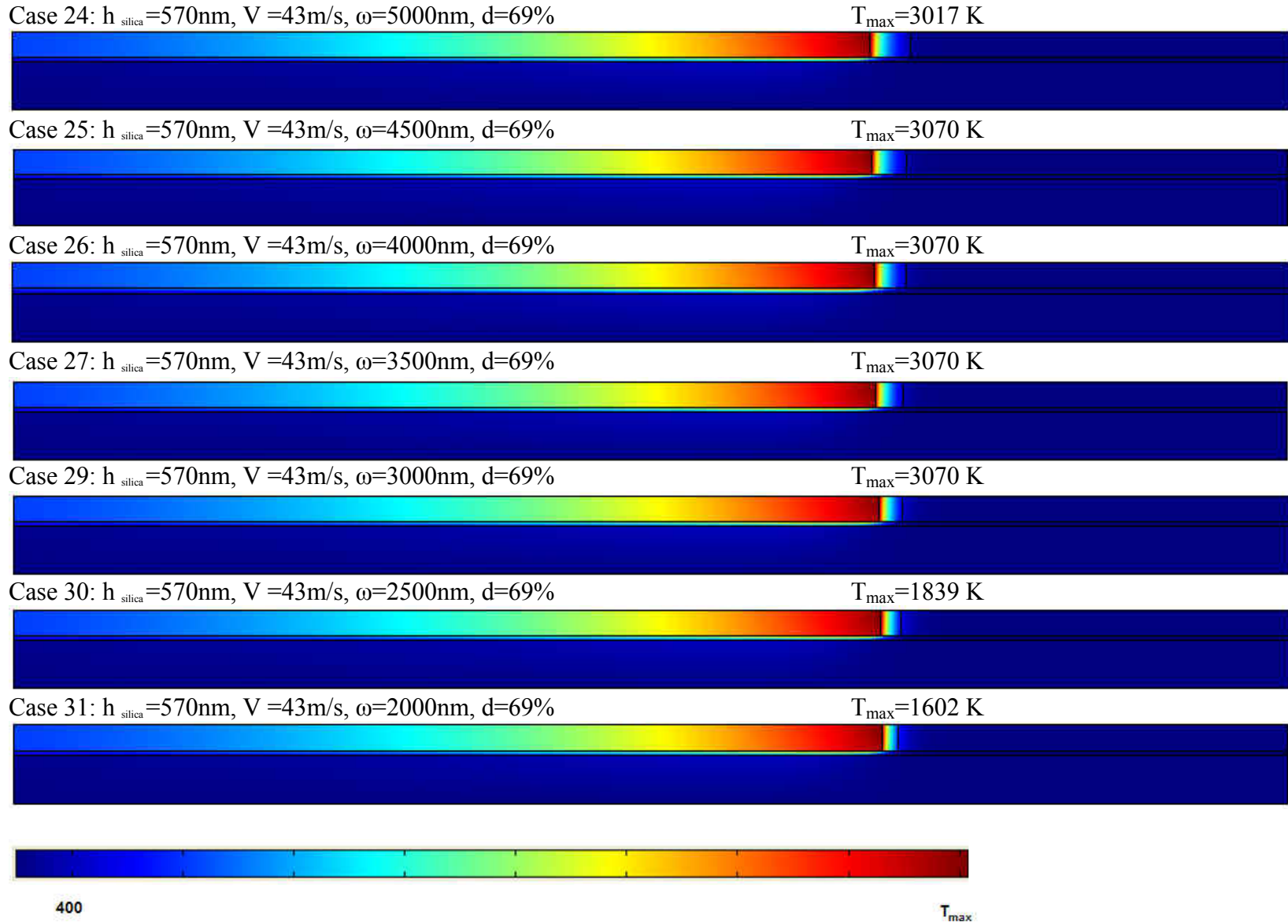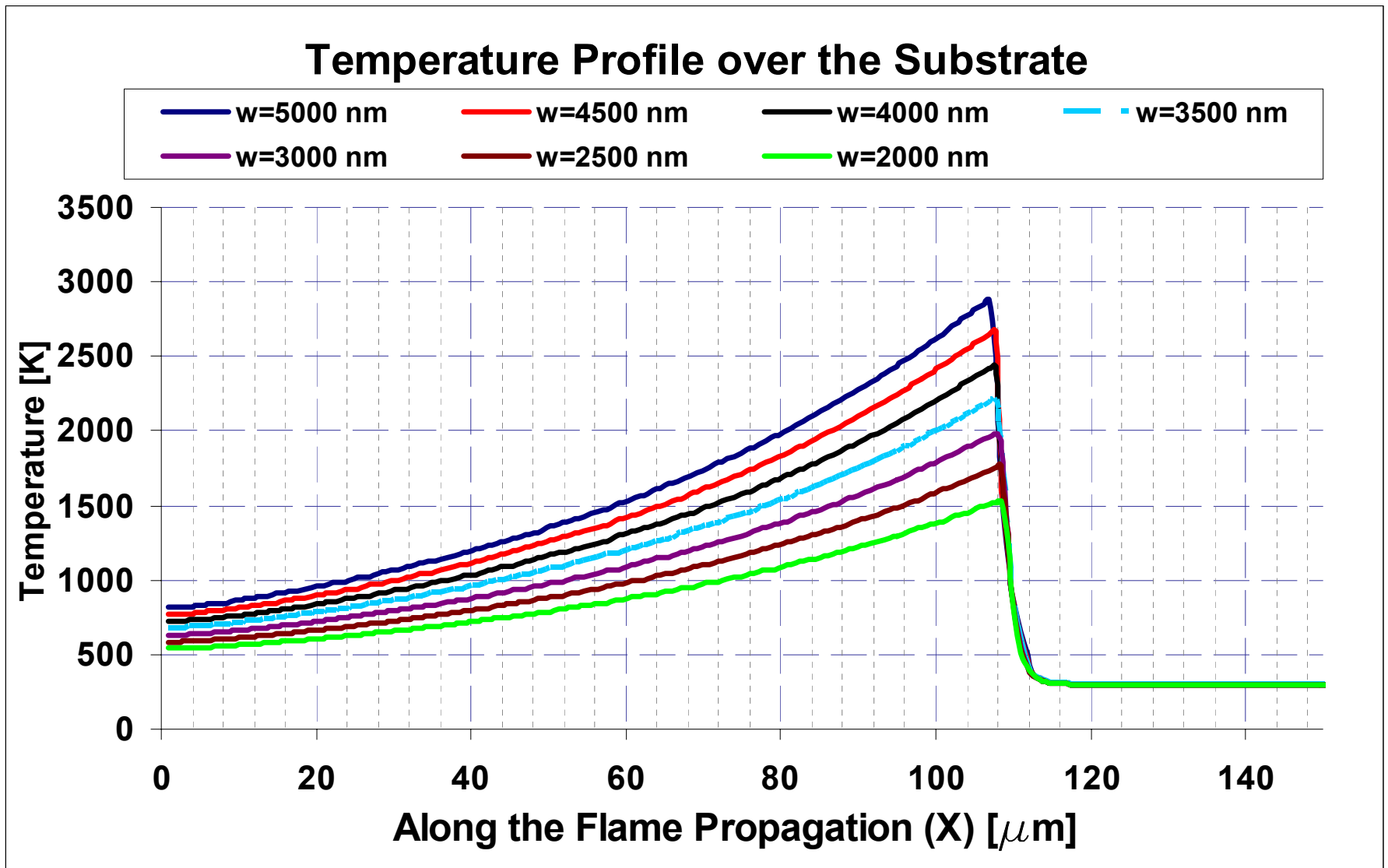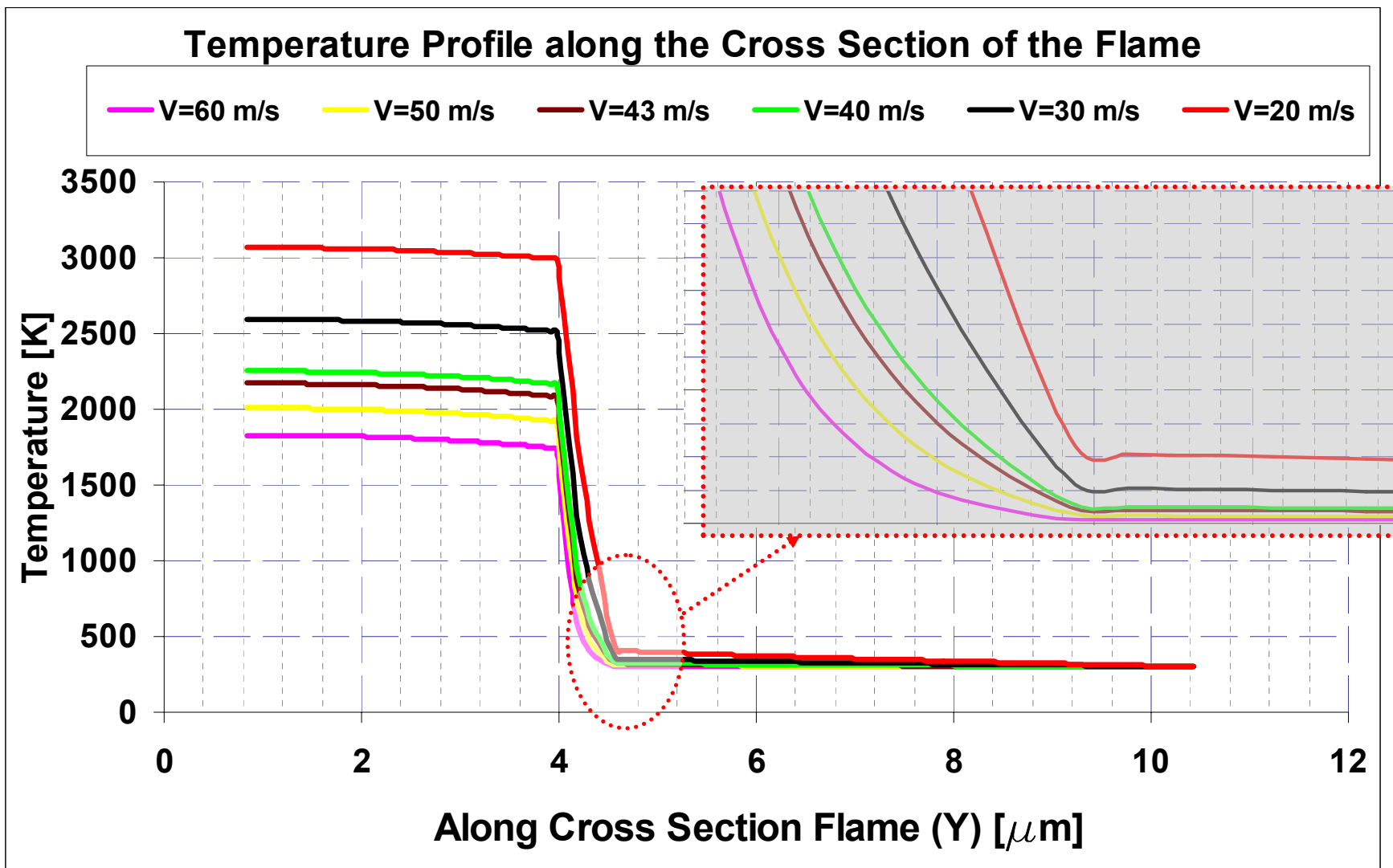
Fig. 4-28. Temperature profile at the interface of thin film and silica substrate

Estimate the characteristics of the flame with different speed of flame front

The reaction of the multilayer thin film over the substrate remains steady in a self-sustained mode if the heat loss stays at a specific range. To find the proper and comparable heat loss, composite substrate was used; therefore, the heat loss can be comparable as silica reaches the thickness of maximum penetration depth or higher. The flame also propagates with proper length of the flame and creates a unique product with specific density in unique speed. Flame front is increased as the thickness of the bi-layer decreases; however, the flame front speed is unique for any conditions. Finding these unique values is the main goal of this portion of study. The numerical model was solved for a number of cases with constant the speed of the flame front as the length of flame and density of the product was modified until maximum flame temperature meets the expected value.

Table 2 simplified the process in the following steps for a flame with the speed of 50m/s. 2900nm is the initial estimation for the length of the flame at this speed, and the expected heat penetration depth is 503 nm. In order to calculate the maximum heat penetration depth, thickness of silica was increased and maximum temperatures were compared. The flame temperature stabilizes when the thickness of silica passes 600 nm so the expected penetration does not match with the calculated value and the length of the flame should be modified. The length of the flame was modified similarly for 2600 nm and 2500 nm. Comparison shows 2500 nm is the best possible estimation of length for the flame with a speed of 50 m/s. the density of the product gradually was reduced to 47% in order to match the maximum flame temperature with the expected value. In

summary, flame front with a speed of 50 m/s should propagate with a 2500 nm flame length. Density of the product also drops to 47% due to the air mixture behind the flame.

Table 4-2. Calculation of characteristic of flame for speed V=50 m/s

	V [m/s]	Peneration Depth [nm]	W [nm]	T [K]	W (Model)	Density of product [%]	h	T @ 50m/s	% delta (Local)	% delta	Error [0.5%]
	50	503.2	2900	2255	2900						
Case 1	50	503.2	2900	2255	2900	69	200	1786		20.79822616	0.5000
Case 2	50	503.2	2900	2255	2900	69	300	1841	-2.98750679	18.35920177	0.5000
Case 3	50	503.2	2900	2255	2900	69	400	1866	-1.339764202	17.25055432	0.5000
Case 4	50	503.2	2900	2255	2900	69	450	1873	-0.747463962	16.94013304	0.5000
Case 5	50	503.2	2900	2255	2900	69	500	1880	-0.744680851	16.62971175	0.5000
Case 6	50	503.2	2900	2255	2900	69	600	1884	-0.212314225	16.45232816	0.5000
Case 7	50	476.5	2600	2255	2600	69	200	1669		25.98669623	0.5000
Case 8	50	476.5	2600	2255	2600	69	300	1718	-2.852153667	23.81374723	0.5000
Case 9	50	476.5	2600	2255	2600	69	400	1741	-1.321079839	22.79379157	0.5000
Case 10	50	476.5	2600	2255	2600	69	450	1748	-0.800915332	22.48337029	0.5000
Case 11	50	476.5	2600	2255	2600	69	500	1752	-0.456621005	22.3059867	0.5000
Case 12	50	476.5	2600	2255	2600	69	600	1758	-0.341296928	22.03991131	0.5000
Case 13	50	467.2	2500	2255	2500	69	200	1629		27.76053215	0.5000
Case 14	50	467.2	2500	2255	2500	69	300	1677	-2.862254025	25.63192905	0.5000
Case 15	50	467.2	2500	2255	2500	69	400	1702	-1.468860165	24.5232816	0.5000
Case 16	50	467.2	2500	2255	2500	69	460	1707	-0.488185901	24.30155211	0.5000
Case 17	50	467.2	2500	2255	2500	69	500	1710	-0.438596491	24.16851441	0.5000
Case 18	50	467.2	2500	2255	2500	69	600	1714	-0.233372229	23.99113082	0.5000
Case 19	50	467.2	2500	2255	2500	60	460	1900.5		15.72062084	0.5000
Case 20	50	467.2	2500	2255	2500	50	460	2166		3.946784922	0.5000
Case 21	50	467.2	2500	2255	2500	40	460	2507		-11.1751663	0.5000
Case 22	50	467.2	2500	2255	2500	47	460	2260		-0.22172949	

Case 23: h $_{silica}$=100nm, V =50m/s, ω=2500nm, d=47%   T$_{max}$=1873 K

Case 24: h $_{silica}$=200nm, V =50m/s, ω=2500nm, d=47%   T$_{max}$=2085 K

Case 25: h $_{silica}$=300nm, V =50m/s, ω=2500nm, d=47%   T$_{max}$=2187 K

Case 26: h $_{silica}$=400nm, V =50m/s, ω=2500nm, d=47%   T$_{max}$=2241 K

Case 27: h $_{silica}$=500nm, V =50m/s, ω=2500nm, d=47%   T$_{max}$=2270 K

Case 28: h $_{silica}$=600nm, V =50m/s, ω=2500nm, d=47%   T$_{max}$=2285 K

Case 29: h $_{silica}$=1000nm, V =50m/s, ω=2500nm, d=47%   T$_{max}$=2288 K

Case 30: h $_{silica}$=1500nm, V =50m/s, ω=2500nm, d=47%   T$_{max}$=2290 K

400   T$_{max}$

Fig. 4-29. Temperature distribution within computational domain
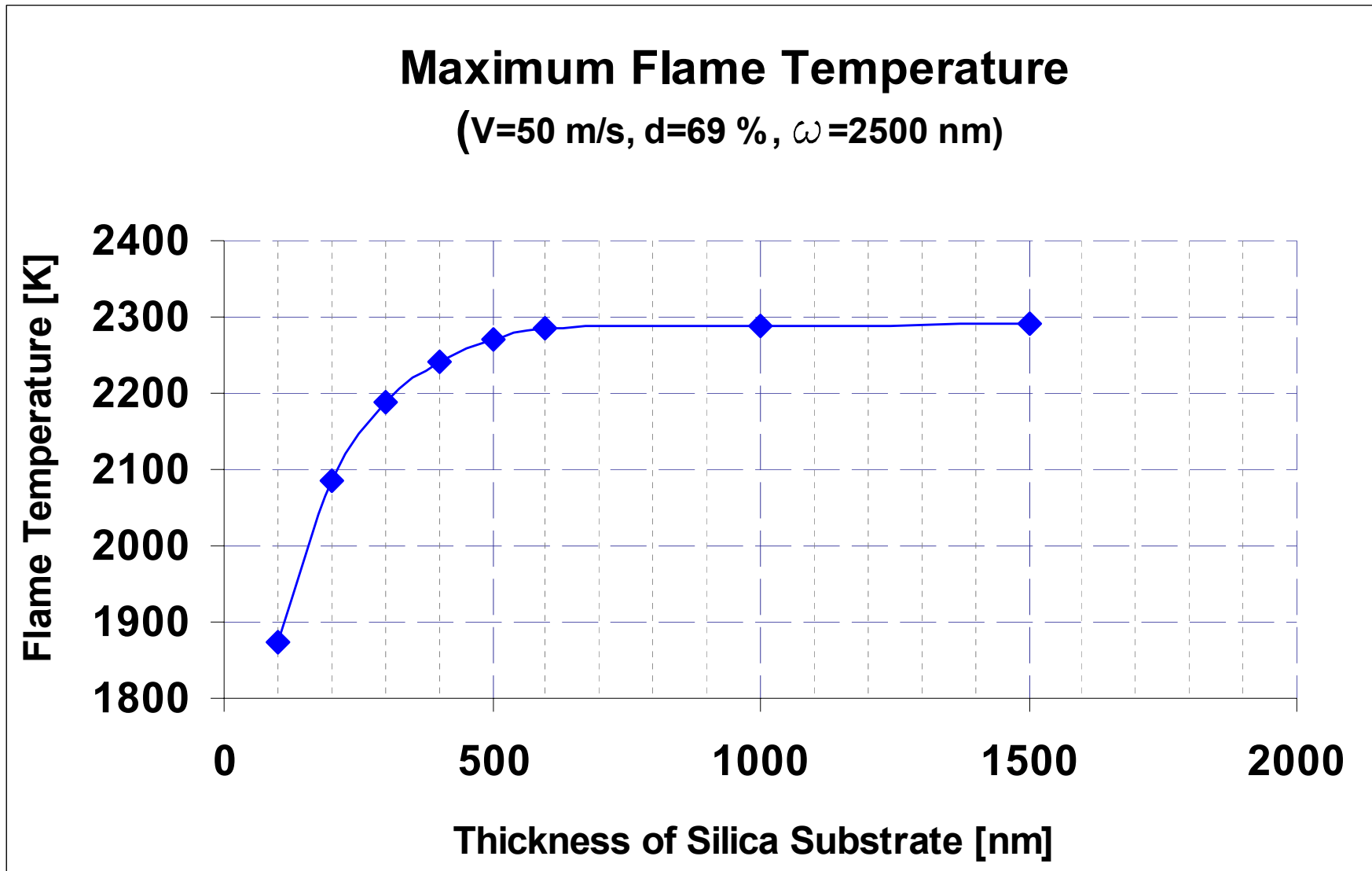
Fig. 4-30. Calculated temperature within penetration depth of substrate

112
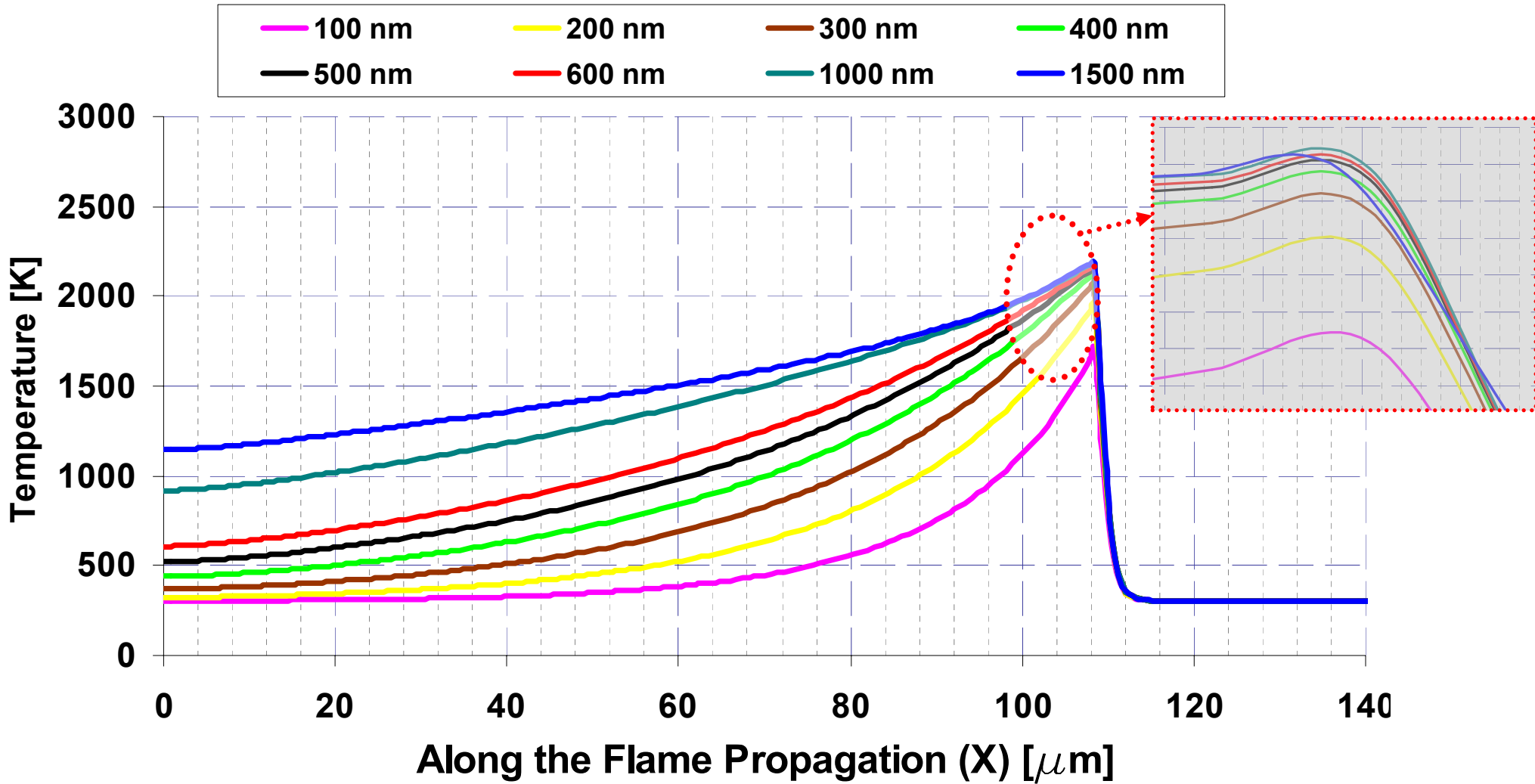
Fig. 4-31. Temperature profile at the interface of thin film and silica substrate
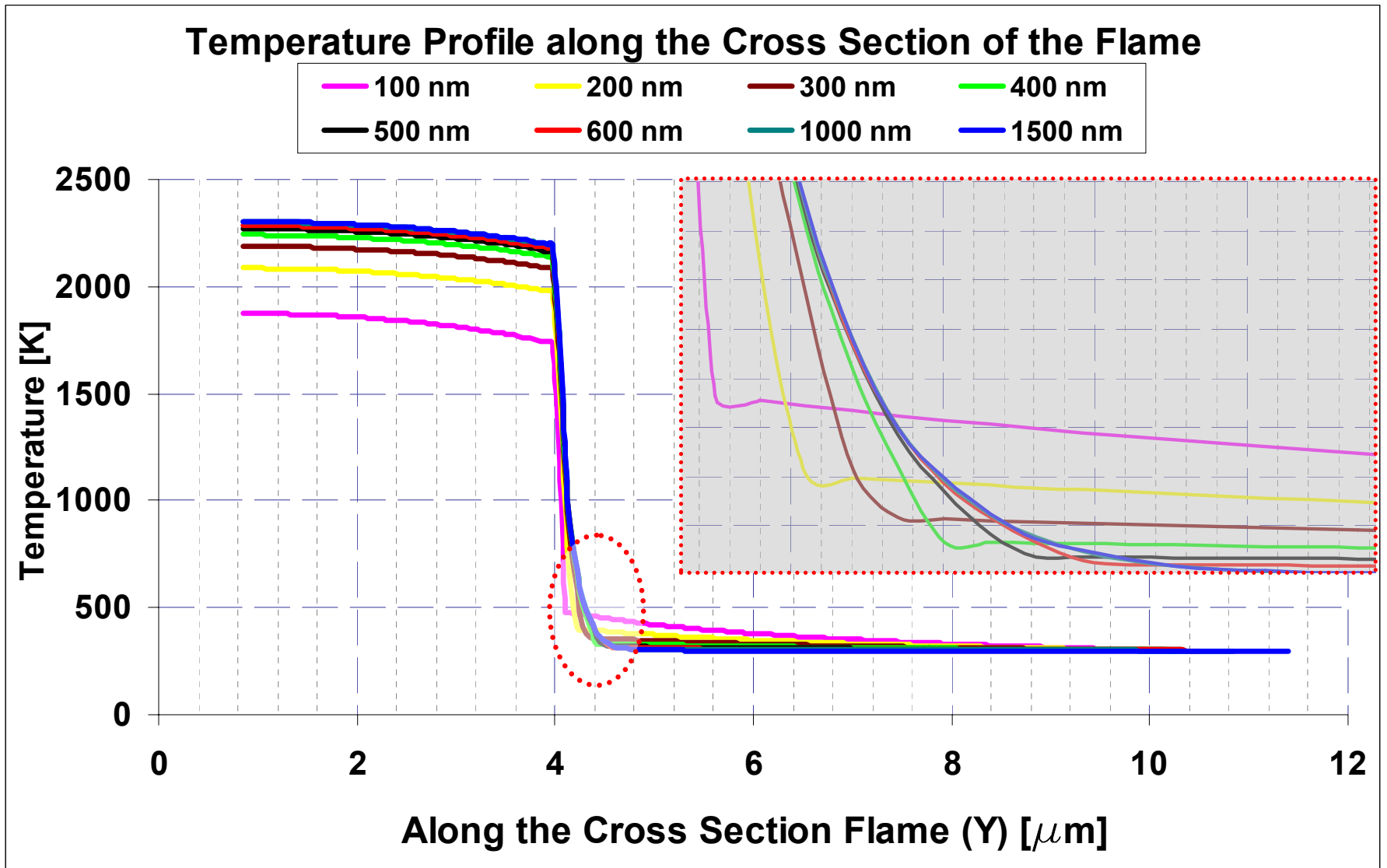
Fig. 4-32.Temperature profile at the cross-section of flame and the substrate

Fig. 28 demonstrates the temperature profile as the thickness of silica gradually is increased. Similarly the maximum flame temperature profile becomes self-similar as the thickness of silica reaches the maximum heat penetration (Fig. 29-30). The temperature at the interface of the silicon and silica drop to the lowest value as well (Fig. 31).

A similar exercise was repeated for flame speeds 30, 40, and 60 m/s (appendix A). Fig. 32 shows the final result for the length of flame, the density of the product behind the flame, and the maximum flame temperature. Extrapolation of the following trends can properly estimate the characteristics of the flame for any other speed of flame in this area.

Characteristics of Flame
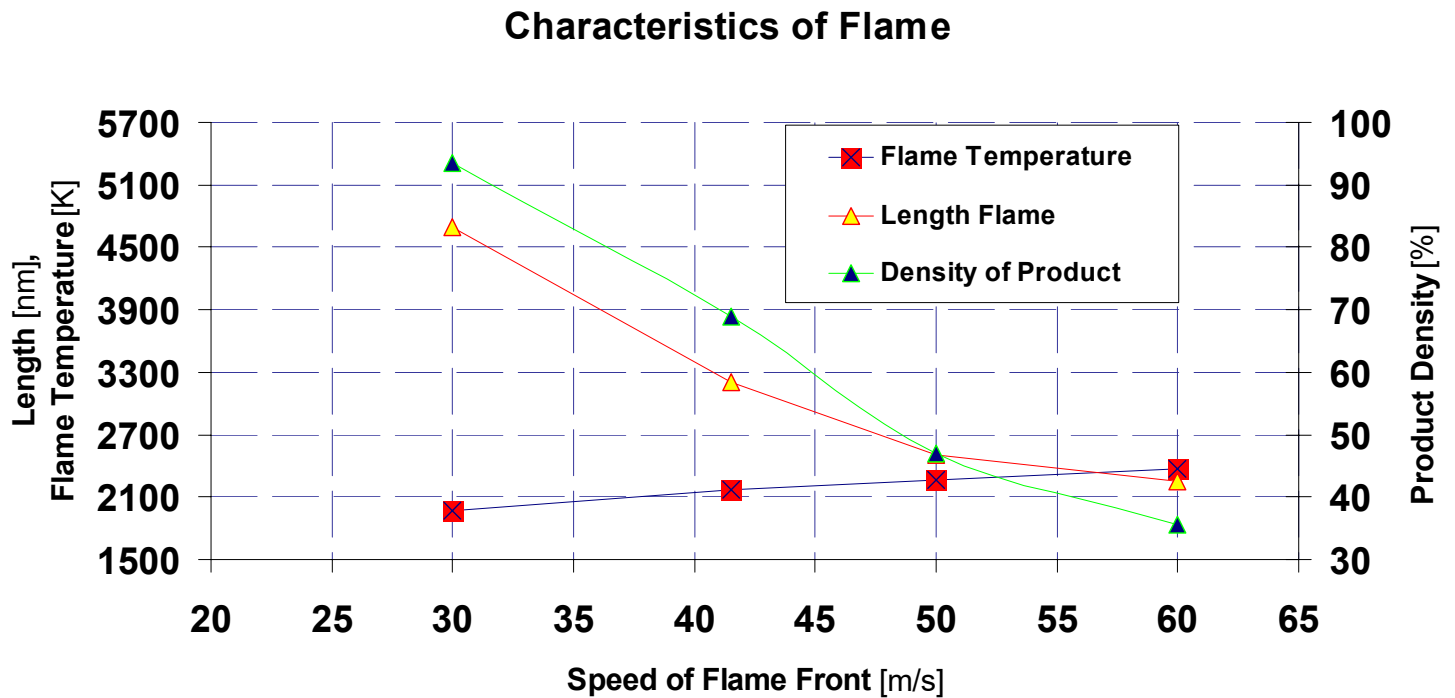
Fig. 4-33. Characteristic of the flame

Fig. 33 compares the maximum temperature of the flame when the density of the product behind the flame assumes to be constant at 69% or it is corrected based on the speed of flame front. As the density of the product corrected properly in all nominated

115

flame front speeds, the maximum flame temperature gets close to the initial estimation of the combustion flame temperature (Fig. 3).

Correction of Product Density
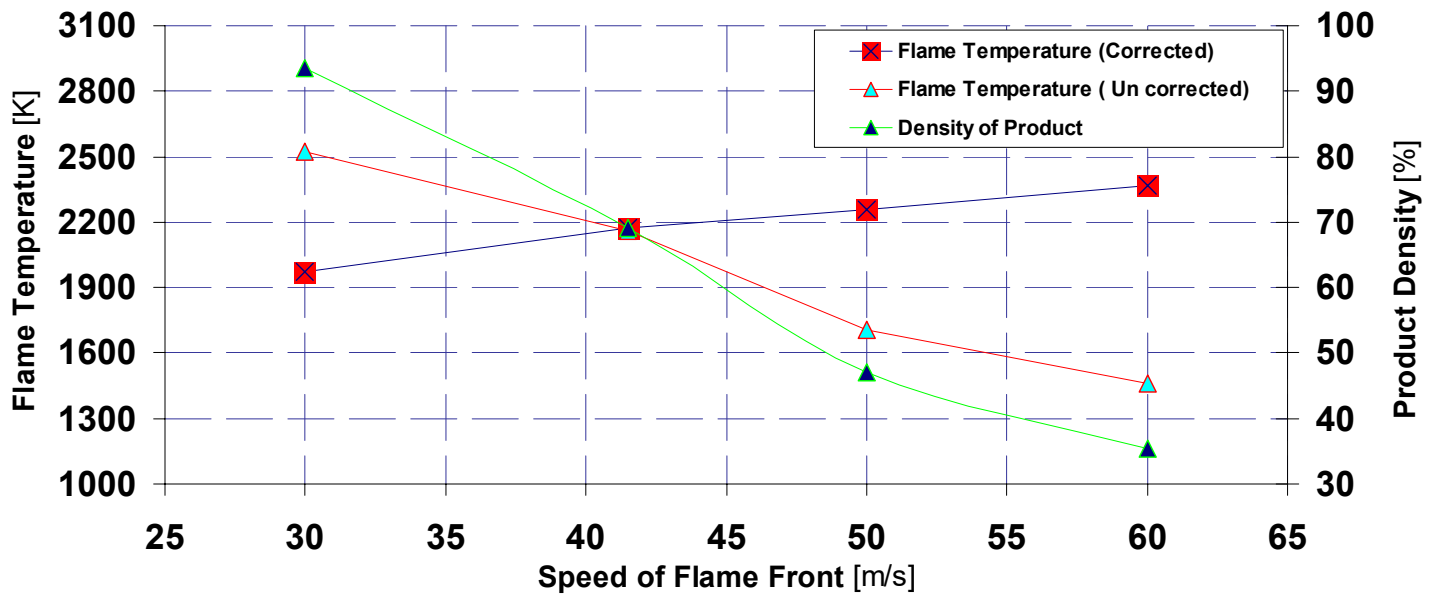
Fig. 4-34. Maximum flame temperature w/o correction of product density

Density of the product is related to the curvature of the flame front speed. Fig. 34 demonstrates the proportionality of the calculated density of the product and the square of the reverse speed. The coefficient of determination (R^2) 0.988 presents a proper linear regression between these two characteristics (the flame speed and the density of the product), and it is another way to justify the final result.

Flame Speed - Distribution of Product

$$d\% = 45475/V^2 + 8.8255$$
$$R^2 = 0.9993$$
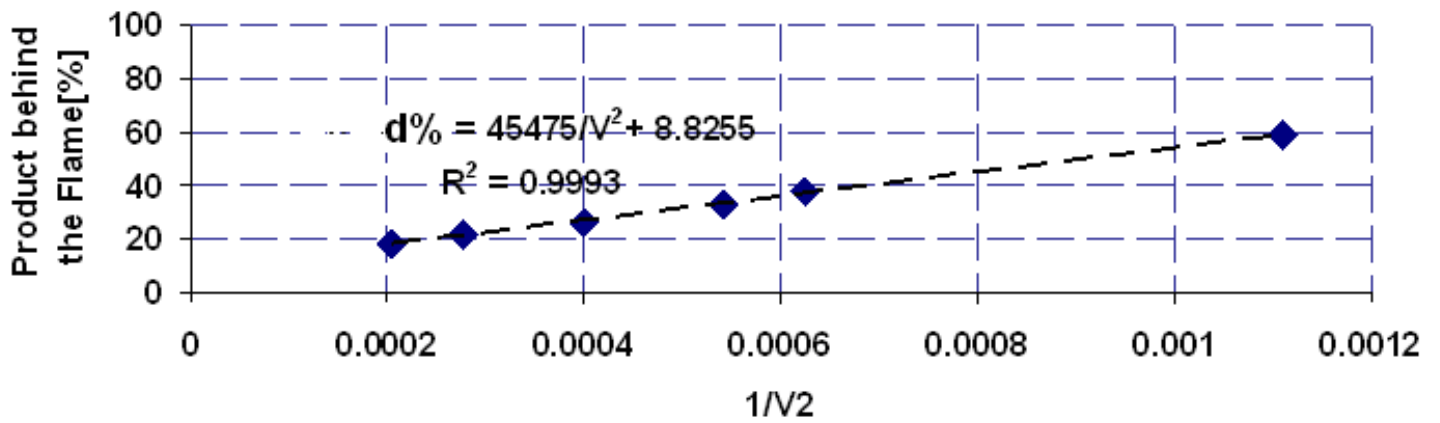
Fig. 4-35. Product density & speed of flame front

CHAPTER 5
SUMMARY

Significant progress has been made in understanding the reaction of nEM in dense film . This problem has been solved in 3 steps that are tied together, flame front speed and the reaction heat loss were the main targets in the first portion of this study. Time-of-flight technique has been developed to measure the speed of flame front with an accuracy of 0.1 m/s. This measurement technique was used to measure the speed of propagation on multilayer nEM over different substrate material up to 65 m/s. A controllable environment (composite silicon\silica) was created for the multilayer standard thin film of aluminum and copper oxide to control the reaction heat loss through the substrate. A number of experimental results show that as the thickness of silica decreases, the reaction is completely quenched. Reaction is not in self-sustain mode if the silica's thickness is less than 200 nm. It is also observed that by increasing silica's thickness in substrate, the quenching effect is progressively diminished. The speed of reaction seems to be constant at slightly over 40 m/s for the silica with thickness greater than 500 nm. This would be the maximum heat penetration depth within the silica substrate, so the flame length was calculated based on the measured speed.

A numerical analysis of the thermal transport of the reacting film deposited on the substrate was combined with a hybrid approach in which a traditional two-dimensional black box theory was used, in conjunction with the sandwich model, to estimate the maximum flame temperature. The appropriate heat flux of the heat sources is responsible for the heat loss to the surroundings. A procedure to estimate this heat flux using stoichiometric calculations is based on the previous author's work. This work highlights two important findings. One, there is very little difference in the temperature profiles

118

between a single substrate of silica and a composite substrate of silicon\silica. Secondly, by increasing the substrate thickness, the quenching effect is progressively diminished at given speed. These results also show that the average speed and quenching of flames depend on the thickness of the silica substrate and can be controlled by a careful choice of the substrate.

In final portion of this study, a numerical model was developed based on the moving heat source for multilayer thin film of aluminum and copper oxide over composite substrate of silicon\silica. The maximum combustion flame temperature corresponding to the speed of flame front is the main target of this model. Composite substrate was used as a mechanism to control the heat loss during the reaction. Thickness of the substrate, the length of flame front, and the density of the product were utilized for the standard multilayer thin film with 43 m/s flame front speed. The calculated heat penetration depth in this case was compared to the experimental result for the same flame front speed. Numerical model was also used to estimate three major variables for a range of 30-60 m/s. In fact, the maximum combustion flame temperature that corresponds to flame speed along with the length of the flame, density of the product behind the flame, and maximum penetration depth in steady reaction, were calculated.

Future Work

This study demonstrates a numerical process to estimate the maximum flame temperature and other characteristics of the flame for multilayer thin film over the substrate. In order to reduce the number of variables, the thickness of the thin film is considered to be constant while the total number of bi-layers is varied for representation of the variation of flame speed. This restriction should be removed in the next stage of this study, and the numerical model should be used for a variety of thicknesses of

119

multilayer thin film.   Fig. 36 shows the predicted speed of the flame relative to the number of bi-layers in previous studies. Also the estimated maximum temperature and the length of flame are presented as the speed of the flame front varied for a thickness (3200 nm). Plot 35 can be expanded further to predict characteristics of the flame as the total thickness of multilayer thin film is varied.

$$v_x^2 = \frac{3 A \lambda^2 R T^2_{MAX}}{\delta^2 E \left(T_{MAX} - T_0\right)} e^{\left(\frac{-E}{RT}\right)}$$

Final Temperature - Length of Flame
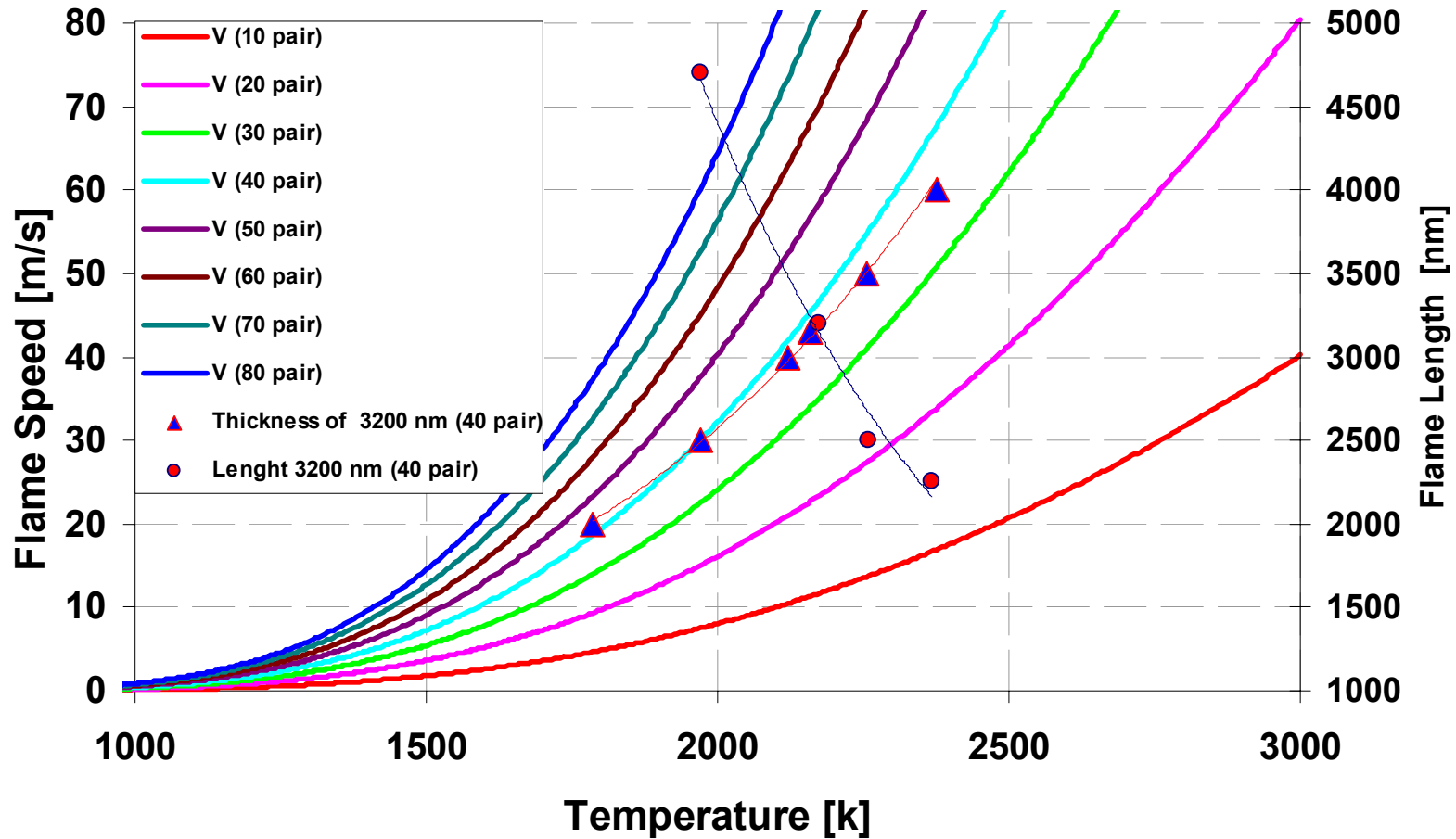
Fig. 5-1. Maximum flame temperature and length of flame

121

APPENDIX A
PROPERTIES OF THE MATERIALS

Table A-1Physical Properties of Reactants and Product

	Density (g/cm3)	Melting point (K)	Latent heat (cal/g)	Boiling point (K)	Latent heat of vaporization (cal/g)	C_p (J/ kg .k)
Al	2.702	933	94.8	2723	2720	903
Cu	8.933	1356	32	2793	1210	385
CuO	6.310	1358	35.4			[14]
Cu$_2$O	6.000	1503	93.6	2073		[14]
Al$_2$O$_3$	3.965	2325	250.6	3273	1130	[14]

APPENDIX B
SANDWICH MODEL

This chapter discusses the one-dimensional modeling and characterization of the propagation velocity of the exothermic reaction in multilayer foils. Mann et al. [57] developed a new model consisting of the so-called sandwich model of Armstrong and Koszykowski [51-53] by characterizing the rate of reaction for any multilayer pair of thin films. The sandwich model has a specific description for multilayer foils. Based on this description, the basic equation for atomic diffusion, and the general equation for thermal transport, they calculated the equation of the reaction rate of multilayer function.

The model, which was developed by [57], is the only classical approach for a multilayer geometry in thin film. Their experimental results for Al/Ni, support this numerical model. The physical model is explained below and two experimental values of the speed of propagation of the Al-CuO film were compared with the model. The corresponding temperature profiles for the two speeds are also compared.

Analysis

Description of multilayer foils
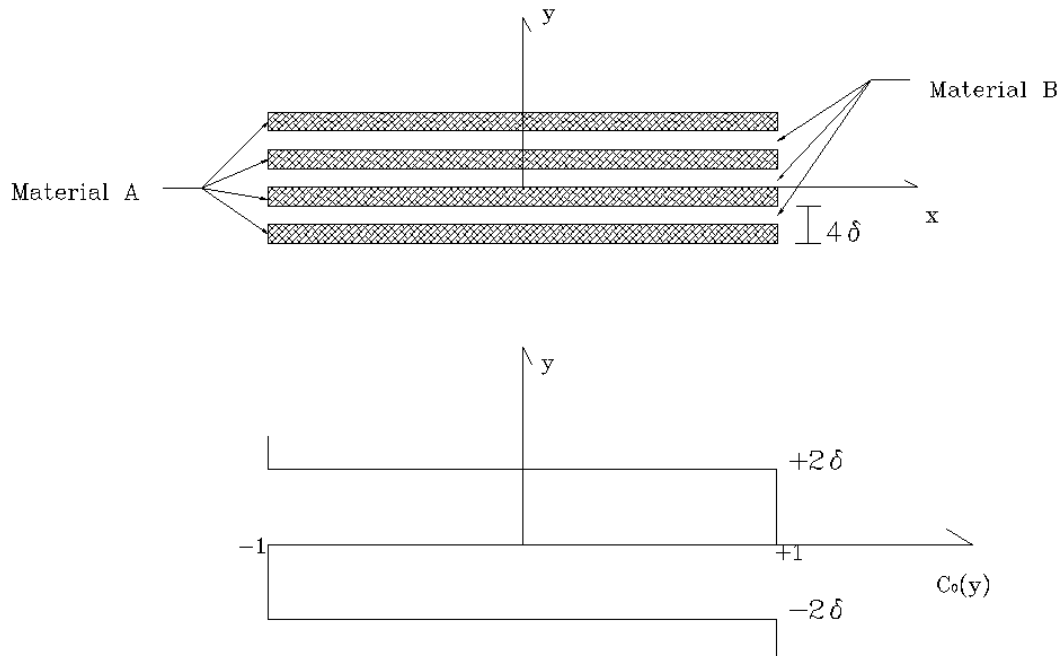
Fig. B-1. Ideal profile for composition, C

Material A: C=1

Material B: C=-1   (B.1)

Between layers: C=0

Theory of Atomic Diffusion

Basic Diffusion Function

$$\frac{dC}{dt} - \nabla D(\nabla C) = 0$$ (B.2)

Sandwich Theory

C is function of x, y, z, t and propagation in x direction

$$\frac{dC}{dt} = \frac{\partial C}{\partial t} + V_X \frac{\partial C}{\partial x}$$ (B.3)

126

3-D Equation for composition, C:

$$\frac{dC}{dt} - \nabla D(\nabla C) = [\frac{\partial D(\frac{\partial C}{\partial x})}{\partial x} + D(\frac{\partial^2 C}{\partial x^2})] + [\frac{\partial D(\frac{\partial C}{\partial y})}{\partial y} + D(\frac{\partial^2 C}{\partial y^2})] + [\frac{\partial D(\frac{\partial C}{\partial z})}{\partial z} + D(\frac{\partial^2 C}{\partial z^2})] \qquad \text{(B.4)}$$

Diffusion is neglected in y and z directions. Therefore,

$$\frac{\partial D(\frac{\partial C}{\partial y})}{\partial x} + D(\frac{\partial^2 C}{\partial x^2}) = 0 \qquad \text{(B.5)}$$

$$\frac{\partial D(\frac{\partial C}{\partial z})}{\partial z} + D(\frac{\partial^2 C}{\partial z^2}) = 0 \qquad \text{(B.6)}$$

$$\frac{\partial C}{\partial t} + V_X \frac{\partial C}{\partial x} + [\frac{\partial D(\frac{\partial C}{\partial x})}{\partial y} + D(\frac{\partial^2 C}{\partial y^2})] = 0 \qquad \text{(B.7)}$$

Arrhenius Relationship

$$\frac{D}{\lambda} = A \cdot e^{\left(\frac{-E}{RT}\right)} \qquad \text{(B.8)}$$

where,

λ = Thermal Diffusion Coefficient

D = Atomic Diffusion Coefficient

A = Arrhenius Constant

R = Ideal Gas Constant

E = Activation Energy

Substituting (B.8) in (B.7)

127

$$\frac{1}{\lambda}\frac{\partial C}{\partial t} + \frac{V_X}{\lambda}\frac{\partial C}{\partial x} + A.\frac{\partial\left(e^{\left(\frac{-E}{RT}\right)}\right)}{\partial y}\frac{\partial C}{\partial t} + A.e^{\left(\frac{-E}{RT}\right)}\frac{\partial^2 C}{\partial y^2} = 0 \tag{B.9}$$

Steady state

$$\frac{1}{\lambda}\frac{\partial C}{\partial t} = 0 \tag{B.10}$$

Temperature is constant along the y direction

$$\frac{\partial\left(e^{\left(\frac{-E}{RT}\right)}\right)}{\partial y} = 0 \tag{B.11}$$

Substituting (B.10) and (B.11) in (B.9) $\hspace{4cm}$ (B.12)

$$\frac{V_X}{\lambda}\frac{\partial C}{\partial x} + A.e^{\left(\frac{-E}{RT}\right)}\frac{\partial^2 C}{\partial y^2} = 0 \tag{B.13}$$

$$F = \int_{-\infty}^{x} e^{\left(\frac{-E}{RT}\right)} \tag{B.14}$$

Solving eq. (B.13) by separation of variables

$$C(F,y) = \sum_{n=odd}\left[k_n.\sin(\alpha_n y)e^{\left(-\alpha_n\lambda AF/v_x\right)} \right] \tag{B.15}$$

$k_n and \alpha_n$ are the Fourier coefficients and Eigen-values of the sine series for $C_0(y)$ in Fig. 1, and are given by:

$$\alpha_n = n\pi/2\delta \tag{B.16}$$

$$k_n = \frac{1}{2\delta} \int\limits_{-2\delta}^{2\delta} C_0(y)\sin(\alpha_n y)dy \qquad (B.17)$$

Thermal Transport

General thermal equation

$$c_p.\rho.\frac{dT}{dt} - c_p.\rho.\lambda.\nabla^2 T = \frac{dQ}{dt} \qquad (B.18)$$

$$\frac{dT}{dt} = \frac{\partial T}{\partial t} + v_x \frac{\partial T}{\partial x} \qquad (B.19)$$

For any chemical reaction

$$Q - Q_0 = c_P.\rho.(T_f - T_0) - \Delta C \qquad (B.20)$$

Where ΔC is the heat released in reaching a composition C when starting from pure A and B (see Fig.1)

$$\frac{d(Q-Q_0)}{dt} = \frac{d[c_P.\rho.(T_f - T_0)]}{dt} - \frac{d\Delta C}{dt} \qquad (B.21)$$

$$\frac{d[c_P.\rho.(T_f - T_0)]}{dt} = 0 \qquad (B.22)$$

$$\frac{dQ}{dt} = \frac{d\Delta C}{dt} \qquad (B.23)$$

ΔC is only a function of x and time, based on the initial assumption

$$\frac{d\Delta C}{dt} = \frac{\partial \Delta C}{\partial t} + v_x \frac{\partial \Delta C}{\partial x} \qquad (B.24)$$

Substituting (19) and (24) in (18)

$$c_p.\rho\left[\left(\frac{\partial T}{\partial x} + v_x \frac{\partial T}{\partial x}\right) - \lambda \nabla^2 T\right] = \frac{\partial \Delta C}{\partial t} + v_x \frac{\partial \Delta C}{\partial x} \qquad (B.25)$$

129

T is function of x only. Therefore,

$$\nabla^2 T = \frac{\partial^2 T}{\partial x^2}$$ (B.26)

$$c_p . \rho \left[\left(\frac{\partial T}{\partial x} + v_x \frac{\partial T}{\partial x} \right) - \lambda \frac{\partial^2 T}{\partial x^2} \right] = \frac{\partial \Delta C}{\partial t} + v_x \frac{\partial \Delta C}{\partial x}$$ (B.27)

Assuming Steady state,

$$\frac{\partial \Delta C}{\partial t} = 0$$ (B.28)

Incorporating the approximation,

$$\frac{\partial T}{\partial x} \langle\langle \frac{\partial^2 T}{\partial x^2} \qquad\qquad v_x \frac{\partial T}{\partial x} \langle\langle \lambda \frac{\partial^2 T}{\partial x^2}$$ (B.29)

Both $\frac{\partial T}{\partial x}$ and $v_x \frac{\partial T}{\partial x}$ are negligible

Equation (B.21) becomes

$$c_p . \rho \left[- \lambda \frac{\partial^2 T}{\partial x^2} \right] = v_x \frac{\partial \Delta C}{\partial x}$$ (B.30)

Velocity of Self-Propagation

Based on eq. (B.30) and (B.15), we can derive the rate of reaction.

If we assume that ΔC is a linear function of C as shown in fig (B.2).
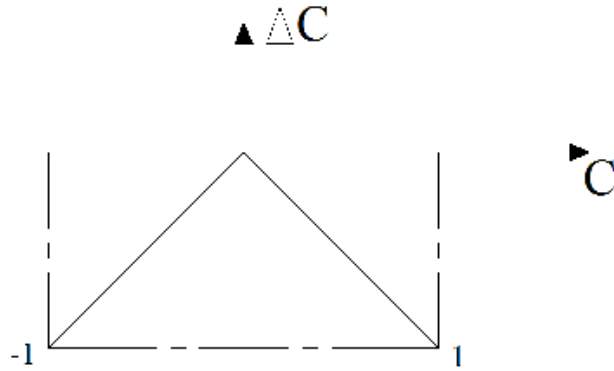
Fig. B-2. Linear function of C

$$\Delta C = c_p . \rho . (T_f - T_0) C$$

Then the reaction rate:

$$v_x^2 = \left(\sum_{n=odd} k_n \Big/ \alpha_n^3 \right)^{-1} \frac{\lambda^2 RT_f^2 A\delta}{E(T_f - T_0)} e^{\left(\frac{-E}{RT}\right)} \tag{B.31}$$

b) If we assume that ΔC is a function of C^2 as shown in fig (B.3).
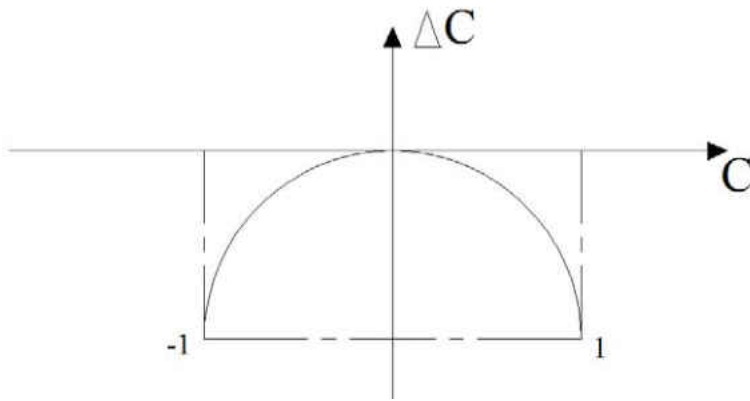
Fig. B-3. None-Linear Function of C

$$\Delta C = c_p . \rho . (T_f - T_0) C^2$$

Then the reaction rate:

131

$$v^2{}_x = \left(\sum_{n=odd} k_n{}^2 \bigg/ \alpha_n{}^2 \right)^{-1} \frac{4\lambda^2 RT_f{}^2 A}{E(T_f - T_0)} e^{\left(\frac{-E}{RT} \right)}$$ (B.32)

In this analysis, we will use the linear profile as given in eq. (B.31).

Velocity of Self-Propagation CuO$_x$ and Al

For a thin film of two material eq. (B.31) can be written as

$$v^2 = \frac{3\lambda D \left(\dfrac{RT_f}{E} \right)}{\delta^2 \left(T_f - \dfrac{T_0}{T_f} \right)} e^{\left(\frac{-E}{RT_f} \right)}$$ (B.33)

APPENDIX C
GOVERNING EQUATIONS_BLACK BOX

Governing Equation

To define flame propagation, conservation of mass, species and energy are applied in the two-dimensional control volume.

Mass Conservation

The general form for mass conservation is defined as:

$$\frac{\partial \rho}{\partial t} + \nabla \cdot (\rho \cdot v) = 0 \tag{C.1}$$

$\frac{\partial \rho}{\partial t}$ is rate of gain of the mass per unit volume

$\nabla \cdot (\rho \cdot v)$ is net rate of mass flow out per unit volume

For steady flow,

$$\nabla \cdot (\rho \cdot v) = 0 \tag{C.2}$$

For the axisymmetric system, equation (C.2) is expanded to

$$\frac{1}{r} \frac{\partial}{\partial r} (r.\rho.v_r) + \frac{\partial}{\partial x} (\rho.v_x) = 0 \tag{C.3}$$

Species Conservation

The general form for mass conservation of species is expressed as

$$\frac{\partial \rho.Y_i}{\partial t} + \nabla.m_i'' = m_i''' \tag{C.4}$$

$\frac{\partial \rho.Y_i}{\partial t}$ is the rate of gain of mass of species i per unit volume

$\nabla.m_i"$ is net rate of mass flow of the species i out by diffusion and bulk flow per unit volume

m_i''' is net rate of mass production of species per unit volume

The mass flux of i, m_i is defined by the mass average velocity i, v_i as follows:

$$m_i" \equiv \rho.Y_i.v_i \tag{C.5}$$

The sum of all of the individual species mass flux is the mixture mass flux.

$$\sum m_i" = \sum \left(\rho.Y_i.v_i \right) = m^." \qquad\qquad m^." \equiv \rho.V \tag{C.7), (C.6}$$

The mass average velocity V is:

$$V = \sum \left(Y_i v_i \right) \tag{C.8}$$

This (V) is the velocity known as bulk velocity. The difference between the spices and bulk velocity is defined as diffusional velocity.

$v_{i,diff} \equiv v_i - V$ The diffusion mass flux can be expressed in term of diffusion velocity.

$$m^"_{i,diff} \equiv \rho.Y_i \left(v_i - V \right) = \rho.Y_i v_{i,diff} \tag{C.9}$$

The total species mass flux is the sum of the bulk flow and diffusion contribution.

$$m_{i^i}" = m^."Y_i + m^"_{i,diff} \tag{C.10}$$

$$\rho.Y_I v_i = \rho.Y_i V + \rho.Y_i v_{i,diff} \tag{C.11}$$

Rewriting the general species conservation equation based on mass diffusion:

$$\frac{\partial \rho.Y_i}{\partial t} + \nabla.\left[\rho.Y_i \left(V + v_{i,diff} \right) \right] = m_i''' \tag{C.12}$$

For the axisymmetric geometry the corresponding conservation for the binary mixture is:

$$\frac{1}{r}\frac{\partial}{\partial r}\left(r.\rho.v_r.Y_A \right) + \frac{1}{r}\frac{\partial}{\partial x}\left(r.\rho.v_x.Y_A \right) - \frac{1}{r}\frac{\partial}{\partial r}\left(r.\rho.D\frac{\partial Y_A}{\partial r} \right) = -m_A^." \tag{C.13}$$

Y is the mass fraction

m is the mass

m' is mass flow rate

m" is the mass flux

m'" is mass production rate per unit volume

Energy Conservation

Conservation of energy for laminar premixed flame is simplified by Shvab-Zeldovich. Shvab-Zeldovich energy equation shows total difference between the rate of enthalpy transport by convection and diffusion is equal to the rate of enthalpy production by chemical reaction.

$$\nabla \cdot \left[m^{\cdot} \int c_p dT - \rho \cdot D \nabla \left(\int c_p dT \right) \right] = -\sum \left(h^0{}_f \cdot m_i^{\cdot'''} \right) \qquad (C.14)$$

For the two-dimensional axisymmetric case, the equation is expanded to

$$\frac{1}{r} \frac{\partial}{\partial x} \left(r \cdot \rho \cdot v_x \int c_p dT \right) + \frac{1}{r} \frac{\partial}{\partial r} \left(r \cdot \rho \cdot v_r \int c_p dT \right) - \frac{1}{r} \frac{\partial}{\partial r} \left(r \cdot \rho \cdot D \frac{\partial}{\partial r} \int c_p dT \right) = -\sum h^0{}_f \cdot m_i^{\cdot''} \qquad (C.15)$$

Mass flux can be derived based on the speed of flame

$$m^{\cdot''} = \rho_u \cdot S_L \qquad (C.16)$$

Length of the flame can be calculated based on 95-99% of the final temperature

$$T(\delta) = 95\% T_f \qquad (C.17)$$

APPENDIX D

CALCULATION OFCHARACTERISTIC OF FLAME FOR DIFFERENT SPEEDS

Table D-1. Calculation of characteristic of flame for speed V=30 m/s

	V(m/s)	Peneration Depth (nm)	W(nm)	T(k)	W (MODEL)	Density of product (%)	h	T@30m/s	% delta (Local)	% delta	0.5% error
	30	809.2444393	4500	1975	4500						
Case 1	30	809.2444393	4500	1975	4500	69	600	2698			0.5000
Case 2	30	809.2444393	4500	1975	4500	69	700	2714	0.589535741		0.5000
Case 3	30	809.2444393	4500	1975	4500	69	800	2724	0.367107195		0.5000
Case 4	30	809.2444393	4500	1975	4500	69	900	2730	0.21978022		0.5000
Case 5	30	772.4411385	4100	1975	4100	69	900	2533	-7.777339124		0.5000
Case 6	30	772.4411385	4100	1975	4100	69	850	2530	-0.118577075		0.5000
Case 7	30	772.4411385	4100	1975	4100	69	800	2527	-0.118717847		0.5000
Case 8	30	772.4411385	4100	1975	4100	69	700	2519	-0.317586344		0.5000
Case 9	30	772.4411385	4100	1975	4100	69	770	2525	0.237623762		0.5000
Case 10	30	772.4411385	4100	1975	4100	80	770	2244	-12.52228164		0.5000
Case 11	30	772.4411385	4100	1975	4100	85	770	2135	-5.105386417		0.5000
Case 12	30	772.4411385	4100	1975	4100	90	770	2035	-4.914004914		0.5000
Case 13	30	772.4411385	4100	1975	4100	95	770	1944	-4.681069959	1.569620253	0.5000
Case 14	30	772.4411385	4100	1975	4100	94	770	1962	0.917431193	0.658227848	0.5000
Case 15	30	772.4411385	4100	1975	4100	93.5	770	1971	0.456621005	0.202531646	0.5000

Table D-2. Calculation of characteristic of flame for speed V=60 m/s

	V(m/s)	Peneration Depth (nm)	W(nm)	T(k)	W (MODEL)	Density of product (%)	h	T @60 m/s	% delta (Local)	% delta	0.5% error
	60	426.5092687		2375	2500	69					
Case 1	60	426.5092687		2375	2500	69	200	1527			0.5000
Case 2	60	426.5092687		2375	2500	69	300	1557.8	1.977147259		0.5000
Case 3	60	426.5092687		2375	2500	69	400	1570.52	0.809922828		0.5000
Case 4	60	426.5092687		2375	2500	69	500	1575.52	0.31735554		0.5000
Case 5	60	400.1011591		2375	2200	69	500	1467	-7.39740968		0.5000
Case 6	60	400.1011591		2375	2200	69	400	1462.16	-0.331017125		0.5000
Case (1) 7	60	400.1011591		2375	2200	65	400	1534.2			0.5000
Case (1) 8	60	404.6222196		2375	2250	50	400	1877			0.5000
Case (1) 9	60	404.6222196		2375	2250	40	400	2193.8			0.5000
Case (1) 10	60	404.6222196		2375	2250	30	400	2614			0.5000
Case (1) 11	60	404.6222196		2375	2250	35	400	2346		1.221052632	0.5000
Case (1) 12	61	401.291939		2375	2250	35.5	400	2367	0.887198986	0.336842105	0.5000

139

www.manaraa.com

REFERENCES

1. C. Rossi, K. Zhang, D. Estève, P. Alphonse, P. Tailhades, and C. Vahlas, "Nanoenergetic materials for MEMS", Journal of Micro electromechanical Systems, v 16, n 4, pp. 919-931, 2007.

2. C. Rossi, D. Briand, M. Dumonteuil, T. Camps, P. Q. Pham, and N. F. de Rooij, "Matrix of 10×10 addressed solid propellant microthrusters", Review of the technologies, Sens. Actuators A, Phys., v 126, n 1, pp. 241-252, 2006.

3. D. W. Youngner, S. T. Lu, E. Choueiri, J. B. Neidert, R. E. Black, III, K. J. Graham, D. Fahey, R. Lucus, and X. Zhu, "MEMS megapixel micro-thruster arrays for small satellite station keeping", presented at the 14th Annu. AIAA/USU Conf. Small Satellites, Logan, UT, AIAA Paper SSC00-X-2, 2000.

4. D. H. Lewis, Jr., S.W. Janson, R. B. Cohen, and E. K. Antonsson, "Digital micropropulsion,", Sens. Actuators A, Phys., v 80, n 2, pp. 143–154, 2000.

5. D. Teasdale, V. Milanovic, P. Chang, and K. Pister, "Microrockets for smart dust", Smart Mater. Struc, v 10, n 6, pp. 1145–1155, 2001.

6. W. Lindsay, D. Teasdale, V. Milanovic, K. Pister, and C. F. Pello, "Thrust and electrical power from solid propellant microrockets", Proc. Tech. Dig. 14th IEEE Int. Conf. MEMS, Piscataway, NJ, pp. 606–610, 2001.

7. K. Takahashi, H. Ebisuzaki, H. Kajiwara, T. Achiwa, and K. Nagayama, "Design and testing of mega-bit micro thruster arrays" presented at the Nanotech, Houston, TX, Paper AIAA 2002-5758, 2002.

8. S. Tanaka, R. Hosokawa, S. Tokudome, K. Hori, H. Saito, M. Watanabe, and M. Esashi, "MEMS-based solid propellant rocket array thruster with electrical feed through" Trans. Jpn. Soc. Aeronaut. Space Sci., v 46, n 151, pp. 47–51, 2003.

9. P. Q. Pham, D. Briand, C. Rossi, and N. F. De Rooij, "Downscaling of solid propellant pyrotechnical microsystems", in Proc. 12th Int. Conf. Solid-State Sensors and Actuators (Transducers), Boston, MA, v 2, pp.1423–1426, 2003.

10. Y. Zhao, B. A. English, Y. Choi, H. DiBiaso, G. Yuan, and M. G. Allen, "Polymeric microcombustors for solid-phase conductive fuels", in Proc.17th IEEE Int. Conf. MEMS, Maastricht, The Netherlands, pp. 498–501, 2004.

11. K. L. Zhang, S. K. Chou, S. S. Ang, and X. S. Tang, "A MEMS-based solid propellant micro thruster with Au/Ti igniter", Sens. Actuators A, Phys., v 122, n 1, pp. 113-123, 2005.

12. K. Zhang, C. Rossi, M. Petrantoni, and N. Mauran "A nano initiator realized by integrating Al/CuO-Based nanoenergetic materials with a Au/Pt/Cr micro heater", Journal of Micro electromechanical systems, v 17, n 4, 2008.

13. T. A. Baginski, S. L. Taliaferro, and W. D. Fahey, "Novel electro explosive device incorporating a reactive laminated metallic bridge" J. Propuls. Power, v 17, n 1, pp. 184-189, 2001.

14. Hofmann, H. Laucht, D. Kovalev, V. Y. Timoshenko, J. Diener, N. Kunzner, and E. Gross, "Explosive composition and its use" U.S. Patent 6 984 274, 2006.

15. D. H. Lewis, Jr., S.W. Janson, R. B. Cohen, and E. K. Antonsson, "Digital micropropulsion" Sens. Actuators A. Phys., v80, n 2, pp. 143-154, 2000.

16. C. Rossi, S. Orieux, B. Larangot, T. D. Conto, and D. Esteve, "Design, fabrication and modeling of solid propellant microrocket-application to micropropulsion", Sens. Actuators A. Phys., v 99, n 1/2, pp. 125-133, 2002.

17. K. L. Zhang, S. K. Chou, S. S. Ang, and X. S. Tang, "A MEMS-based solid propellant microthruster with Au/Ti igniter," Sens. Actuators A, Phys., v 122, n 1, pp. 113-123, 2005.

18. Y. Ohkura, Shih-Yu Liu, P. M. Rao and X. Zheng, "Synthesis and ignition of energetic CuO/Al core/shell nanowires", Proc. Combust. Inst. 2010.

19. K.K. Kuo, G.A. Risha, B.J. Evans, E. Boyer, "Potential usage of energetic nano-sized powders for combustion and rocket propulsion", Mater. Res. Soc. Symposium Proceedings, v 800, pp. 3-14, 2004.

20. L. L. Wang, Z. A. Munir, Y. M. Maximov, "Termite reactions: their utilization in the synthesis and processing of materials" J. Mater. Sci., v 28, n 14, 1993.

21. R. Orrum, Sannia, A. Cincotti, G. Cao, "Thermal and mechanochemical self-propagating degradation of chloro-organic compounds: The case of hexachlorobenzene over calcium hydride", Chem. Eng. Sci., v 38, n 9, pp. 3218-3224, 1999.

22. C. Rossi, K. Zhang, D. Estève, P. Alphonse, P. Tailhades, and C. Vahlas, Tailhades, Philippe, "Nanoenergetic materials for MEMS", Source: Journal of Micro electromechanical Systems, v 16, n 4, pp. 919-931, 2007.

23. E. L. Dreizin, "Metal-based reactive nanomaterials", Prog. Energ. Combust, v 35, n 2, pp. 141-167, 2009.

24. T. Troianello, "Precision foil resistors used as electro-pyrotechnic initiators", Proc. 1st Electron. Compon, and Technol. Conf., Orlando, FL, pp. 1413-1417, 2001.

25. H. DiBiaso, B. A. English, and M. G. Allen, "Solid-phase conductive fuels for chemical microactuators", Sens. Actuators A, Phys., v 111, n 2/3, pp. 260-266, 2004.

26. H. Laucht, H. Bartuch, and D. Kovalev, "Silicon initiator, from the idea to functional tests", Proc. 7th Int. Symp. and Exhib. Sophisticated Car Occupant Safety Syst., pp. 12-16, 2004.

27. T. W. Barbee, R. L. Simpson, A. E. Kash, and J. H. Satcher, "Nanolaminate-based ignitors" U.S. Patent WO 2005 016 850 A2, 2005.

28. Michelle L. Pantoja, and John J. Granier, "Combustion behavior of highly energetic thermites: Nano versus micron composites", propellants, explosives, pyrotechnics, v 30, pp. 53-62, 2005.

29. S. H. Fisher, M. C. Grubelich, "Theoretical energy release of thermites, intermetallics, and combustible metals" Proceedings of 24th International Pyrotechnics Seminar, Monterey, California, USA, 1998.

30. Z. A. Munir, U. Anselmi-Tamburini, "Self-Propagating exothermic reactions: The synthesis of high-temperature materials by combustion" Materials Science Reports, v 3, n 7-8, p 277-365, 1989.

31. J. Eckert, J. C. Holzer, C. C. Ahn, Z. Fu, and W. L. Johnson, "Melting behavior of nanocrystalline aluminum powders" , Nanostructured Materials, v 2, n 4, pp. 407-13, 1993.

32. K. Zhang, M. Petrantoni, C. Rossi.," A development of Al/NiO nano energetic material on silica substrate", Applied Physics Letters, v 91, Issue 11, 2008.

33. T.M. Tillotson, A.E. Gash, R.L. Simpson, L.W. Hrubesh, J.H. Satcher Jr., and J.F. Poco, "Nanostructured energetic materials using sol-gel methodologies", Journal of Non-Crystalline Solids, v 285, pp. 338-345, 2001.

34. K.J. Blobaum, M.E. Reiss, J.M.P. Lawrence, and T.P. Weihs, "Deposition and characterization of a self-propagating CuOx/Al thermite reaction in a multilayer foil geometry", Journal of Applied Physics, v 94, pp. 2915-2922, 2003.

35. L. Menon, S. Patibandla, K. Bhargava Ram, S.I. Shkuratov, D. Aurongzeb, M. Holtz, J. Berg, J. Yun, and H. Temkin, "Ignition studies of Al/Fe2O3 energetic nanocomposites", Applied Physics Letters, v 84, pp. 4737-4737, 2004.

36. S.H. Kim and M.R. Zachariah, "Enhancing the rate of energy release from nanoenergetic materials by electrostatically enhanced assembly", Advanced Materials, v 16, pp. 1821-1825, 2004.

37. J.D. Ferguson, K.J. Buechler, A.W. Weimer, and S.T. George, "SnO2 atomic layer deposition of ZrO2 and Al nanoparticles: pathway to enhanced thermite materials" Powder Technology, v 156, pp. 154-163, 2005.

38. M.L. Pantoya and J.J. Granier, "Combustion behavior of highly energetic thermites: nano versus micro composites", Propellants Explosives Pyrotechnics, v 30, pp. 53-62, 2005.

39. B.S. Bockmon, M.L. Pantoya, S.F. Son, B.W. Asay, and J.T. Mang, "Combustion velocities and propagation mechanisms of metastable interstitial composites", Journal of Applied Physics, v 98, pp.7, 2005.

40. Prakash, A.V. McCormick, and M.R. Zachariah, "Tuning the reactivity of energetic nanoparticles by creation of a core-shell nanostructure", Nano Letters, v 5, pp. 1357-1360, 2005.

41. S. Apperson, R.V. Shende, S. Subramanian, et at, "Generation of fast propagating combustion and shock waves with copper oxide/aluminum nanothermite composites", Applied Physics Letters, vol. 91, pp. 3, 2007.

42. L. A. Clevenger, C. V. Thompson, and K. N. Tu, "Explosive silicidation in nickel/amorphous-silicon multilayer thin films", Journal of Applied Physics, v 67, n 6, pp. 2894-2898, 1990.

43. E. Besnoin, Cerutti, S., Knio, O. M., and Weihs, T. P., "Effect of reactant and product melting on self-propagating reactions in multilayer foils" Journal of Applied Physics, Vol. 92, n 9, pp. 5474-5481, 2002.

44. K. R. Coffey, R. Kumar, "Thin Film Energetic Materials,", presented at the 2nd Eglin Symposium on nano-Energetics (ESNE2), Shalimar, Florida, 2006.

45. E. Ma, Thompson, C. V., Clevenger, L. A., and Tu, K. N "Self-propagating explosive reactions in Al/Ni multilayer thin films", Applied Physics Letters, v 57, n 12, pp. 1262-1264, 1990.

46. A. J. Gavens, D. Van Heerden, A. B. Mann, M. E. Reiss, and T. P. Weihs, " Effect of intermixing on self-propagating exothermic reactions in Al/Ni nano-laminate foils" Journal of Applied Physics, v 87, n 3, pp.1255-1263, 2000.

47. A.S. Rogachev, A. E. Grigoryan, E.V. Illarionova, I.G.Kanel, A. G. Merzhanov, A. N., Nosyrev, N. V. Sachkova, V. I. Khvesyuk, and P. A. Tsygankov, "gasless Combustion of Ti-Al Bimetallic Multilayer nanofilms", Combustion, Explosion, and Shock Waves, v 40, n 2, pp. 166-171, 2004.

48. J. C. Gachon, A. S. Rogachev, H. E. Grigoryan, E. V. Illarionova, J. J. Kuntz, D. Yu. Kovalev, A. N. Nosyrev, N. V. Sachkova, and P. A. Tsygankov, "On the mechanism of heterogeneous reaction and phase formation in Ti/Al multilayer Nanofilms", Acta Materialia, v 53, pp. 1225-1231, 2005.

49. L. Takacs, "Self-Sustaining metal-sulfur reaction induced by ball milling, J. Materials synthesis and processing", Journal of Materials Synthesis, v 8, pp 3-4, 2000.

50. A. Bakhshai, R. Pragai, and L. Takacs "Self-Propagating reaction induced by ball milling in a mixture of Cu_2O and Al powders", Metallurgical and Materials Transactions A, n 11, v 33, pp. 3521-3526, 2002.

51. R.C. Armstrong and M.L. Koszykowski, "Combustion theory for sandwiches of alloyable materials", Z.A. Munir and J.B. Holt, Editors, Combustion and plasma synthesis of high-temperature materials, New York, pp. 88-99, 1990.

52. R. Armstrong, "Models for Gasless Combustion in Layered Materials and Random Media", Comb, Sin. Technol, v 71, Issue 4, pp. 155-174, 1990.

53. R. Armstrong, "Theoretical models for the combustion of alloyable materials" Metall. Tran, Springer-Verlag , v 23, Issue 9, 1992.

54. J. Zeck, L. Takacs, and A. Bakhshai "Like SHS, Loose powder ignition a key process within mechanochemical reaction", Goucher college, Baltimore, 2001.

55. A. Bakhshai, V. Soika, M. A. Susol, and L. Takacs , "Mechanochemical reactions in the Sn–Zn–S System further study", J. Solid state chem., v 153, 2000.

56. C. Michaelsen, K. Barmak and T. P. Weihs "Investigating the thermodynamics and kinetics of thin film reaction by differential scanning calorimetry", J. Appl. Phys., v 30, n 23, p 3167-3186, 1997.

57. Mann, A. J. Gavens, M. E. Reiss, D. Van Heerden, G. Bao and T. P. Weihs "Modeling and characterizing the propagation velocity of exothermic reaction in mulilayer foils", J. Appl. Phys, v 82, pp. 3, 2003.

58. S. R. Turns, "An introduction to combustion", John Wiley &sons, New York, 1999.

59. J. Glassman, "Combustion theory", 2th Ed., Academic press, San Diego, CA, 1996.

60. J. C. Gachon, A. S. Rogachev, H.E. Grigoryan, E.V. Illarionova, J. J, Kuntz, D. Yu. Kovalev , A. N. Nosyrev , N. V. Sachkova , P. A. Tsygankov "On the mechanism of heterogeneous reaction and phase formation in Ti/Al multilayer nanofilms" Acta Materialia, v 53, n 4, pp. 1225-1231, 2005.

61. H. J. Feng, J. J. Moore, and D. G. Wirth, "Combustion synthesis of ceramic-metal composite materials", International Journal of Self-Propagating High-Temperature Synthesis, v 1, n 2, pp. 228-38, 1992.

62. J. J. Moore and H. J. Feng, "Combustion synthesis of advanced materials: part I. Reaction parameters", Prog. Mater. Sci., v 39, n 4-5, pp. 243-273, 1995.

63. J. J. Moore and H.J. Feng, "Combustion synthesis of advanced materials: part II. Classification, applications and modeling", Prog. Mater Sci., v 39, n 4-5, pp. 275-316, 1995.

64. L. Menon, S. Patibandla, K. Bhargava Ram, S. I. Shkuratov, D. Aurongzeb, and M. Holtz, "Ignition studies of AlÕFe2O3 energetic nanocomposites", applied physics letters, v 84, n 23, 2004

65. K. Zhang, C. Rossi, M. Petrantoni, and N. Mauran, "A nano initiator realized by integrating Al/CuO-based nanoenergetic materials with a Au/Pt/Cr microheater", Journal of Microelectromechanical Systems, v 17, n 4, pp. 832-6, 2008.

66. C. Zanotti, P. Giuliani, M. Monagheddu, and N. Bertolino, "Modeling of ignition phenomena in combustion synthesis", ICNC-Sorrento, v 11, n 1, pp. 41-9, 2003.

67. S. Alexander, A. T. Tappan, S. T. Gregory T. Long, M. Anita Renlund, and H. Stanley Kravitz, "Micro energetic processing and testing to determine energetic material properties at the mesoscale", AIAA. 2003.

68. Rossi, T. Do Conto, D. Esteve, and B. Larangot "Design, fabrication and modeling of MEMS-based micro thrusters for space application", smart materials and structures, v 10, n 6, pp. 1156-1162, 2001.

69. S. Bhattacharya, "A novel On-Chip diagnostic method to measure burn rates of energetic materials", Journal of Energetic Materials, v 24, n 1-15, 2006.

70. T. Q. Qui, and C. L. Tien, "Heat transfer mechanisms during short-pulse laser heating of metals", ASME J. Heat Transfer, v 115, n 4, pp. 835-841, 1993.

71. T. Q. Qui, and C. L. Tien, "Femtosecond laser heating of multi-layer metals-I analysis", Int. J. Heat Mass Transfer, v 37, n 17, pp. 2789-2797, 1994.

72. A. A. Joshi, and A. Majumdar,"Transient ballistic and diffusive phonon transport in thin films", J. Appl. Phys., v 74, n 1, pp. 31-9, 1993.

73. G. Chen, "Size and interface effects on thermal conductivity of superlattices and periodic thin-film structures", J. Heat Transfer, v 119, n 2, pp. 220-229, 1997.

74. G. Chen, "Thermal conductivity and ballistic-phonon transport in the cross-plane direction of superlattices" Phys. Rev. B, v 57, n 23, pp. 14958-14973, 1993.

75. G. Chen, and M. Neagu, 1997, "Thermal conductivity and heat transfer in superlattices" Appl. Phys. Lett., v 71, n 19, pp. 2761-2763, 1997.

76. M. Asheghi, M. N. Touzelbaev, K. E. Goodson, Y. K. Leung, and S. S. Wong, "Temperature-dependent thermal conductivity of single-crystal silicon layers in SOI substrates" J. Heat Transfer, v 120, n 1, pp. 30-36, 1998.

77. M. Asheghi, K. Kurabayashi, R. Kasnavi, and K. E.Goodson, "Thermal conduction in doped single-crystal silicon films" J. Appl. Phys., v 91, n 8, pp. 5079-5088, 2002.

78. Y. S. Ju, and K. E. Goodson, "Phonon scattering in silicon thin films with thickness of order 100 nm" Appl. Phys. Lett., v 74, n 20, pp. 3305-3307, 1999.

79. K. E. Goodson, and Y. S. Ju, "Heat conduction in novel electronic films", Annu. Rev. Mater. Sci., v 29, pp. 261-293, 1999.

80. Y. S. Ju, "Microscale heat conduction in integrated circuits and their constituent films", Ph.D. thesis, Department of Mechanical Engineering, Stanford University, 1999.

81. N. W. Ashcroft, and N. D. Mermin, "Solid State Physics", Saunders, Philadelphia, 1976.

82. S.V. J. Narumanchi, J. Y. Murthy, Cristina H. Amon, "Submicron heat transport model in silicon accounting for phonon dispersion and polarization", Journal of Heat Transfer, v 126, n 6, pp. 946-955, 2004.

83. C. Kittel, "Introduction to Solid State Physics", Wiley, New York, 1971.

84. A. Majumdar, "Microscale energy transport in solids in microscale energy transport, tien", Washington, D.C., pp. 1-94, 1998.

85. M. I. Flik, B. I. Choi, and K. E.Goodson, "Heat transfer regimes in microstructures", ASME J. Heat Transfer, v 114, n 3, pp. 666-674, 1992.

86. G. Cahill, W. K. Ford, K. E. Goodson, G. D. Mahan, A. Majumdar, H. J. Maris, R. Merlin, and S. R. Phillpot, "Nanoscale thermal transport", J. Appl. Phys., v 93, n 2, pp. 793-818, 2003.

87. D. G. Cahill, K. E. Goodson, G. D. Mahan, A. Majumdar, "Thermometry and thermal transport in micro/nanoscale solid-state devices and structures", ASME J. Heat Transfer, v 124, n 2, pp. 223-241, 2002.

88. K. E. Goodson, "Thermal conduction in nonhomogeneous CVD diamond layers in electronic microstructures", ASME J. Heat Transfer, v 118, pp. 279-286, 1996.

89. A. Majumdar, "Microscale heat conduction in dielectric thin films", ASME J. Heat Transfer, v 115, n 1, pp. 7–16, 1993.

90. G. Chen, "Nonlocal and nonequilibrium heat conduction in the vicinity of nanoparticles", ASME J. Heat Transfer, v 118, n 3, pp. 539-545, 1996.

91. G. Chen, "Phonon wave heat conduction in thin films and superlattices", J. Heat Transfer, v121, n 4, pp. 945-953, 1999.

92. G. Chen, "Particularities of heat conduction in nanostructures", J. Nanopart, Res., v 2, n 2, pp. 199-204, 2000.

93. G. D. Mahan, and F. Claro, "Nonlocal theory of thermal conductivity", Phys. Rev. B, v 38, n 3, pp. 1963-1969, 1988.

94. F. Claro, and G. D. Mahan, "Transient heat transport in solids", J. Appl. Phys., v 66, n 9, pp. 4213–4217, 1989.

95. S. Carslaw, and J. C. Jaeger, "Conduction of heat in solids", Oxford University Press, Cambridge, U.K., pp. 255, 1947.

96. D. Rosenthal, "Mathematical theory of heat distribution during welding and cutting", Welding Journal Welding Journal, v 20, n 5, pp. 220, 1941.

97. T. W. Eagar, and N. S. Tsai, "Temperature fields produced by traveling distributed heat sources", Welding Journal, v 62, n 12, pp. 346-355, 1983.

98. S. K. Jeong, and H. S. Cho, "An analytical solution to predict the transient temperature distribution in fillet arc welds", Welding Journal, v 76, n 6, pp. 223, 1997.

99. J. Goldak, A. Chakravarti, and M. Bibby, "A double ellipsoid finite element model for welding heat sources", International Journal of Thermal Sciences, v 48, n 10, pp. 1923-31, 2009.

100. N. T. Nguyen, A. Ohta, K. Matsuoka, N. Suzuki, Y. Maeda, "Analytical solutions for transient temperature semi-infinite body subjected to 3D moving heat sources", Welding Research Supplement, Welding Journal, pp. 265-274, 1999.

101. A. Kaplan, "A model of deep penetration laser welding based on calculation of the keyhole profile", J Phys , v 27, pp. 1805-1814, 1994.

102. H. J. Blobaum, A. J. Wagner, J. M. Plitzko, D. Van Heerden, D., and T. P. Weihs, "Investigating the reaction path and growth kinetics in CuO_x /Al multilayer foils", J. Appl. Phys, v 94, 2003.

103. N. Aminimanesh, S. Basu, and R. Kumar, "Experimental flame speed in multi-layered nano-energetic materials Experiments and numerical studies in dense layered nano-energetic materials", Combustion and Flame, v 157, n 3, p 476-480, 2010.

104. Z. A. Munir, "Synthesis of high temperature materials by self-propagating combustion methods", American Ceramic Society Bulletin, v 67, n 2, p 342-9, 1988.

105. Z. A. Munir, "Combustion & plasma synthesis of high temperature materials", VCH, New York, 1990.

106. S. Tappan, A. N. N. Renlund, G. T. Long, S. H. Kravitz, K. L. Erickson, W. M. Trott, M. R. Baer "Micro energetic processing and testing to determine energetic material properties at the mesoscale", 12th International Detonation Symposium, 2002.

107. C. Rossi, T. Do Conto, D. Esteve, and B. Larangot, "Design, fabrication and modelling of MEMS-based micro thrusters for Space application", smart materials and Structures, v 10, n 6, pp.1156-1162, 2001.

108. S. A. Mukasyan, A. S. Rogachev, A. Varma. "Mechanisms of reaction wave propagation during combustion synthesis of advanced materials", Chemical Engineering Science, v 54, n 15-16, pp. 3357-3367, 1999.

109. H. Okamoto and T. B. Massalski, Eds., "Binary Alloy Phase Diagrams. Metal Park", OH: ASM International, pp. 381–383, 1990.

110. R. Weichert, and K. Schonert, "Temperature distribution produced by a moving heat source", Quarterly Journal of Mechanics and Applied Mathematics, v 31, n 3, p 363-79, 1978.

111. S. V. Patankar, "Numerical Heat Transfer and Fluid Flow", Mc Graw Hill, 1980.

112. A.V. Prakash, McCormick, M. R. Zachariah, "Aero-Sol-Gel Synthesis of Nanoporous Iron-Oxide Particles: A Potential Oxidizer for Nanoenergetic", Materials Chemistry of Materials, v 16, n 8, pp. 1466-71, 2004.

113. S. F. Son, J. R. Busse, B. W. Asay, P. D. Peterson, J. T. Mang, B. Bockmon, M. L. Pantoya, "Propagation Studies of Metastable Intermolecular Composites (MIC)" presented at the 29th Int. Pyrotechnics Seminar, Westminster, CO, 2002.

114. M.E. Brown, S. J. Taylor, M. J. Tribelhorn, "Fuel-Oxidant particle contact in binary pyrotechnic reactions" Propellants, Expolos, Pyrotech, v 23, n 6, pp. 320-327, 1998

115. W. Miziolek, "Nanoenergetics: An Emerging Technology Area of National Importance", AMPTIAC Quarterly, Vol. 6, n 1, pp. 43-48, 2002.

116. TB. Massalski, "Binary alloy phase diagrams", ASM, v 1, 2000.

117. P. H. Renard, C. Roldan, DE. Thevenin, and S. Candel, "Dynamics of flame/vortex interactions" Combust. Flame, v 26, n 3, pp. 225-282, 2000.

118. P. A. Ramakrishna, P. J. Paul, and H. S. Mukunda, "Sandwich propellant combustion: modeling and experimental comparison", Proc. Combust. Symp, v 29, 2002.

119. J. Subrahmanyam, and M. Vijayakumar, "Self-propagating high-temperature synthesis", J. Mater. Sci., v 27, pp. 6249–6273, 1992.

120. S. Michaelson, K. Barmak, and T. P. Weihs, "Investigating the thermodynamics and kinetics of thin film reaction by differential scanning calorimetry", J. Appl. Phys., v 30, 1997.

121. J. F. Tu, K. N. Lankalapalli, M. Gartner, and K. H. Leong, "On-Line Estimation of Laser Weld Penetration" Journal of Dynamic Systems Measurement and Control, v 119, n 4, pp.791, 1997.

122. H. N. Najm, P. H. Paul, C. J. Mueller and P. S. Wyckoff "On the adequacy of certain experimental observables as measurements of flame burning rate", Combust Flame, v 113, pp. 312–332, 1998.

123. M. Song, and R. Kovacevic, "Thermal modeling of friction stir welding in a moving coordinate system and its validation", International journal of machine tools & manufacture, v 43, n 6, pp. 605, 2003.